DESIGN & DEVELOPMENT OF PLANAR SOLID OXIDE FUEL CELL STACK

POLITECNICO DI TORINO
Dipartimento Energia

Ph.D. Thesis

DESIGN & DEVELOPMENT OF PLANAR SOLID OXIDE FUEL CELL STACK

GUSTAVO ADOLFO ORTIGOZA VILLALBA

Academic advisor: Prof. Massimo Santarelli

May 2013, Turin (Italy)

Abstract

In the present work, planar anode-supported Solid Oxide Fuel Cell short-stacks have been designed, assembled, tested and characterized.

The design of the stacks and its components (frame, housing, interconnect, compressive and bonded seals) required a great attention to the materials properties (i.e. thermal expansion coefficient compatibility, durability, strength and oxidation resistance, conductivity and so on), as well as to the fluid-dynamic analysis focused on flow field and gas distribution. Then, a careful analysis was done based on a multidisciplinary approach to select the stack components materials, geometries, and dimensions; in order to assure a high performing stack at elevated temperatures with cost reduction of materials, parts manufacturing and assembly procedure.

The materials selected were: Crofer®22APU for the interconnect and the frame; AISI 316L for bolts and housing; Thermiculite® 866 for the compressive seal placed between the frame and the interconnect plate; Flexible Mica Paper for the compressive seal positioned between the interconnect endplate and the housing; SiO_2-CaO-Al_2O_3-Na_2O glass-ceramic sealant for the bonded seal to join the frame with the cell.

On the other hand, the stack assembly was focused on the implementation of innovative and simple procedures, which allowed power capacity scale-up in accordance to power requirements. In this work, two different stack configurations were produced: with one cell (for initial testing of the materials and fluid-dynamic selected solutions) and with three cells. It must be mentioned that all developed stacks in this research were assembled with commercial cells “ASC3” from H.C. Starck.

Also, calculations at ambient temperature and 800°C were done in the stack compression system to determine the proper tightening torque to be applied: this value was 50N. Although this calculation took into consideration the loss of tightening torque at high temperatures, some marks were found in housing and micas during the stack inspection after disassembly. These marks are a clear indicator of gas leakage.

Additionally, a study was carried out related to the effect of the protective $Mn_{1.5}Co_{1.5}O_4$ coating deposited on interconnect surface to prevent the cathode Cr poisoning. This experiment was executed in the stack of one cell configuration. No voltage degradation was observed during the galvanostatic experiment of 360 h at 800°C.

Acknowledgements

Completion of this doctoral dissertation was possible with the support of several people. I would like to express my sincere gratitude to all of them.

First and foremost I want to thank my advisor Prof. Massimo Santarelli and Energy Department of Politecnico di Torino, for his valuable guidance, technical inputs and consistent encouragement I received throughout the research work,

My colleagues, Dr. Pierluigi Leone and Dr. Andrea Lanzini, have all extended their support in a very special way, and I gained a lot from them, through their personal and professional interactions, their suggestions at various points of my research program.

I gratefully acknowledge the funding sources that made my Ph.D. work possible. It was carried out in the framework of MULTISS, PRIN 2008 and SOFCOM.

I would also like to thank the Department of Applied Science and Technology of Politecnico di Torino, specially to Dr. Federico Smeacetto and Prof. Milena Salvo.

Lastly, I would like to thank my wife, Isabel, for her love, kindness and support; during the last years she has encouraged me to finalize this thesis. Furthermore, I would also like to thank my parents and my brother for their endless love and support.

Table of Contents

List of Figures

List of Tables

Introduction

1.1 Fuel Cells for Energy Supply

Ever since the beginning of industrialization, fossil fuels (coal, oil and natural gas) have been the major source of energy supply. However, it is certain that the supply of cheap, conventionally produced oil will peak and decline this century. The predictions about “peak oil” run from 2010 by ASPO (Association for the Study of Peak Oil and Gas) to a peak approximately in 2035 by IEA (International Energy Agency) [1]. Then at the latest, an energy revolution to alternative energy sources such as solar and wind will have taken place to cover the worldwide growing need for energy.

Meanwhile there are fundamental economic [2], environmental and strategic interests [3] for a responsible dealing with fossil fuels. For example, the first 11 years of the 21st century experienced notably higher temperatures compared to the middle and late 20th century, so the economic costs of the climate change range between 5% and 20% of the worldwide gross domestic products (several trillion Euros). Therefore, governmental and non-governmental organizations strive to solve present and future energy problems on an international level [4].

Regardless of what the driving force may eventually be, political reason or increasing energy prices, the importance of a more efficient use of energy has been recognized as a key issue for technology development. Considerable aspirations in this context are

connected with fuel cells. Interest in these alternative energy-conversion devices has increased rapidly in recent years, whereas the basic principles of fuel-cell operation are known since the early experiments of Schönbein and Grove in the first half of the 19th century. These fuel cells with high-energy conversion efficiency and low emission are promising systems for replacing combustion-based electrical generators at all sizes.

In fact, fuel cells represent a revolutionary technology for power generation by fuel. In conventional electrical power generation the fuel is oxidized spontaneously in an irreversible combustion reaction, recovering the chemical energy in the fuel as heat, which has to be converted first to mechanical and then to electrical energy. In fuel cell-based power generation the oxidation reaction is carried out in an electrochemical cell, keeping the reactants apart and forcing the electron-transfer involved in the reaction to take place through an external circuit, such that most of the chemical energy can be recovered directly as electrical energy.

The electric efficiency of conventional power generation is 33–38%, while that of power generation with high-temperature fuel cells may be 60% [5]. Moreover, the oxidation process in fuel cells takes place, with the aid of a catalyst, at temperatures much lower than the flame temperature, and therefore emits negligible NOx even in high-temperature fuel cells. Fuel cell-based power generation does not emit any particulates or noise either.

It therefore makes sense to invest heavily in research and development of this technology to preserve fossil fuels and protect the environment.

1.2 Fuel cells overview

A general introduction is given on fuel cells. The history, different types, advantages and drawbacks of fuel cells are discussed.

1.2.1 Definition

Fuel cells are electrochemical devices that directly convert chemical energy, from a reaction between a fuel and an oxidant, into electrical energy. The basic elements of a typical fuel cell, as depicted in Figure 1-1, consist of an electrolyte phase in intimate

contact with a porous anode (negative electrode) and a porous cathode (positive electrode). The fuel and oxidant gases flow along the surface of the anode and cathode, respectively, and react electrochemically in the three-phase-boundary region established at the gas / electrolyte / electrode interface. A fuel cell can theoretically produce electrical energy for as long as fuel and oxidant are fed to the porous electrodes, but the degradation or malfunction of some of its components often limits the practical life span of a fuel cell.

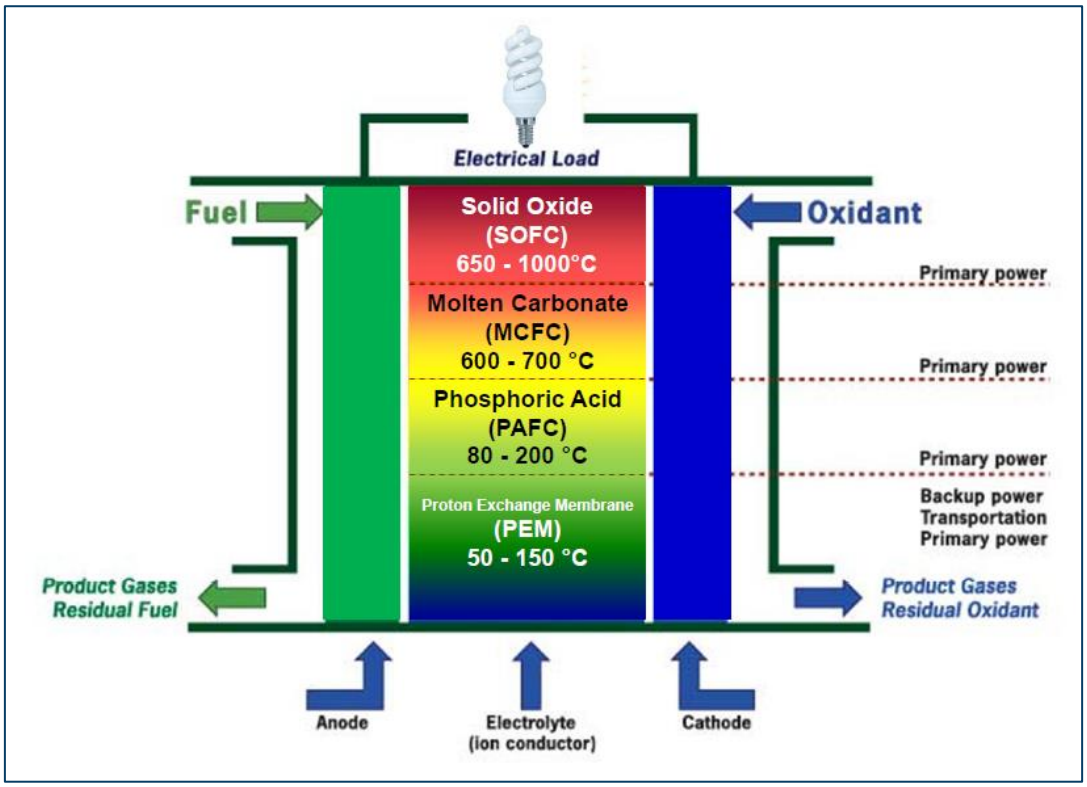

Figure 1-1: Schematic representation of a fuel cell

Different fuels can be used, such as hydrogen, ethanol, methanol, or gaseous fossil fuels like natural gas. Solid or liquid fossil fuels need to be gasified first before they can be used as a fuel. Oxygen or air can be used as oxidant.

1.2.2 Types of fuel cells

The various types of fuel cells are usually classified by the applied electrolyte (see Table 1-1) and include the following:

- Polymer electrolyte fuel cell (PEFC),
- Alkaline fuel cell (AFC),
- Phosphoric acid fuel cell (PAFC),
- Molten carbonate fuel cell (MCFC),
- Solid oxide fuel cell (SOFC).

Table 1-1: Typical components, operating conditions and electrochemical reactions in Fuel Cells. [a] Space Shuttle Orbiter, [b] Apollo Program, [c] Fluorinated sulfonic acid, registered trademark of E.I. du Pont de Nemours & Company, Inc.

	PEM	AFC[a]	AFC[b]	PAFC	MCFC	SOFC
Anode	Pt black or Pt/C	80%Pt-20%Pd	Ni	Pt/C	Ni-10%Cr	Ni-YSZ cermet
Cathode	Pt black or Pt/C	90%Au-10%Pt	Li-doped NiO	Pt/C	Li-doped NiO	Sr-doped $LaMnO_3$
Electrolyte (mol%)	Nafion [c]	35-45% KOH	85% KOH	100% H_3PO_4	62 Li_2CO_3-38K_2CO_3	Yttria stabilized ZrO_2 (YSZ)
Abs pressure (MPa)	0.1-0.5	0.4	~0.4	0.1-1	0.1-1	0.1
Temperature (°C)	80	80-90	260	200	650	1000
Anode reaction	$H_2 \rightarrow 2H^+ + 2e^-$	$H_2 + 2OH^- \rightarrow 2H_2O + 2e^-$	$H_2 + 2OH^- \rightarrow 2H_2O + 2e^-$	$H_2 \rightarrow 2H^+ + 2e^-$	$H_2 + CO_3^{2-} \rightarrow H_2O + CO_2 + 2e^-$	$H_2 + 2O^{2-} \rightarrow H_2O + 2e^-$
Cathode reaction	$O_2 + 4H^+ + 4e^- \rightarrow 2H_2O$	$O_2 + 2H_2O + 4e^- \rightarrow 4OH^-$	$O_2 + 2H_2O + 4e^- \rightarrow 4OH^-$	$O_2 + 4H^+ + 4e^- \rightarrow 2H_2O$	$O_2 + 2CO_2 + 4e^- \rightarrow 2CO_3^{-2}$	$O_2 + 4e^- \rightarrow 2O^{-2}$

Large differences exist in application, design, size, cost and operating range for the different type of fuel cells. The fuel cells above are listed in order of increasing operating temperature, ranging from ~80°C for PEFC to 1000°C for SOFC. The low temperature fuel cells (PEFC, AFC, PAFC) utilise aqueous electrolytes in which H^+ or OH^- ions are the dominant ionic current carriers.

At higher temperatures, CO_3^{2-} ions in the molten salt electrolyte of the MCFCs and O^{2-} ions in the solid electrolyte of the SOFC are the ionic current carriers. The operating temperature has consequences for design, the efficiency of the fuel cell, the choice of other materials needed in and around the fuel cell and the kind of fuel that may be used. For low temperature fuel cells (PEFC, AFC and PAFC) the operating temperature is too low to enable direct oxidation of hydrocarbon fuels like natural gas, therefore fuels like hydrogen and methanol are used. Low temperature fuel cells are generally seen as interesting for small scale applications, for example mobile applications like cars (PEFC), notebooks, phones etc.

For high temperature fuel cells (MCFC and SOFC) it is possible to use natural gas which can be reformed internally into hydrogen and carbon monoxide (depending on operating temperature a catalyst will be necessary). The high temperature fuel cells, but also PAFC, are interesting for the decentralised production of electricity and heat (distributed CHP).

1.2.3 Advantages and drawbacks

The advantages and drawbacks of fuel cell systems are determined by their type and application. As it can be useful to compare a SOFC or MCFC system with traditional generators, a small fuel cell developed for applications as notebooks or mobile phones should be compared with traditional batteries. The advantages and drawbacks given here are mostly based on SOFC systems, but in general part of it will be valid for other types of fuel cells.

The main advantages are:

- *High energy conversion efficiency*. Because of the direct conversion of free enthalpy into electrical energy the usual losses from fuel to electrical energy, due to the conversion of fuel to heat, heat to mechanical energy and mechanical energy to electrical energy is avoided. The global efficiency is further improved when the by-product heat is fully utilized.
- *Environmental compatibility*. Fuel cells are capable of using practical fuels as an energy source with minor environmental impacts (less CO_2 and NO_x produced per

kWatt power), since they do not produce particulate matter neither Volatile Organic Compounds (VOCs).

- *Modularity*. Fuel cells have the characteristic of modularity, i.e. cells can be made in modular sizes. The size of a fuel cell can be easily increased or decreased and its electric efficiency is relatively independent of size.
- *Siting flexibility*. Because fuel cells can be made in a variety of sizes they can be placed at different locations with minimum siting restrictions. Fuel cell operation is quiet because a fuel cell has no moving parts. Consequently fuel cells can be easily located near points of use such as urban residential areas.

Unfortunately, there are some drawbacks which have caused a slow introduction of solid oxide fuel cells on the energy market:

- *Material problems in relation with costs*: For SOFC there are roughly two design types, tubular and flat plate. For the tubular cell material problems are less, but fabrication costs are high. For the flat plate design fabrication costs are less, but more material problems arise.
- *Economics*. Introduction on the energy market would presently involve a high capital cost-to-performance ratio.

1.3 PhD investigation objectives

This PhD thesis is concerned with design, build and experimental analysis of planar Solid Oxide Fuel Cell stack. The general objective is the development and in-house production of short SOFC stacks of planar anode-supported geometry for dealing with multiple fuels.

The following general considerations have been taken into account to establish the specific objectives of this research:

- Chemical and Mechanical stability: at the cathode side under oxidizing conditions and at the anode side under reducing conditions, for temperatures up to 800°C.
- Material selection: the thermal expansion coefficients similar between the contact layer materials.
- Gas tightness: can be obtained by using adequate sealant materials and their proper placement.

- Thermal management: the temperature field must be as homogeneous as possible, whereas the reactant distribution system in both sides of the cell must be uniform.
- Electrical behavior analysis of materials (ceramics, metallic and cermets) at high temperatures.
- High electrical performance of the cell interconnection for reducing as much as possible the ohmic losses in the stack.
- The sealing materials must avoid the gas leakages.
- Moderate costs.

In consequence, the specific objectives are:

1. Testing of commercial anode-supported cell (“ASC3” NiO/YSZ anode, YSZ electrolyte, LSM cathode) to determine the stack geometry.
2. Design and production of the components (interconnectors, housing, frame, seal and cell geometry) for a planar SOFC stack, with particular attention to:
   - Reactant distribution system with homogeneous flows field in the cell and small thermal stresses into the cell interconnection at the same time.
   - Electrochemical performance in the final configuration: high open circuit potential and minimum polarization losses must be ensured.
   - Good mechanical stability and high electrical conductivity of the interconnectors.
   - Capability to resist high temperature conditions under oxidizing atmosphere of the interconnector surface without material degradation.
3. Building of short planar anode-supported SOFC stacks by using innovative procedures, which allow power capacity scale-up in accordance to requirements.
4. Electrochemical testing of SOFC short-stacks under steady state conditions with non-conventional fuels and experimental analysis
5. Stacks disassembly and post mortem characterization of the SOFC stack components (interconnectors, frame, sealant, protective coating and ASC cells) by means of Scanning Electron Microscopy (SEM) and Energy Dispersion Spectroscopy (EDS). This activity was carried out in collaboration with Department of Applied Science and Technology (DISAT) of the Politecnico di Torino.

This PhD Dissertation has been organized in six chapters as briefly described hereafter:

- Chapter 1 introduces the reader into the importance of Fuel Cells as an energy alternative to fossil fuels. In addition, the basic concepts, advantages and drawbacks of the different types of fuel cells are here exposed. Next, the objectives of this research work are presented in this Chapter.

- Chapter 2 summarizes the Solid Oxide Fuel Cells historical background to present the evolution of this technology up to date. The SOFC working principles are also explained. Additionally, this Chapter deals with some key elements of SOFC technology: main configurations (tubular and planar) with particular attention in planar ones; technical requirements of components (interconnect materials, sealant materials, protective coatings) to assembly single stacks, and its use with different fuels. Furthermore, a brief review regarding materials used for stack building as sealant and interconnect materials is presented.

- Chapter 3 deals with the development of stack materials and components as well as the engineering processes (based on the in-house production) to build a short anode-supported planar SOFC stack; with particular attention to reduce costs, and to improve the reliability and robustness of the stack systems against conditions that occur in actual operating systems.

- Chapter 4 shows and analyzes the performance and electrochemical test results obtained with short planar anode-supported stacks of mono cell and multi cells configuration at different H_2 gas flow conditions and different Fuel Utilization.

- Chapter 5 presents the post mortem examination and results (in terms of mechanical structure, material compatibility and durability) of stacks previously tested. Also, the cathode protection from Cr poisoning is analyzed by microstructure investigation in those stacks with the protective coating.

- Chapter 6 summarizes the conclusions drawn from the results of this work, as well as outlining possible future developments and application of the present investigation.

Solid Oxide Fuel Cells Overview

A brief historical background related SOFC is here described to present the evolution of this technology up to date. Next, the basic thermodynamic principles of SOFCs are explained.

In addition, this Chapter deals with some key elements of SOFC technology: main configurations (tubular and planar) with particular attention in planar ones; technical requirements of components (interconnect materials, sealant materials, protective coatings) to assembly single stacks, and its use with different fuels. Furthermore, a brief review regarding materials used for stack building as sealant and interconnect materials is presented.

2.1 Historical background

The fuel cell concept dates from the beginning of the 19th century and is ascribed to Sir Humprey Davy. The possibility of making it a reality was demonstrated by Sir William Grove, who operated a successful hydrogen-oxygen cell in 1839, generally stated as the start of fuel cell history. Grove built a cell in which the reaction of hydrogen and oxygen produced water, and generated an electric current. He stated: '*A shock was given which could be felt by five persons joining hands, and which when taken by a single person was painful*'.

The history of the solid oxide electrolytes can be considered to commence at the end of the 19th century, when Nernst produces his 'glower'. Nernst discovered that the very high electrical resistance of pure solid oxides could be greatly reduced by addition of certain

other oxides. The most promising of these mixtures consisted mainly of zirconia (ZrO_2) with small amounts of added yttria (Y_2O_3). This is still the most widely used electrolyte material in the Solid Oxide Fuel Cells (SOFC).

The first working SOFC was demonstrated by Baur and Preis (1937), using stabilised zirconia as electrolyte and coke and magnetite as a fuel and oxidant, respectively. At a current density of approximately 0.3mA/cm^2 the cell voltage was 0.65V. Although the operation of the first SOFC was demonstrated, the current output of this cell was too low for practical purposes.

A first period of intense activity in SOFC research began in the early 1960s, with intensive research programs driven by new energy needs mainly for military, space and transport applications. At that time basic research dealt with the improvement of electrolyte conductivity and the first steps in SOFC technology. A second period of high activity began in the mid-1980s and goes on today, focusing on electrode materials and technology.

Efforts thus far have resulted in ‘almost’ commercial units which are part of our power generation facilities. Leading companies in SOFC commercialization are; for instance, Siemens and Sulzer (Europe), Westinghouse Electrical Cooperation (USA) and Fuji Electric Corporate Research and Development, Ltd and Tokyo Electric Power Co. (Japan).

2.2 Operating Principles

A simplified functional principle of a solid oxide fuel cell (SOFC), a concept that is regarded as one of the most promising systems due to its high efficiency and its flexibility in terms of the fuel gas, is schematically shown in Figure 2-1. The reactant gases are separated by an ionically conducting oxide membrane, which is usually made of doped zirconium oxide. The chemical potential difference between the reactant gases initiates a driving force for gas compensation through the oxygen ion-conducting electrolyte. The electrodes facilitate the incorporation and removal of oxygen ions into and from the electrolyte.

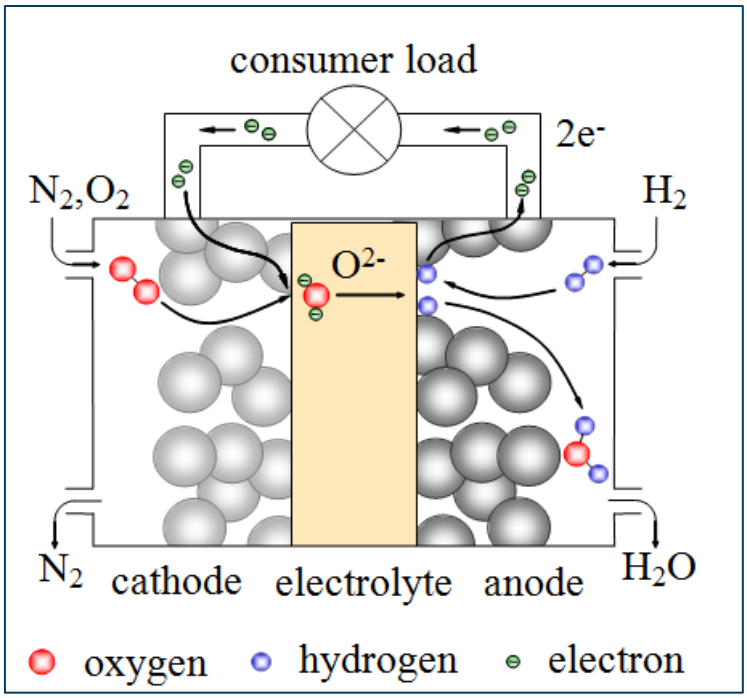

Figure 2-1: Schematic SOFC concept: Oxygen and fuel (here H_2) react via a dense, oxide ion-conducting electrolyte; the spatial separation of reduction and oxidation reaction enables the utilization of the electrons involved in the redox process [6]

The heart of any SOFC is a multilayer ceramic cell, which allows the generation of power by electrochemically oxidizing the fuel. A simple overview of the ceramic cell's function and architecture is shown in Figure 2-2 . As can be seen, rare earth elements are used throughout the layers of the cell and cobalt is commonly used in the cell's cathode.

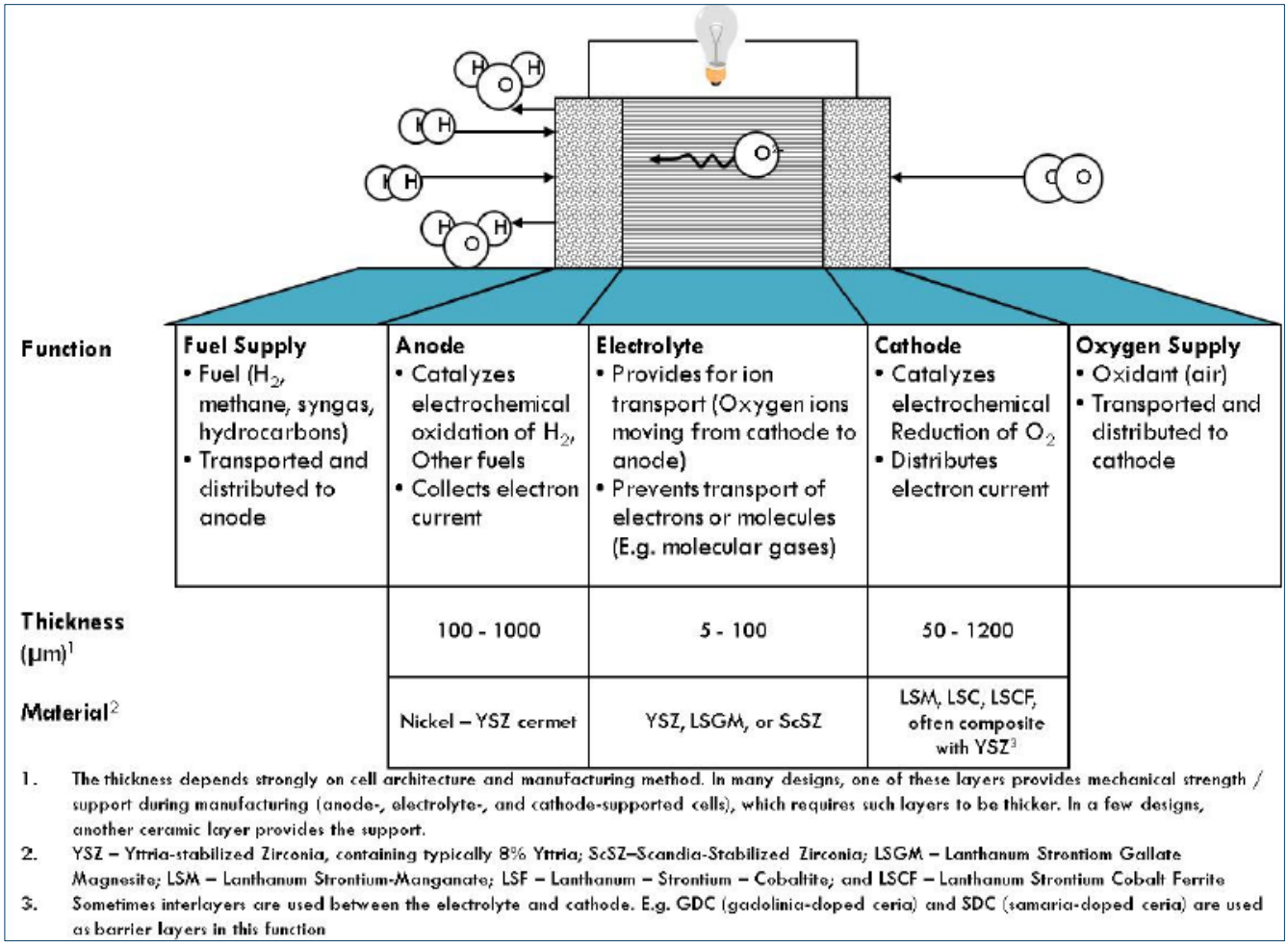

Figure 2-2: Overview of Architecture, Function, and Materials of SOFC [7]

The solid electrolyte can be an oxygen ion, a proton, or a mixed oxygen ion–proton conductor, but it must be an electronic insulator (prohibiting the conduction of electrons or electron holes) and gas impermeable (in a dense membrane form). While SOFCs based on proton conductors (e.g., $BaZr_{0.1}Ce_{0.7}Y_{0.2}O_{3-\delta}$—base electrolytes) have attracted much attention in recent years, the most studied SOFC systems to date are based on oxygen ion conductors such as yttria-stabilized zirconia electrolyte (YSZ, with a composition of 8 mol.% Y_2O_3—92 mol.% ZrO_2, sometimes referred as 8YSZ); the anode is a porous nickel-YSZ cermet; and the cathode is a porous composite that usually contains YSZ and $La_{1-x}Sr_xMnO_{3-\delta}$ (LSM, usually x varies from ~0.15 to ~0.20). YSZ-based SOFCs usually operate at high temperatures (750–1000°C) to be efficient because of the limited transport and catalytic properties of the SOFC materials at low temperatures. To reduce the operating temperature, doped ceria (such as $Ce_{0.9}Gd_{0.1}O_{2-\delta}$ or GDC and $Ce_{0.9}Sm_{0.1}O_{2-\delta}$ or

SDC) have been used as the electrolyte and $La_{0.6}Sr_{0.4}Co_{0.2}$-$Fe_{0.8}O_{3-\delta}$ (LSCF) as the cathode for SOFCs to be operated at low temperatures (<700°C).

If, for example, hydrogen is used as fuel gas (see Figure 2-1), the following electrochemical reactions occur at the two electrodes:

Cathode: $\frac{1}{2}O_2(g) + 2e'(cathode) \rightarrow O^{2-}(electrolyte)$ Equation 1

Anode: $O^{2-}(electrolyte) + H_2(g) \rightarrow H_2O(g) + 2e'(anode)$ Equation 2

Sum: $\frac{1}{2}O_2(g) + H_2(g) \rightarrow H_2O(g)$ Equation 3

The electronically conducting SOFC cathode (typically lanthanum strontium manganite, LSM) leads the oxidant through its porous channels to the electrolyte, where the oxygen-reduction mechanism takes place (Eq. 1). The region where the electronic conducting phase (cathode), gas phase (porous cathode channels) and ionic conducting phase (electrolyte) meet, is called triple-phase boundary (tpb); the concentration of these active sites determines the electrochemical performance of the cathode. Before incorporation of the oxygen ions into the electrolyte, a variety of steps including adsorption of the molecules, dissociation into oxygen atoms and ionization take place at the cathode. Due to the chemical potential difference, the oxygen ions travel through the electrolyte towards the anode where the redox reaction occurs (Eq. 2). The electrons, which are involved in the electrochemical reaction, are forced to flow through an outer circuit performing electrical work. In case of an open circuit, the Nernst voltage U_N arises between cathode and anode:

$$U_N = \frac{RT}{2F} \cdot ln \sqrt{\frac{pO_2\,(cathode)}{pO_2(anode)}} \qquad \text{Equation 4}$$

where R is the general gas constant, T the absolute temperature, F Faraday's constant and pO_2 the respective oxygen partial pressure at cathode and anode.

For a certain oxygen partial pressure at the cathode, $pO_{2\,c}$, the magnitude of E_r depends on the anode oxygen partial pressure, $pO_{2\,a}$, and thus on the type and composition of the fuel fed to the anode. For example, when H_2 is fed to the anode, the following cell reaction takes place:

$$H_{2\,a} + \frac{1}{2}O_{2\,c} \overset{K_i}{\leftrightarrow} H_2O_{\,a} \qquad \text{Equation 5}$$

Where K_i is the equilibrium constant of Eq. 5. The equilibrium oxygen partial pressure at the anode is given by

$$pO_{2\,a} = \left(\frac{pH_2O_a}{pH_{2\,a}K_i}\right)^2 \qquad \text{Equation 6}$$

Substituting the equation for the anode oxygen partial pressure (Eq. 6) into (Eq. 8) yields

$$E_r = E^0 + \frac{RT}{4F}\ln pO_{2c} + \frac{RT}{2F} ln \frac{pH_{2a}}{pH_2O_a} \qquad \text{Equation 7}$$

where E^0 is the reversible voltage at the standard state and is given as

$$E^0 = \frac{RT}{4F} lnK_i \qquad \text{Equation 8}$$

At the standard state, E_r equals E^0, and the following equation is established for any fuel

$$E^0 = -\frac{\Delta G^0}{zF} = -\frac{\Delta H^0 - T\Delta S^0}{zF} \qquad \text{Equation 9}$$

where ΔG^0 is the standard Gibbs free energy change of the combustion reaction of the fuel, ΔH^0 the standard enthalpy change, ΔS^0 the standard entropy change and z the number of electrons involved in the reaction to convert a single fuel molecule. The maximum energy obtained in this case is given by $-\Delta G^0$ and the ideal thermodynamic efficiency, ε_T, represented by $\Delta G^0/\Delta H^0$. Table 2-1 gives ΔG^0, ΔH^0, E^0 and ε_T for the use of H_2 as fuel.

Table 2-1: Thermodynamic data and efficiency (ε_T) for the hydrogen oxidation reaction

T (K)	ΔG^0 (kJ)	ΔH^0 (kJ)	E^0 (V)	ε_T
1000	-192.5	-247.3	0.997	0.78
1250	-178.2	-249.8	0.924	0.71

However, the respective electrochemical processes in the cell exhibit ohmic losses which arise during the transport of charge carriers in the electrodes and in the electrolyte, where the latter (diffusion losses of the oxygen ions) dominate the ohmic part of the total losses. Additionally, polarization losses evolve during the conversion of electronic current into ionic current. Both the ionic transport in the electrolyte and the electrochemical reaction at

the electrodes are thermally activated; thus, the ohmic and polarization losses increase with decreasing temperature. Due to the losses, the cell voltage $\boldsymbol{U_C}$ always undercuts the Nernst voltage $\boldsymbol{U_N}$:

$$\boldsymbol{U_C = U_N - j_L \cdot \sum_k ASR_k} \qquad \text{Equation 10}$$

with j_L as load current and $\boldsymbol{k}$ the contributing loss portions, which are given by their respective area specific resistance (ASR).

During operation, oxygen molecules are adsorbed, dissociated, and reduced on the cathode surface to ionic oxygen species before incorporated into the lattice as oxygen ions, which then move through the electrolyte to the anode and combine with fuel molecules to form water and carbon monoxide/dioxide (if a hydrocarbon fuel is used). Outside the cell, electrons move from the anode to the cathode through an external circuit, converting chemical energy of the fuel to electrical energy. In Kroger's notation, oxygen reduction on the cathode can be described as follows:

$$\boldsymbol{\frac{1}{2}O_2 + 2e + V_{\ddot{O}} = O_O^X} \qquad \text{Equation 11}$$

At the same time, fuel molecule (e.g., hydrogen) is oxidized on the anode by combining with oxygen ions and release electrons:

$$\boldsymbol{H_2 + O_O^X = H_2O + 2e + V_{\ddot{O}}} \qquad \text{Equation 12}$$

The combination of Eq. 11 and 12 yields the overall reaction of the fuel cell,

$$\boldsymbol{H_2 + \frac{1}{2}O_2 = H_2O} \qquad \text{Equation 13}$$

For practical applications, SOFCs have different structures, and each of them has its own advantages and disadvantages, though the materials for cell components in these different designs are either the same or very similar in nature.

i. Fuel Cell Efficiency

The overall efficiency of an SOFC, ε_{FC}, is the product of the electrochemical efficiency, ε_E, and the heating efficiency, ε_H. The electrochemical efficiency is, in turn, the product of the

thermodynamic efficiency, ε_T, the voltage efficiency, ε_V, and the Faradaic or current efficiency, ε_J, of the fuel cell.

Thus, $$\boldsymbol{\varepsilon_{FC} = \varepsilon_E \cdot \varepsilon_H = \varepsilon_T \cdot \varepsilon_V \cdot \varepsilon_J \cdot \varepsilon_H}$$ Equation 14

The heating efficiency must be considered when the fuel contains inert gases, impurities and other combustibles in addition to the electrochemically active species. Then, the heating value efficiency, ε_H, is defined as:

$$\boldsymbol{\varepsilon_H = \frac{\Delta H^0}{\Delta H_{com}}}$$ Equation 15

where ΔH^0 represents the enthalpy of fuel species available in the fuel cell to generate electricity and ΔH_{com} is the enthalpy included in all combustible species in the fuel gases fed to the fuel cell.

On the other hand, the thermodynamic efficiency is given by the ratio of the free enthalpy change of the cell reaction, ΔG, which may be totally converted to electrical energy and the enthalpy of the reaction. Thus, a fuel cell has an intrinsic (maximum) thermodynamic efficiency expressed as follows.

$$\boldsymbol{\varepsilon_T = \frac{\Delta G}{\Delta H} = 1 - \frac{T\Delta S}{\Delta H}}$$ Equation 16

In an operating SOFC, the cell voltage is always less than the reversible voltage. As the current is drawn from the fuel cell, the cell voltage is reduced due to various losses. The reduction in the cell voltage under current load depends on current density and several factors such as temperature, pressure, gas flow rate, gas combustion and cell material. The voltage efficiency, ε_V, is defined as the ratio of the operating cell voltage under load, E, to the equilibrium cell voltage, E_r, and is given as

$$\boldsymbol{\varepsilon_V = \frac{E}{E_r}}$$ Equation 17

The difference between the operating cell voltage and the expected reversible voltage is termed polarisation or overpotential and is presented as η. The total polarisation of a cell is the sum of four types of polarisation: charge transfer or activation polarisation, η_A, diffusion

or concentration polarisation, η_D, reaction polarisation, η_R, and resistance or ohmic polarisation, η_Ω:

$$\boldsymbol{\eta = \eta_A + \eta_D + \eta_R + \eta_\Omega} \qquad \text{Equation 18}$$

Polarisation cannot be eliminated but can be minimised by material choice and cell design. Temperature, pressure, electrolyte composition and electrode material certainly influence cell polarisation.

Electrochemical reactions involve an energy barrier that must be overcome by reacting species. This energy barrier, called the activation energy, results in activation or charge transfer polarisation, η_A. Activation polarisation is related to current density, i, by the following equation:

$$\boldsymbol{i = i_0\, exp\left(\frac{\beta_a \cdot \eta_A \cdot F}{RT}\right) - i_0 \exp\left(-\frac{\beta_c \eta_A F}{RT}\right)} \qquad \text{Equation 19}$$

Where β is the symmetry coefficient and i_0 is the exchange current density. The symmetry coefficient is considered as the fraction of the change in polarisation which leads to a change in the reaction rate constant. The exchange current density is related to the balanced forward and reverse electrode reaction rates at equilibrium. A high exchange current density means a high electrochemical reaction rate and, in that case, a good fuel cell performance is expected. The exchange current density can be determined experimentally by extrapolating plots of log i versus η to η=0. For large values of η (either negative or positive) one of the bracketed terms in Eq. 19 becomes negligible. After rearranging one obtains

$$\boldsymbol{\eta_A = a \pm b \cdot \log i} \qquad \text{Equation 20}$$

which is usually referred to as the Tafel equation. Parameters a and b are constants which are related to the applied electrode material, type of electrode reaction and temperature

Diffusion or concentration polarisation, η_D, becomes eminent when the electrode reaction is hindered by mass transport effects, i.e., when the supply of reactant and/or the removal of reaction products by diffusion to or from the electrode is slower than that corresponding to the charging/discharging current i. When the electrode process is governed completely by diffusion, the limiting current, i_L, is reached. The limiting current can be calculated from the diffusion coefficient of the reacting species, D, their concentration, c_M, and the thickness of the diffusion layer, δ, by applying Fick's law as follows:

$$i_L = \frac{zFD\Delta c_M}{\delta}$$ Equation 21

For an electrode process free of activation polarisation, the diffusion or concentration polarization can be expressed as

$$\eta_D = \frac{RT}{zF}\ln\left(1 - \frac{i}{i_L}\right)$$ Equation 22

In general, mass transport is a function of temperature, pressure and concentration of the species involved. In SOFC's the reactants must diffuse through the porous anode and cathode, emphasising the importance of the microstructure and design of electrodes.

The reaction polarisation, η_R, appears when the rate of the electrode process is influenced by a chemical reaction. A possible reaction includes the incorporation of oxygen in the oxide sublattice at the cathode.

The ohmic polarisation is caused by the resistance of the conducting ions (through the electrolyte), electrons (through the electrodes and current collectors) and contact resistances between cell components. The ohmic polarisation, η_Ω, is given as

$$\eta_\Omega = iR_i$$ Equation 23

where R_i represents the total ohmic cell resistance, including both ionic and electronic resistances.

With respect to the current efficiency, for 100% conversion of a fuel, the amount of current density, i_F, produced is given by the Faraday's law as:

$$i_F = zF\frac{df}{dt}$$ Equation 24

Where df/dt is the molar flow rate of the fuel. For the amount of fuel actually consumed, the current density produced is given by

$$i_F = zF\left(\frac{df}{dt}\right)_{consumed}$$ Equation 25

The current efficiency, εJ, is the ratio of the actual current produced to the current available from complete electrochemical conversion of the fuel as can be seen next.

$$\varepsilon_J = \frac{i}{i_F}$$ Equation 26

In the case of fuel cells, the current efficiency is commonly expressed as fuel utilization.

2.3 SOFC stack technologies

A wide range of SOFC stack and cell technologies has been developed, differing from each other in terms of:

- Cell materials used.
- Thickness and morphology of cell materials.
- Shape of cells.
- Means and architecture of interconnects.
- Means and architecture of gas flow manifolds.
- Manufacturing methods used for each layer in the cell structure.

These differences can strongly impact the cost of the materials as well as the cost of manufacturing. There is a large number of cell/stack architectures to considerer among tubular and planar configurations, not to mention the range of material combinations and manufacturing methods.

2.3.1 Planar versus tubular configuration

Earlier studies in SOFCs were focused on high temperature tubular SOFC systems; since the late 1990s, accompanied with the reduction of electrolyte thickness in the planar SOFC technology, the development of planar SOFC systems has drawn great interest due to its apparent advantages in power density and the ease of fabrication. However, tubular SOFC is still favorable for portable applications where rapid start-up and cool-down are required.

In SOFC tubular configurations (see Figure 2-3), the electrode (either cathode or anode) is usually made into a long-tube with a porous wall. Outside the electrode tube are the electrolyte and then another electrode. Cells are also connected in series through interconnects. Another example of a tubular-type cell is the transverse stripe type tubular cell. The schematic is shown in the figure below. In this type of cell, the single cells are arranged in series on one tube. Therefore, each tube can be regarded as a small stack. Numerous other tubular designs have been proposed, but are no longer pursued.

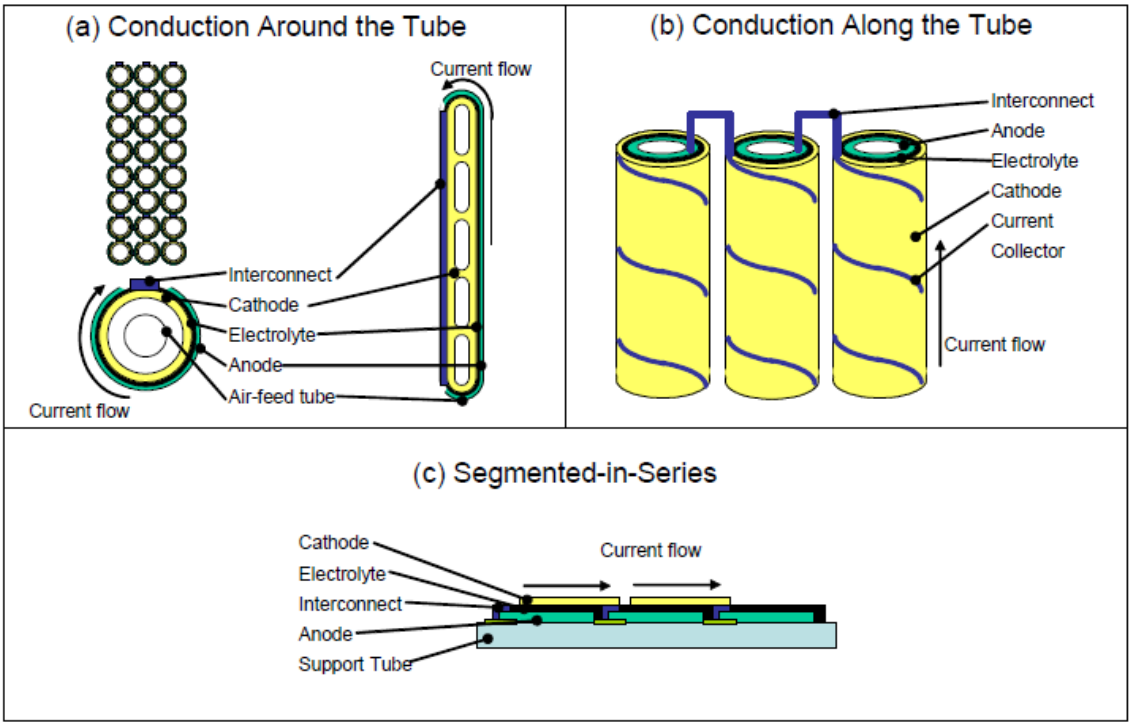

Figure 2-3: Overview of Three Types of Tubular SOFC: a) Conduction around the Tube; b) Conduction along the Tube; c) Segmented in Series [8].

Large- diameter tubular SOFCs have been the most successful so far. Their main advantage is the seal-less stack design; the disadvantages are the low power density, the long start-up times, and the expensive fabrication techniques.

Microtubular SOFCs are especially useful for smaller systems, providing rapid start-up; the reason for this is the small diameter of the cells and the low wall thickness which prevent the build-up of damaging thermal stresses. Start-up in about a minute is possible and leaks can be prevented by bringing the microtubes through the insulation for sealing in the cold zone. On the negative side, cell interconnection and assembly issues are significant, and it seems likely that microtubular systems will mainly be applicable in small systems.

In planar stack SOFCs, each cell is made into a flat disk, square, or rectangular plate. The cells are put in series and connected by the interconnect plates, as schematically shown in Figure 2-5: Schematic for the cross-section of self-supported SOFC.

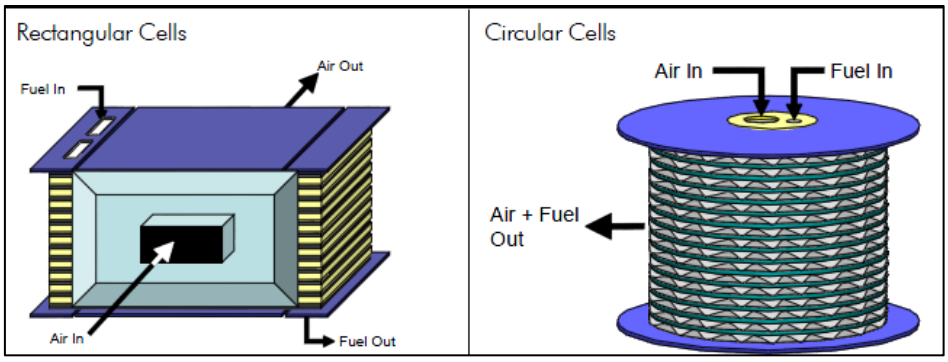

Figure 2-4: Overview of two different SOFC planar stacks designs studied by the National Energy Technology Laboratory /U.S. DOE [9]

Planar SOFCs employ the same materials for the single cell as other cell designs. The most common cell materials are yttria-stabilised zirconia (YSZ) for the electrolyte, lanthanum strontium manganite (LSM) for the cathode and nickel/zirconia cermet (Ni/YSZ) for the anode. The planar cells can be broadly classified into two categories: self-supporting and external supporting. In the self-supporting configuration, one of the cell components (often the thickest layer) acts as the cell structural support. Thus, single cells can be designed as electrolyte supported, anode supported, or cathode supported. In the external-supporting configuration, the single cell is configured as thin layers on the interconnect or a porous substrate. The key features of each configuration are summarised Table 2-2.

- Self-supporting: where one of the cell components (often the thickest layer) acts as the cell structural support. Thus, the single cell can be designed as electrolyte, anode or cathode supported, as schematically shown in Figure 2-5. This figures also reports that the anode-supported is the best choice from the polarization standpoint.

    - *Electrolyte-supported*. Early planar cells were mostly electrolyte-supported. This requires a relatively thick electrolyte (>100 but typically around 200 µm, with both electrodes at about 50 µm) which leads to high resistance, requiring high-temperature operation (about 900-1000°C) to minimise electrolyte ohmic losses.

    - *Cathode-supported. This allows for a thinner electrolyte than electrolyte*-supported cells, but mass transport limitations (high concentration polarization) and manufacturing challenges (it is difficult to achieve full density in a YSZ electrolyte

without oversintering an LSM cathode) make this approach inferior to anode-supported thin-electrolyte cells.

- *Anode-Supported*. Advances in manufacturing techniques have allowed the production of anode-supported cells (supporting anode of 0.5 to 1 mm thick) with thin electrolytes. Electrolyte thicknesses for such cells typically range from around 3 to 15 μm (thermomechanically, the limit in thickness is about 20 to 30 μm). The cathode remains around 50 μm thick, given the difference in thermal expansion between the anode and the electrolyte). Such cells provide potential for very high power densities (up to 1.8 W/cm^2 under laboratory conditions, and about 600 to 800 mW/cm^2 under commercially-relevant conditions) [8].

  For cell configurations with thin (5-20 μm) YSZ electrolytes, the cell can operate at reduced temperatures (< 800°C). The advantages of reduced-temperature operation for the SOFC include a wider choice of materials (especially low-cost metallic materials for the interconnect), longer cell life, reduced thermal stress, improved reliability, and potentially reduced cell cost. The main disadvantages are potential slow electrode reaction kinetics (thus high polarisations) and the reduced thermal energy that can be extracted from the hot exhaust stream by a turbine or a heat exchanger.

- External supporting: the single cell is configured as thin layers on the interconnect or a porous substrate.

  - Metal Interconnect-supported. This configuration minimizes mass transfer resistance and the use of (expensive) ceramic materials. In such cells, the electrodes are typically 50 μm thick and the electrolyte around 5 to15 μm. While the benefits are obvious, the challenges are to find a materials combination and manufacturing process that avoids corrosion and deformation of the metal and interfacial reactions during manufacturing as well as operation.

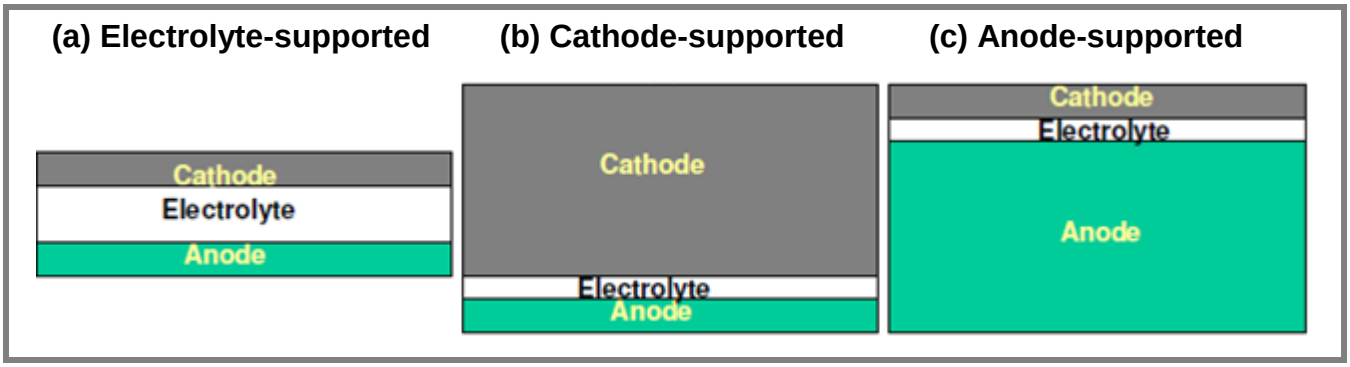

Lowest Performance	Intermediate Performance	Highest Performance
Cathode: ~50 µm Anode: ~50 µm Electrolyte: ~150 µm	Cathode: ~2000 µm Anode: ~50 µm Electrolyte: ~20 µm	Cathode: ~50 µm Anode: ~500-1000 µm Electrolyte: ~10 µm
1) High ohmic contribution 2) Low cathode concentration polarization 3) Low anode concentration polarization	1) Low ohmic contribution 2) High cathode concentration polarization 3) Low anode concentration polarization	1) Low ohmic contribution 2) Moderate anode concentration polarization 3) Low cathode concentration polarization

Figure 2-5: Schematic for the cross-section of self-supported SOFC.

Table 2-2: Features of different designs of planar single cell [8].

	Cell configuration	Advantage	Disadvantage
Self-supporting	**Electrolyte Supported**	- Relatively strong structural support from dense electrolyte. - Less susceptible to failure due to anode re-oxidation.	- Higher resistance due to lower electrolyte conductivity. - Higher operating temperatures required to minimise ohmic loses.
	Anode Supported	- Highly conductive anode. - Lower operating temperature via use of thin electrolyte.	- Mass transport limitations due to thick anodes. - Potential anode re-oxidation
	Cathode Supported	- No oxidation issues. - Lower operating temperature via use of thin electrolyte.	- Lower conductivity. - Mass transport limitation due to thick cathodes
External supporting	**Interconnect supported**	- Thin cell components for lower temperature. - Stronger structures from metallic interconnects.	- Interconnect oxidation. - Flowfield design limitations due to cell support requirement.
	Porous substrate	- Thin cell components for lower operating temperature. - Potential for use of non-cell material for support to improve properties.	- Increased complexity due to addition of new materials. - Potential electrical shorts with porous metallic substrate due to uneven surface.

More recently, planar SOFC systems with high power densities operating at lower temperatures (650 to 850 °C instead of 900 to 1000 °C as was previously the norm) have been developed. Combined with the ability of SOFC to use conventional fossil fuels, this could help reduce the cost of the fuel cell because less-expensive materials of construction could be used at lower temperatures. This would improve the economy of applications ranging from small-scale stationary power (down to ~2 kW) to auxiliary power units for vehicles and mobile generators for civilian as well as military applications. There is even the possibility that SOFC could eventually be used for part of the prime power in vehicles. The present challenge for developers is to produce robust, high-performance stack technologies based on suitable low-cost materials and fabrication methods. Derivatives from SOFC technology, such as oxygen sensors used in automobiles, are already in widespread commercial use.

Planar SOFCs provide very high areal (W/cm2) and volumetric (W/cm3) power densities and can be manufactured by low-cost conventional ceramic processing techniques; however, sealing around the edges of the cells and the control of temperature gradients which can cause cell cracking remain issues to be resolved.
To summarize, a comparison between the main features of planar and tubular structures of SOFC is presented in Table 2-3.

Table 2-3: Comparison of main features for planar an tubular structure for solid oxide fuel cells [10]

	Planar	***Tubular***
Power per unit area	Higher	Lower
Power per unit volume	Higher	Lower
Ease of fabrication	Easier	Difficult
Cost of fabrication	Higher	Lower
Ease of sealing	Difficult	Easy
Long-term stability	Fair	Excellent
Thermo-cycling stability	Fair	Good

2.3.2 Gas Flow configuration in Planar SOFC

The most important design feature of the Planar SOFC relates to gas flow configuration and gas manifolding which can be arranged in several ways.

- *Gas flow configurations*. Fuel and oxidant flows in planar SOFCs can be arranged to be cross-flow, co-flow, or counter-flow. The selection of a particular flow configuration has significant effects on temperature and current distribution within the stack, depending on the precise stack design. Various flow patterns can be implemented in the different flow configurations including Z-flow, serpentine, radial, and spiral patterns (see
- Figure 2-6). Flow fields (flow channels) are used in planar SOFCs to increase uniformity of gas distribution and to promote heat and mass transport in each cell. In addition, the flow field is often designed to have sufficient pressure drop through the cell to promote cell-to-cell flow uniformity within the stack. Thus, defining the flow field for both fuel and oxidant flows is an important aspect in designing planar SOFCs. For a specific design, the shape and arrangement of the flowfield can be varied to improve/optimise stack design. Figure 2-7 shows two examples of flowfield design used in planar SOFCs [10]. Flowfields are commonly designed as part of the interconnect although certain planar designs include the flowfield in the electrodes. Since the flowfield electrically connects the interconnect and the electrodes, contact area (between the flowfield and the electrodes) must be considered in the design to minimise contact resistance losses.

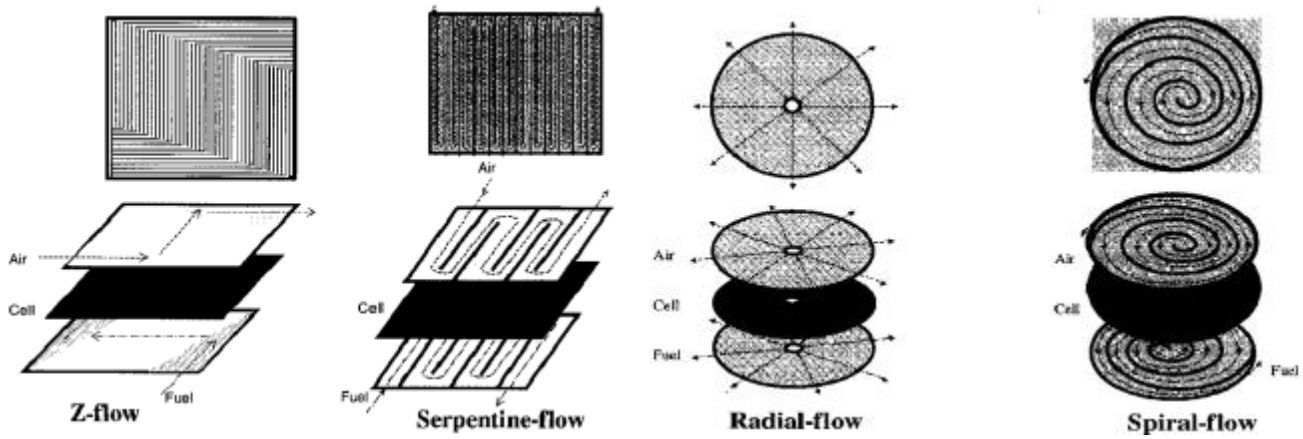

Figure 2-6: Flow patterns in planar SOFCs [11]

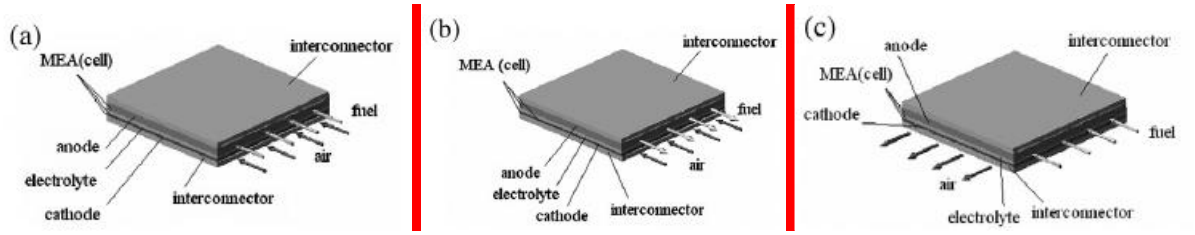

Figure 2-7: Sketch for flow configurations; (a) co-flow; (b) counter-flow; (c) crossflow. [12]

- *Gas manifolding.* Any stack design must include gas manifolds for routing gases from a common supply point to each cell and removing unreacted gases and reaction products. Gas manifolds can be classified as external or integral. External manifolds are constructed separately from the cell or interconnect component of the stack. Figure 2-8 is an external manifold concept for crossflow planar SOFCs. Integral manifolds are formed and designed as part of the cell or interconnect and one example is found in Figure 2-9. Depending on the design, gas manifolds often require sealing to prevent gas leakage or crossover. The manifold seal is insulating to prevent cell-to-cell electrical shorts. In principle, the manifold must be designed to have low pressure drop (relative to individual cell pressure drop) to provide uniform flow distribution to the stack.

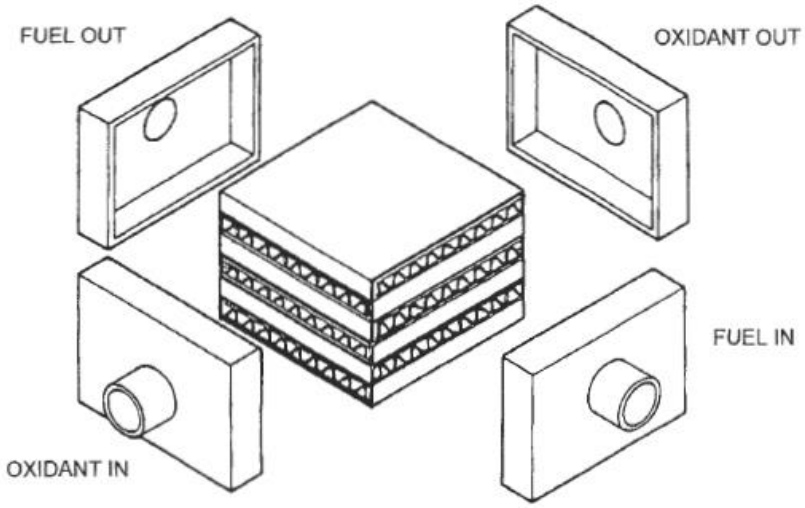

Figure 2-8: Examples of external manifold

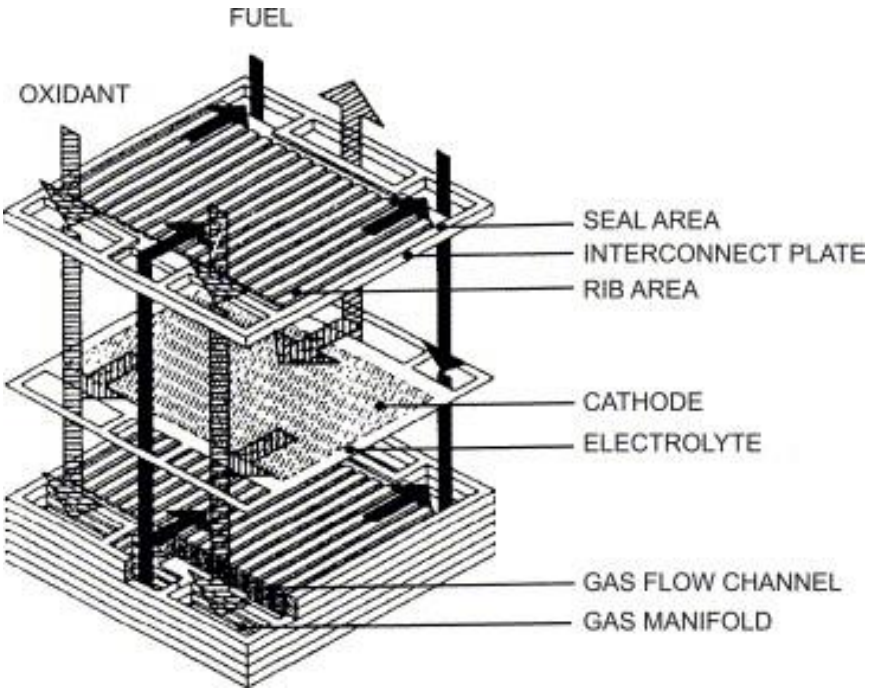

Figure 2-9: Example of integral manifolds.

2.4 Technical requirements of planar SOFCs and components for stack building

The major components of an individual SOFC cell include the electrolyte, the cathode, and the anode. Fuel cell stacks contain an electrical interconnect, which links individual cells together in series or parallel. The electrolyte is made from a ceramic such as yttria-stabilized zirconia (YSZ) and functions as a conductor of oxide ions. Oxygen atoms are reduced into oxide ions on the porous cathode surface by electrons, and then flow through the ceramic electrolyte to the fuel rich porous anode where the oxide ions react with fuel (hydrogen), giving up electrons. The interconnect serves to conduct the electrons through an external circuit.

In this section, the requirements of planar SOFC design, the characteristics that the leading candidate materials possess with particular attention in the stack components (metallic interconnectors, sealing materials and protective coatings) are discussed.

2.4.1 Key requirements for planar SOFC design

Advances in ceramic technology, especially in synthesising fine powders, engineering material compositions, tailoring composition/property/microstructure relationships, and fabricating/processing intricate structures, have contributed to the increased interest in planar SOFCs since early 1980s. Significant progress has now been made on the demonstration of fabricability, performance, and operation of planar SOFCs.

A planar SOFC, like any other cell configuration, must be designed to have the desired electrical and electrochemical performance, along with required thermal management and mechanical/structural integrity to meet operating requirements of specified power generation applications. The key requirements are briefly discussed as follow and they are summarised in Table 2-4.

- Electrical performance. It means that the design must minimise ohmic losses in the stack. Thus, the current path in the components (especially those having low electrical conductivity) must be designed to be as short as possible. There must be good electrical contact and sufficient contact area between the components. The current collector must also be designed to facilitate current distribution and flow in the stack.
- Electrochemical performance. The stack design must provide for full open circuit voltages and minimal polarisation losses. Thus, any significant gas leakage or cross-leakage and electrical short must be avoided. Fuel and oxidant must be distributed uniformly not only across the area of each cell but also to each cell of the stack. The gases must be able to quickly reach the reaction sites to reduce mass transport limitation.
- Thermal management. This requirement means that the design must provide stack cooling and more uniform temperature distribution during operation. The design must permit the highest possible temperature gradient across the stack.
- Mechanical/structural integrity. Any planar SOFC stack must be designed to have adequate mechanical strength for assembly and handling. Thus, mechanical and thermal stresses must be kept to minimum to prevent cracking, delamination, or detachment of the components under the variety of operating conditions the stack is expected to experience (e.g., normal operating temperature gradients, off-design temperature gradients, thermal shock

conditions such as sudden power change and cold start-up, and mechanical loading expected during installation, moving, and vibration loading).

Table 2-4: Design requirements for planar SOFC design [11]

	Property requirement	Design target
Electrical performance	Minimal ohmic loss	Short current path Good electrical contact and sufficient contact area. Current collector design for uniform and short current path.
Electrochemical performance	Full open circuit voltage Low polarisation loss	Insignificant gas leakage or cross-leakage (no or minimal sealing). No electrical short. Uniform gas distribution between cells and across cells. Easy gas access to reaction sites.
Thermal management	Cooling and uniform temperature distribution. Highest possible temperature gradient across stack.	Simple and efficient means for cooling. Appropriate gas flow configuration. Design to withstand thermal stress.
Mechanical/structural integrity	Mechanical strength for assembly and handling.	Minimal mechanical stress.

2.4.2 Cell and Stack Performance

Planar SOFCs of various sizes have been fabricated and operated under various conditions. Single cells have been shown to have extraordinarily high areal power densities. For example, power densities of up to 1.8 W/cm^2 at 800°C and 0.8 W/cm^2 at 650°C have been obtained for anode-supported planar cells with hydrogen fuel and air oxidant [13].

The planar cell design offers high power density but currently has a number of significant issues such as requiring high-temperature gas seals at the edges of the cell components to isolate oxidant from fuel. Difficulties in successfully developing such high-temperature seals have slowed the development and use of planar design cells for SOFC generators.

However, SOFC stacks in 1-25 kW size utilising planar cells are now beginning to be designed, fabricated, and electrically tested.

2.4.3 Interconnect materials

Two roles of the interconnect in high-temperature solid oxide fuel cells (SOFCs) are the electrical connection between cells and the gas separation within the cell stack. The fact that the interconnect must be compatible with all of the cell components as well as be stable with respect to both oxidising and reducing gases places very stringent materials requirements on it. These requirements plus the additional constraints of cost and ease of fabrication tend to limit the possible choices to only a few materials. These materials come from either perovskite-type oxide ceramics based on rare earth chromites for operating temperatures in the 900-1000°C range or metallic alloys for lower temperature cell operation.

The properties which an interconnect must possess are rather extensive and somewhat dependent upon the particular SOFC configuration. However, typical requirements are:

- High electronic conductivity with low ionic conductivity
- Chemical stability in both fuel and air
- Thermal expansion match to other cell components
- High mechanical strength
- High thermal conductivity
- Chemical stability with regard to other cell components

Depending upon the particular SOFC design, additional requirements such as the ease of fabrication to gas-tight density, the ability to make gas-tight seals with other cell components, and the material cost also play an important role.

In order to meet all these requirements, two classes of materials are commonly used for interconnects, namely ceramic and metallic materials.

The first three requirements listed above are crucial and tend to eliminate most candidate materials. In fact, for operation at temperatures above 800°C, the only oxides that fit these criteria are the doped rare earth chromites.

In particular, compositions from the system (La,Sr,Ca)(Cr,Mg)O_3 are the leading interconnect materials. However, due to the electrical conductivity required, lanthanum chromites cannot be used at temperatures lower than 800 °C. In addition, lanthanum chromites show undesirable swelling in reducing atmospheres caused by the reduction of Cr^{4+} ions to Cr^{3+} and the formation of oxygen vacancies [14] leading to strong internal stresses and possible cracking during operation. Nevertheless, compositions from the system (Y,Ca)CrO_3 also have acceptable properties. These rare earth chromites satisfy most of the requirements, but have problems in fabrication and have high cost.

Apart from these physical handicaps, costs are high for the $LaCrO_3$ and for the processing of the layers. Hence, the advantages of metallic interconnects are obvious: high electrical conductivity, good ability for processing and lower costs. The disadvantages, however, are corrosion in combination with increasing resistance during operation, chromium evaporation and unsatisfactory high-temperature strength.

The long-term stability of the metallic interconnect is essentially governed by the corrosion characteristics. The materials used for interconnects are alloys which form chromium oxide, thus ensuring sufficiently high conductivity for thin oxide scales. Meanwhile, several ferritic steels have been developed especially for SOFC application containing only very small amounts of aluminium and silicon to avoid the formation of highly resistive oxide scales and low amounts of manganese for the formation of $(Cr,Mn)_3O_4$ spinels as the outer corrosion scale [15, 16].

The main focus in interconnect development is still the improvement of corrosion behaviour, but also the reduction of the contact resistance of the oxide scales or in combination with coatings and the reduction of chromium evaporation to avoid a detrimental poisoning of the cathode with chromium species [17, 18]. All these phenomena make a major contribution to the observed degradation of stack voltage during operation, although it is not yet clarified to what extent.

The interconnects can be fabricated by machining, pressing or, in the case of powder metallurgical alloys, by near-net-shape sintering. The gas distribution is usually realised by parallel channels whilst the ridges separating the channels serve as electrical contact with the electrodes. An example of these channels was observed previously in Figure 2-7. A bipolar interconnect plate is shown in Figure 2-10, which serves several functions: a) gas barrier between anode and cathode; b) electrical connector between anode and cathode

(series); distribution of fuel and oxidant (flow field). A bipolar interconnector also must meet several requirements [19] as follows:

- Impermeability.
- Mechanical strength.
- Flatness and dimensional tolerance.
- Electrical bulk conductivity.
- Contact resistance.
- Pressure drop (flow field design).
- Manufacturability.
- Material stability.
- Cost.

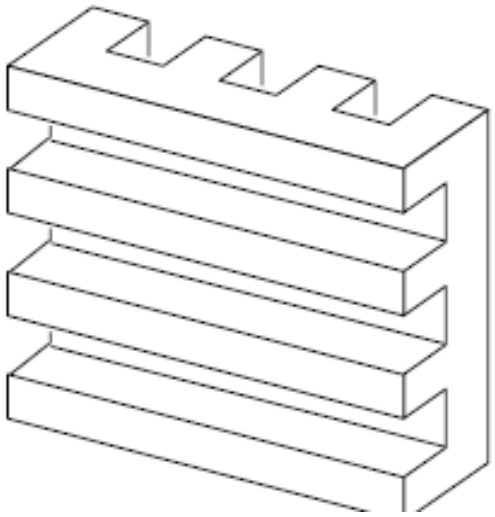

Figure 2-10: Interconnect design for cross-flow bipolar.

Recently, a high temperature ferritic stainless steel known commercially as Crofer ® APU 22 has been used in an extensive way for the interconnection of planar anode-supported cells. This alloy was especially developed for SOFC application. At temperatures up to 900°C a chromium-manganese oxide layer is formed on the surface of Crofer ® 22APU which is thermodynamically very stable and possesses high electrical conductivity.

The low coefficient of thermal expansion is matched to that ceramics typically used for high temperature fuel cells in the range from room temperature to 900°C. However, the high chrome content of this alloy (see Table 2-5) results in a relatively high materials cost (around 30 €/kg) and lead to poisoning the cathode with chromium leading to its deposition at the three phase (LSM/YSZ/gas) boundary and causing rapid de-activation of the cathode.

Table 2-5: Crofer ® 22APU chemical composition (%wt) *[from material data sheet, May 2010 by ThyssenKrupp VDM]*

	Cr	Fe	C	Mn	Si	Cu	Al	S	P	Ti	La
Min.	20.0	Bal.		0.30						0.03	0.04
Max	24.0		0.03	0.80	0.50	0.50	0.50	0.020	0.050	0.20	0.20

2.4.4 Protective and contact coatings

Many attempts have been made to reduce the damaging effect of chromium vapours on the cathode side by suitable protective layers. The first approach was plasma-sprayed coatings of lanthanum chromite as a protective method to minimise the evaporation of volatile Cr species [20]. The function of these coatings as diffusion barriers against volatile Cr species strongly depends on the quality of the layers (gas tightness, crack density) and may not always be as effective as expected. In addition, for anode-supported cells, the plasma-sprayed chromite coatings are characterized by high contact resistances and high fabrication costs in comparison to ceramic methods using slurries or pastes. However, the reactivity of lanthanum chromite with metals, either with Cr- or Fe-based alloys, is low and the metal/ceramic interface is very stable under operating conditions.

Chemical interactions between coatings and interconnect material increase when the alkaline earth content in the ceramic is increased. Often perovskite materials have been brought in contact with Cr-based alloys or steels and the formation of chromates (e.g. $CaCrO_4$ or $SrCrO_4$) was observed [21, 22] leading to the progressive decomposition of the perovskite material and a brittle interface. As a consequence of these interactions, the application of cobalt oxide or cobalt manganese spinel between the perovskite and alloy was investigated [23,24] and showed stable contact resistance over time.

Coating the ferritic steel Crofer22APU by wet powder spraying with a porous Co_3O_4 layer or a metallic Co layer leads to the formation of a new dense Cr-free reactive layer under SOFC operating conditions [25]. As a reaction product of Mn from the oxide scale of the steel and the Co_3O_4 layer, this dense layer may act as a barrier against the vapour phase transport of volatile Cr species.

Contact materials are electrically conductive ceramics applied to improve the contact between interconnect and electrode. Whereas for the anode side metallic materials are

used (as mesh, foam or paste), the cathode side is often coated with ceramic cathode-like compositions having conductivities in the range of 50–500 S/cm. Because there are no electrochemical requirements to be obeyed for the contact materials, they can vary significantly from the electrode materials and be optimised with regard to other physical and chemical properties than the electrodes. Apart from the electrical conductivity, the most important properties are the thermal expansion and sintering behaviour at assembling temperatures in the range of 800–1100°C. Because the contact layer thickness may vary between 30 and 200 µm and ceramic materials heat treated below 1000°C are usually very porous, the specific conductivity of the material should be high. This is, in fact, the case for lanthanum cobaltites which have specific conductivities up to 1700 S/cm [26]. In contrast, the thermal expansion of these cobaltites has a strong mismatch with the other cell components. For electrically conductive ceramics, therefore, a compromise between acceptable conductivity and tolerable mismatch in thermal expansion has to be made as for the cathode materials.

2.4.5 Sealing materials

The challenges of sealing the oxidant from fuel in planar SOFC stacks is significant. The function of SOFC seals includes:

- Prevent mixing of fuel and oxidant.
- Prevent mixing of reactants with the ambient environment.
- Provide mechanical bonding of components.
- Provide electrical insulation between stack components.

Planar designs typically require multiple seals per repeat unit, and even in planar designs the length of the seals can vary by two or three orders of magnitude for a given area cell depending on design. A number of possible seal types is shown in Figure 2-11 for a rectangular planar cell with metal interconnects.

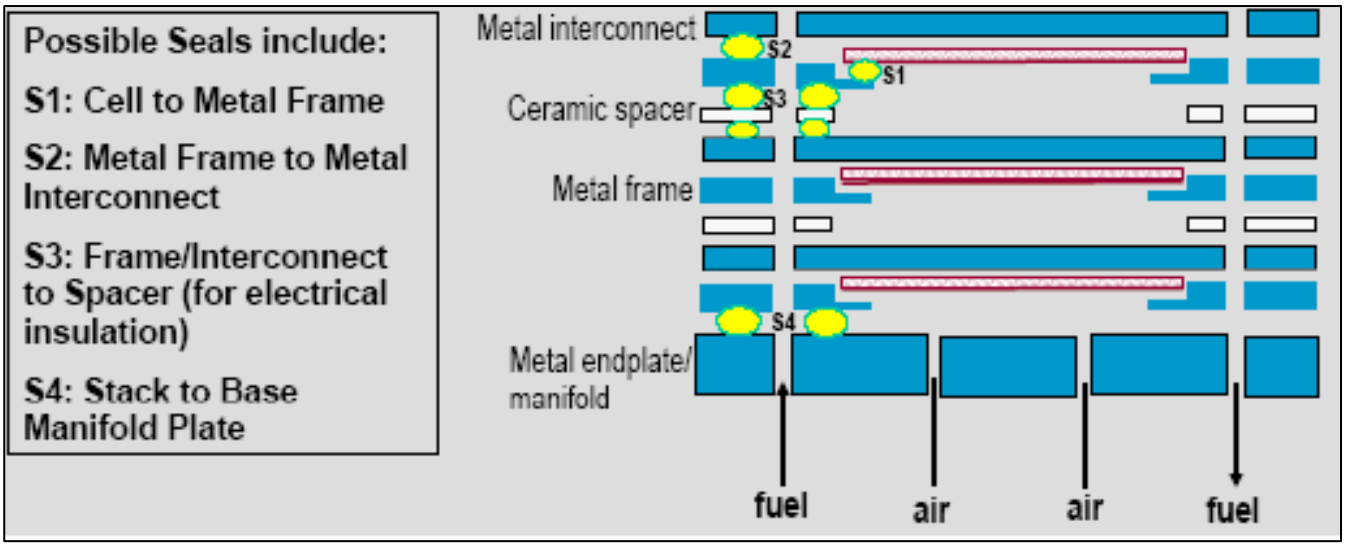

Figure 2-11: Possible Seal Types in a Planar SOFC [8]

The requirements, material choices, and general sealing concepts are common to most planar SOFC stack designs. Fundamentally, two different types of seals are being developed for SOFC: bonded and compressive seals.

Bonded Seals

Bonded seals can be rigid or compliant. A hermetic seal is achieved through adhesive forces between the seal material and both surfaces against which the seal is to work. The seal material must have good adhesive properties (good wettability of the material to be sealed).

Some are designed to remain flexible over the operating range of the cell, while others are meant to be rigid. To use the rigid type of seal, the thermal expansion coefficient of the seal material and all other components must be closely matched. If the seal is compliant, the thermal expansion coefficient matching requirements are somewhat relaxed. The bonding temperature for this type of seal should lie between the operating temperature and the stability limit for the other cell materials. There are several common sub-types of bonded seals currently under consideration for SOFC applications. Glass and glass-ceramic seals are perhaps the most common. This type of seal is attractive because:

- Viscous/wetting behavior of glass facilitates hermetic sealing.
- They are inexpensive and easy to manufacture and apply.

- Wide range of compositions of glass and ceramics allows tailoring some of the key properties (e.g. thermal expansion coefficient glass transition temperature).
- Glass-ceramics can be designed to avoid viscous flow and uncontrolled progressive crystallization during operation.

However, glass-ceramic seals also exhibit disadvantages:

- They are brittle, leading to seal and even cell failures during cool-down;
- Despite control, few glass systems allow a match of thermal expansion coefficient to other important cell materials (typically alkaline earth-alumina-silica glasses). In any case, the cell materials do not match each other close enough to allow a rigid seal in larger cells.
- Many glasses interact with adjacent cell components, especially with the interconnects.
- Some of the constituents of glass volatilize during operation (e.g. silica, borate, and alkali metals). These constituents will likely foul or poison the electrode catalyst or interact in an undesirable manner with other cell components.

Metal brazes, which use a molten metal filler to ensure sealing, provide some attractive features:

- Molten metal facilitates hermetic sealing.
- Easy to fabricate.
- Properties can be tailored by judicious choice of composition.

However, several factors limit their application in SOFC:

- Brazes are electrically conductive, making them unsuitable of most seal types.
- Few braze materials are compatible with SOFC operating conditions. Noble metals are considered too expensive in most SOFC stack designs. Silver is less expensive, but its use in a dual (oxidizing and reducing) environment can lead to chemical instability.

In addition to the benefits listed above, bonded seals result in compact structures, as no load- frame or other means to apply pressure is required. However, in cells with metal interconnects, the mismatch in thermal expansion may be too great for the use of rigid seals.

As mentioned before, glass or glass ceramics are frequently applied for joining metals, especially the joining of steels [27]. Many of these products are available commercially, but most of the sealing products are produced for low-temperature joining and for room temperature applications. However, no commercial product fulfills the requirements of a thermal expansion coefficient in the range of 10–13 x 10^{-6} K^{-1} up to high temperatures. Therefore, many SOFC developers started their own sealing development.

Compressive Seals

A hermetic seal is achieved by pressing the seal material between the surfaces to be sealed. The seal material must be elastic over the operating temperature range, and sufficiently soft to fill the micro-roughness on the surfaces to be sealed. Compressive seals offer several advantages:

- Mechanically “de-couple” adjacent stack components, thus reducing thermal stress during cycling.
- Thermal expansion matching requirements between cell components may be somewhat relaxed (though electrical contact considerations may still require this)
- Some are easy and inexpensive to fabricate.

However, there are also barriers to overcome:

- Difficult to achieve a hermetic seal with some materials unless “soft seat” interlayer is provided.
- Few materials and structures are compliant and provide a hermetic seal at the operating temperatures.
- A load frame is required to provide compression to all seals. This type of hardware is potentially bulky and expensive. If (portions of the) load frame must be kept at lower temperatures than the stack itself, packaging and insulation is significantly

complicated, especially if multiple stacks are to be combined for larger-capacity systems.

- Other stack components must be designed to withstand prolonged pressure. This can be a challenge, given that creep strength of the metals used in the interconnect is typically very low (in the 700 to 800 °C operating temperature range typical for state-of-the-art planar cells).
- To the extent that electrical contact between cell components depends on controlled pressure, balancing these pressure requirements with those of the seal can be a challenge for the cell designer.

Recently, mica and hybrid mica seals have been developed as a viable technology. Mica seals were found to have many desirable characteristics, such as the ability to withstand thermal cycling, but exhibited unacceptable leak rates. When a thin layer of glass is inserted on either side of the seal to fill the voids between the seal and the other stack components, the leak rate was substantially reduced while other desirable properties were retained.

2.4.6 Summary

The research work on solid oxide fuel cells is mainly based on their characterization according to theoretical thermodynamics and electrochemistry, fundamentals and suitability of materials, fuel issues, experimental measurements on single cells and stacks degradation mechanisms and demonstration projects. The design of single cell units is an interesting challenge concerning the issues of lowering costs (lower operating temperatures, minimize expensive materials), increasing performance (higher conductivity electrolyte, more active electrodes, reduction of leakages), durability (lower operating temperatures, better seals, improved current collection); and robustness (metal-supported, oxidation-tolerant anodes) [28,29,30]. Concerning the issue of fuels for SOFCs, efforts are devoted to measure current-voltage characteristics of cells with various feedstocks, the effect of sulphur poisoning of anodes, design of the thermal management and control of systems [31]. Many works are focused in the characterization of SOFCs short stacks with the aim of investigate reliable measurement procedures of performance of single cell units

and stack, possible scale-up problems during multi-cell stacking, practical viability of the stack and stack components via log-term operation and thermal cycling tests, performance dependence upon fuel and air flow, pointing both to flow homogeneity between cells in a stack and flow distribution within a repeating unit [32].

An extensive simulation activity can be found in open literature. Several models approach the simulation of SOFC systems, computational fluid-dynamic of single cell units and stacks; a promising approach is represented by mesoscopic models (Lattice Boltzmann methods- LBMs) [33, 34].

Furthermore, one of the major challenges for implementation of SOFC (planar configuration) is the development of suitable sealant material to separate the air and the fuel. The seals must be stable in a wide range of oxygen partial pressure (air and fuel) and be chemically compatible with other fuel cell components, while minimizing thermal stresses during high temperature operation [35, 36].

Glasses and glass-ceramics, in principle, meet most of the requirements of an ideal sealant by choosing suitably the components of the glasses and their proportion [37]. Glass ceramics, which can be prepared by controlled sintering and crystallization of glasses, possess superior mechanical properties and higher viscosity at the SOFC operating temperature. To develop a suitable glass-ceramic sealant, it is therefore necessary to understand the crystallization kinetics both from the point of view of its sealing properties and of its chemical interactions when in contact with other components of the cell. For example, barium aluminosilicate sealants showed a high reactivity with the metallic interconnect [38], while phosphate and borate glasses are not sufficient stable in the humidified fuel gas environment.

One of the keys to commercialisation of SOFC-based power generation systems is a major reduction in costs of the SOFC stack. It is now widely accepted that planar cell and stack configurations offer the best prospect for commercially viable SOFC systems. Such geometries offer high power densities and the potential for low-cost production of the cell and stack components; for example the cells could be produced by conventional, mass-production processes such as tape-casting.

The development of planar SOFC technology has been the subject of worldwide programmes for more than ten years and considerable progress has been made in improving cell performance and in gaining a greater understanding of the underlying materials and design issues. However, there have been few demonstrations of planar SOFC stack technology at a significant scale due to the difficulties in achieving a sealed and mechanically robust design and problems with the stability of the materials in the stack operating environment.

At this stage the most viable route for lowering stack operating temperatures is to use the anode as the structural support for a very thin electrolyte (~10 µm). The concomitant reduction in electrolyte resistance removes a major barrier to efficient operation of the SOFC stack at temperatures below 800°C. There may also be benefits in improved mechanical robustness of the anode- supported cells compared to electrolyte-supported cells. Given these potential advantages, anode-supported cells technology is currently the subject of development programmes at a number of companies and research institutes around the world.

Reducing the stack operating temperature is one way to reduce degradation rates and potentially to allow the use of lower cost materials in the stack and system. This would be particularly attractive if it allowed the stack interconnect plate to be produced from ferritic stainless steel or similar low- cost metal. To date, planar SOFC technology development has mainly focused on cells in which the structural member is the electrolyte, which needs to be at least 100 µm in thickness in order to retain the mechanical integrity of the cell. With the conventionally used electrolyte materials (generally, yttria- stabilised zirconia or YSZ) this dictates that the cells should operate at temperatures above about 850°C in order to keep the electrolyte resistance to acceptable levels. This restricts the materials choice for the interconnect plate to expensive alloys or electronically conducting ceramics.

High stack operating temperatures also add to overall system costs since this requires that the surrounding system components such as afterburners and heat exchangers are also produced from expensive, heat resistant materials. However, as long as the SOFC stack operating temperature does not fall significantly below 700°C, sufficient heat should still be available to allow steam reforming of the fuel and therefore maintain high system efficiency.

Two principal routes for reducing the operating temperature of the planar stack can be considered. One route is to replace the conventional materials with those having better electrical and catalytic performance at lower temperature. This applies to replacement of the YSZ electrolyte with a material of inherently higher oxygen ion conductivity as well as employing improved electrode materials. New materials are being investigated but limitations such as mechanical strength and chemical stability are still being addressed and they will not realistically be available for use in stacks for some years.

e. Goals and importance of SOFC Development

Solid Oxide Fuel Cells have the potential to become a major source of electrical energy in the coming decades. They combine very high electrical efficiency (in the range 45-60%) with extremely low emissions of major local air pollutants (CO, NO_x and unburned hydrocarbons). They can potentially be operated on a range of fuels, including pipeline natural gas and bio-mass, without a significant loss of efficiency or increase in system complexity and cost. Being essentially modular, SOFC systems will be highly attractive for the distributed power market where units can be sized and configured to meet a particular local power generation demand.

Efficiency and long-term stability are the two main goals of SOFC development, particularly with regard to new applications. Besides commercially available stationary systems, mobile applications like auxiliary power units (APU) [39, 40] or µ-SOFCs [41] as battery replacement are of increasing interest. In the course of that, the operating temperature of the systems need to be reduced from 800 °C ≤ T ≤ 1000 °C to T ≤ 750 °C for APU application and to T ≤ 600 °C for µ-SOFC application. In general, a reduction of the operating temperature offers advantages and bears drawbacks. The material requirements of the system and developing costs are reduced substantially for intermediate-temperature SOFCs (IT-SOFCs) at 500 °C ≤ T ≤ 750 °C. For example, the bipolar plate facilitating the electrical contacting of the fuel cells and providing the supply of the gaseous fuels can be made of highly alloyed ferritic steel as opposed to ceramic interconnects at operating temperatures below 800 °C, which makes the production of the plate suitable for a cheap mass production. Additionally, decreasing operating temperature leads to increased long-term stability and simplified thermal management of the SOFC system. On the other hand, the thermally activated transport processes in solid oxide fuel

cells decrease in principle with decreasing operating temperature entailing an increase of ohmic (predominantly electrolyte based) and electrode polarization losses and thereby causing a decrease of SOFC efficiency. However, the increase of power density is a central approach in world-wide SOFC research [42] to further the competitiveness to existing energy systems. Therefore, the development of highly efficient electrolytes and catalytically effective electrodes at 500 °C ≤ T ≤ 750 °C is of decisive relevance.

On the electrolyte-site the first step to meet these demands was the introduction of thin-film electrolytes (thickness t ≈ 10 µm) in anode-supported cells (ASC), which are able to significantly reduce the portion of ohmic losses in comparison to electrolyte-supported cells (ESC, t ≈ 150 µm). Besides geometrical optimization, two approaches for higher oxygen-ion conduction of the electrolyte itself are pursued: a) the development of new materials (e.g. doped lanthanum gallate, (La,Sr)(Ga,Mg)O3-δ, LSGM [43]) with high oxygen-diffusion properties and b) the usage of a tailored microstructure of the electrolyte taking advantage of potential grain-size effects.

For the development of high-performance cathodes, the following requirements have been stipulated [44]: beneficial chemical diffusion and oxygen-exchange properties of the cathode material (I), adjusted coefficients of thermal expansion (TEC) (II) and chemical compatibility (III) between cathode and substrate and a tailored microstructure (IV).

Some of these requirements have already been fulfilled: Mixed ionic-electronic conducting (MIEC) iron- and cobalt-containing perovskites from the (La,Sr)(Co,Fe)$O_{3-\delta}$ (LSCF) material group are already known for their high oxygen permeability (I) [45] and high electrocatalytic activity [46, 47]. These MIEC materials significantly enlarge the area where the oxygen reduction can take place and thereby provide lower cathode polarization losses compared to solely electronic conducting cathode materials like (La,Sr)(Mn)$O_{3-\delta}$ (LSM). The TEC of the cathode (II) is usually adjusted by the stoichiometry on the B-site (Co, Fe) [48]; the chemical compatibility (III) is ensured by the introduction of a ceria-based interlayer between cathode and electrolyte [49]. The role of the microstructure (IV), however, is still unclear.

SOFC stack development & assembly

The research carried out in this PhD focuses on materials, structure optimization and engineering techniques for developing anode supported planar SOFC stack components. Preliminary technical aspects were approached in order to obtain a behavior improvement of stack.

Engineering processes developed are based on the in-house production. The aims are primarily to reduce costs, and to improve the reliability and robustness of the stack systems against conditions that occur in actual operating systems.

3.1 Stack SOFC Components & Materials

3.1.1 Standard Repeat Units (SRU)

The main structure of the SRU with single cell was designed and assembled as shown in Figure **3-1**. This design takes into account its reproducibility in a higher scale for multi-cells configuration.

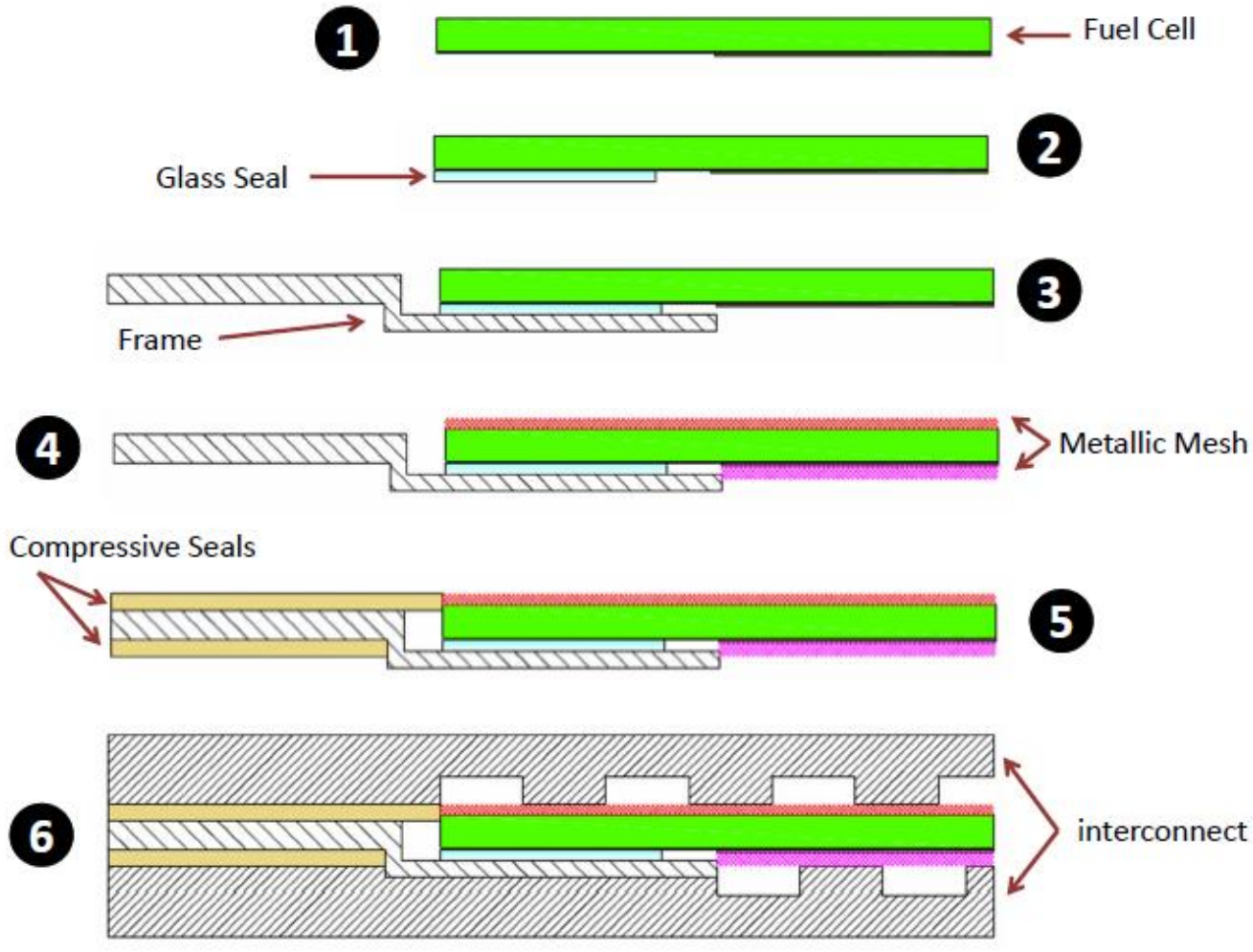

1. Fuel Cell
2. Glass-Ceramic Seal
3. Metallic Frame
4. Metallic Mesh
5. Compressive Seal
6. Interconnect

Figure 3-1: Main structure of the SRU with single cell

This configuration includes the separation between anodic and cathodic gas by means of the glass-ceramic seal. Also, the Compressive Seals were utilized for electric insulation and manifolds sealing. In addition, it was necessary to include the metallic mesh (Ni at the anode side and Platinum at the cathode side) to improve the electrical contact between the electrode and interconnect plates of the system. The frame is a metallic component made in CroFer® (ferritic stainless steel) which is the sealing gasket for glass-ceramic seal.

The SRU material selection was done taking into consideration the thermal expansion coefficients compatibility among the cell and stack components, as observed in Figure 3-2 and Figure 3-3, where can be evidenced that the mismatch in thermal expansion at 800°C

between the cell and the metallic interconnect is too great for using rigid seal. This is the reason to use the glass-ceramic seal to join the electrolyte to the metallic frame.

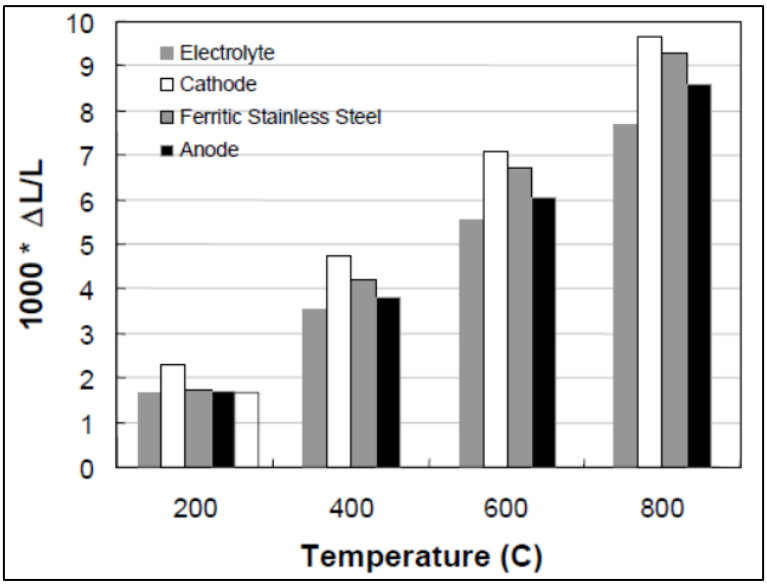

Figure 3-2: Expansion of Typical Cell Components in a 10 cm x 10 cm Planar SOFC with Ni-YSZ anode, YSZ Electrolyte, LSM Cathode, and Ferritic Steel Interconnect. [50]

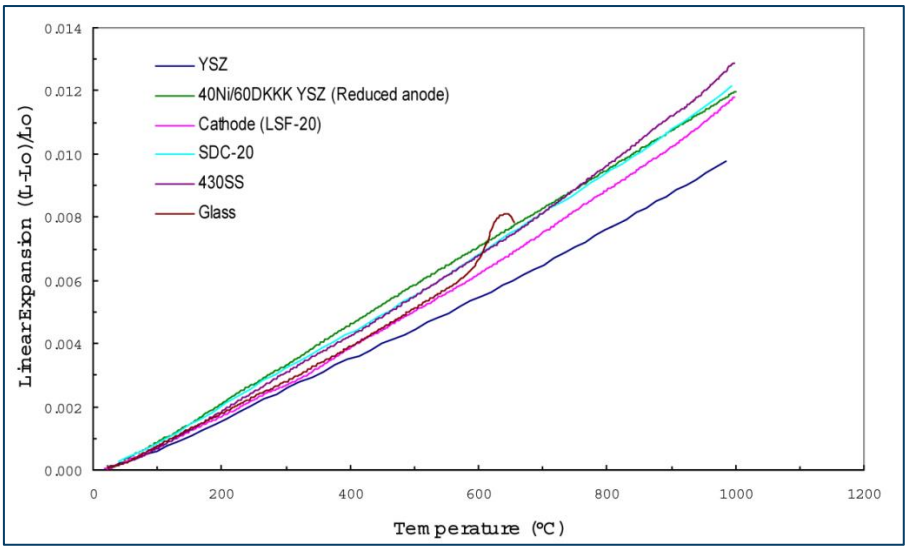

Figure 3-3: Thermal Expansion coefficients of Cell and Stack Materials [51]

3.1.2 Housing

This element is formed by two plates as schematically shown in Figure 3-4. The housing constitute the mechanical support due to it maintains pressure equalized in fuel cell stack (tightening torque: 50N) during test. A second function is to distribute the gases (Air and Fuel) in the stack because of the inlet manifolds. Each housing plate must be coupled with

the respective counterpart, because each of them has the external manifolds, one for the inlet gas and the other for the outlet gas.

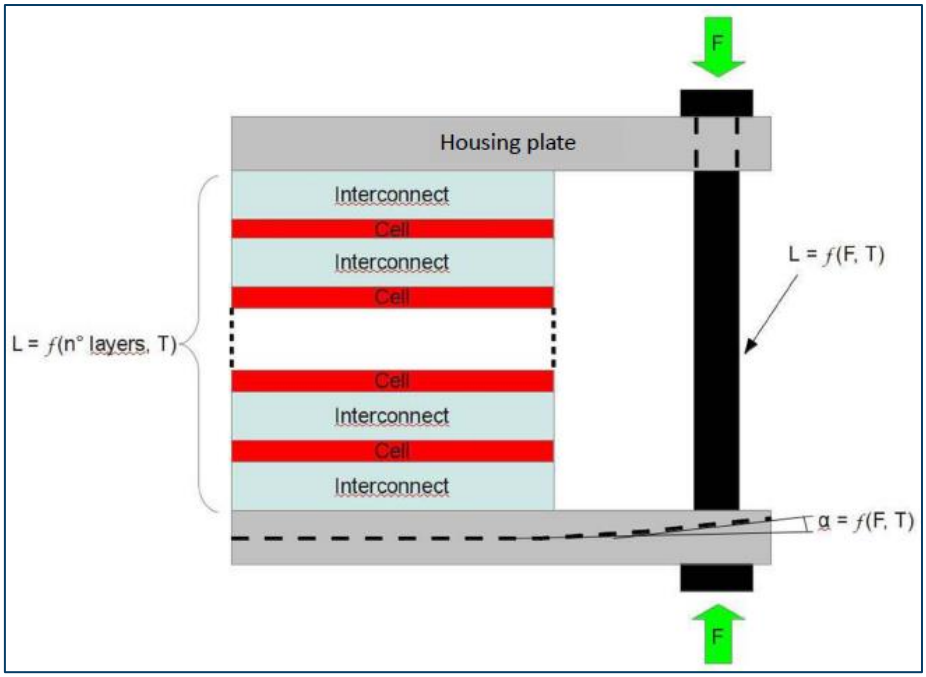

Figure 3-4: Schematic of the housing plates and the bolts. [53]

These parts are made in Stainless steel AISI 316L. This alloy offers higher creep, stress-to-rupture, and tensile strength at elevated temperature. In addition, AISI 316L has lower carbon content than AISI 316. This characteristic is important to avoid the susceptibility for intergranular corrosion at high temperatures [52].

Table 3-1: Chemical composition of AISI 316 and 316L [from IMS S.p.a.]

AISI 316							
C	Mn	Si	Cr	Ni	Mo	N	Others
≤0.070	≤2.00	≤1.00	16.50÷18.50	10.00÷13.00	2.00÷2.50	≤0.11	S≤0.030 P≤0.045
AISI 316L							
C	Mn	Si	Cr	Ni	Mo	N	Others
≤0.030	≤2.00	≤1.00	16.50÷18.50	10.00÷13.00	2.00÷2.50	≤0.11	S≤0.030 P≤0.045

In this work, a simple integrated compression system was developed to guaranty a hermetic enclosure of the planar SOFC stack. Basically, the two housing plates (see Figure 3-4) are characterized by the load of the bolts and the plates deformation depends on load and temperature (as per Young modulus).

The distance between the two plates also depends on the temperature (through thermal expansion coefficients) and the number of layers (through friction and roughness). A numerical routine procedure suggest that the pressure to be applied to the housing plates has to be one and a half times higher respect to the required one during operation for three cells stack shows in Figure 3-4. This value increases as the number of layer does [53].

In this PhD investigation, the housing plates were designed as shown in Figure 3-5 a). These components were designed to contain the stack, to distribute the gases and to lock hermetically the stacks and its pieces. This figure notes also the position of the metallic interconnector on housing plate (b); two pictures of the prototype with a detail of bolts positioning (c); and after building completion (d).

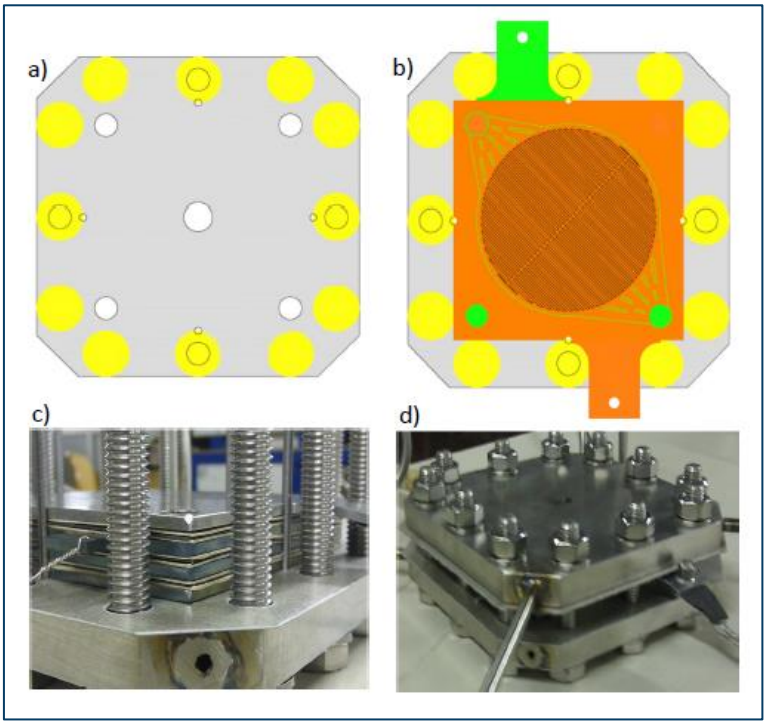

Figure 3-5: a) Drawing of the housing plates used; b) Drawing of the housing plate with the interconnector; c) Detail of bolts positioning during the prototype assembly; d) Prototypical stack after building completion.

Thanks to the development of the compression system described above, the prototypes properly functioned more than 500 hours at standard operation conditions.

Additionally, it must be noted that this system does not work under thermal cycle conditions due to the loss of bolts mechanical properties after the first thermal cycle. This happens because of the high mechanical loads at high temperatures. The solution adopted in this research was the use of a new set of bolts in each stack.

A possible optimization for future developments would be the improvement of the compression system by means of springs, braces, or hydraulic controlled system.

Besides the functions of housing explained before, this component also works as interconnector since it was manufactured to have the flow field for cathodic and anodic gases. The figure below exhibits the two housing designs and the one used in this investigation (see Figure 3-6 b), which enhanced the bolts position as shown in Figure **3**-**5** b).

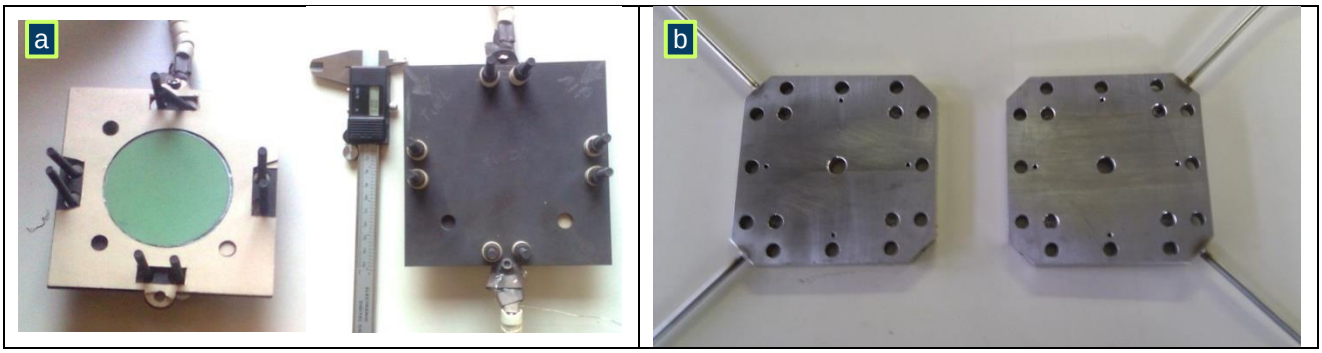

Figure 3-6: Housing Stack: a) first version; b) improved version.

3.1.3 Compressive Seal

These kinds of seals must be guaranteed two functions: electrical insulation; and sealing between the stack structure and housing component.

During the stack assembly, two types of compressive seals were used. The first one is the Flexible Mica Paper from Fuel Cell Materials. Mica paper is a commonly used material for compressive sealing in SOFC stacks, due to it offers excellent thermal, electrical and moisture resistance. The mica paper dimensions used was 170 x 170 mm with thicknesses of 0.50 mm. In addition, a laser cutting was employed to obtain exactly the manifolds and the holes for bolts positioning, as noticed in Figure 3-7 a).

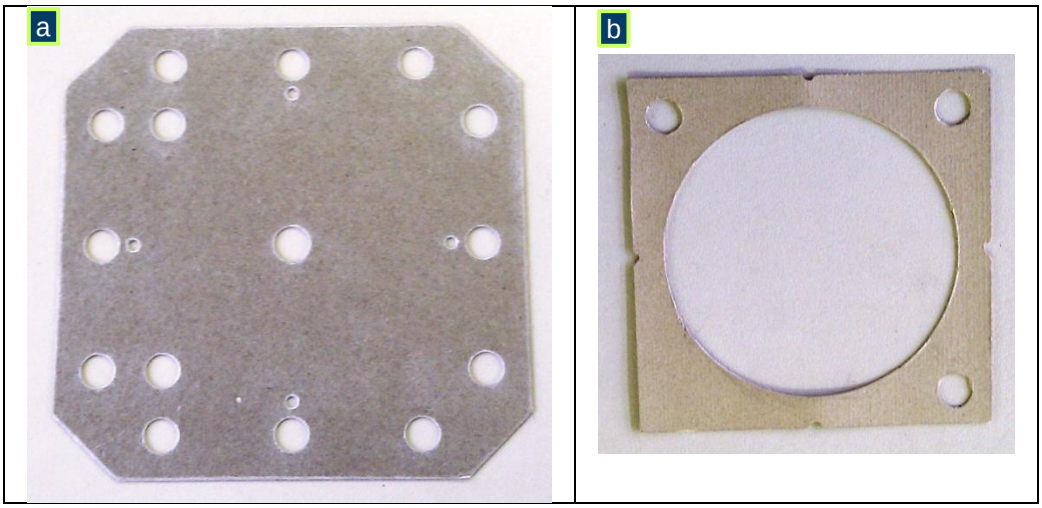

Figure 3-7: Compressive seal types: a) Mica paper; b), Thermiculite® 866 by Flexitallic

The second type of seal is illustrated in Figure 3-7 b). This seal has a high performance material and it is supplied in cut gasket or sheet form. The material is composed of a blend of chemically exfoliated vermiculite and steatite and is totally free from organic material consequently the material will not release thermal decomposition products during elevated temperature service. This seal can be applied for requirements as: low stress sealing, electrical isolation, non-contaminating and complex gasket geometry.

3.1.4 Glass-ceramic Seal

This seal is positioned between the cell and the frame. It is also known as “bonded seals”. The seal used in this PhD Thesis was developed by DISAT-Politecnico di Torino in the framework of the Regional Project “MULTISS” and in cooperation with the development of the prototypical stack in this research.

A schematic view of the metallic frame is presented in Figure 3-8.The process for developing the seal joint between the cell and the frame is illustrated in Figure 3-9 and a description of this process is mentioned hereafter.

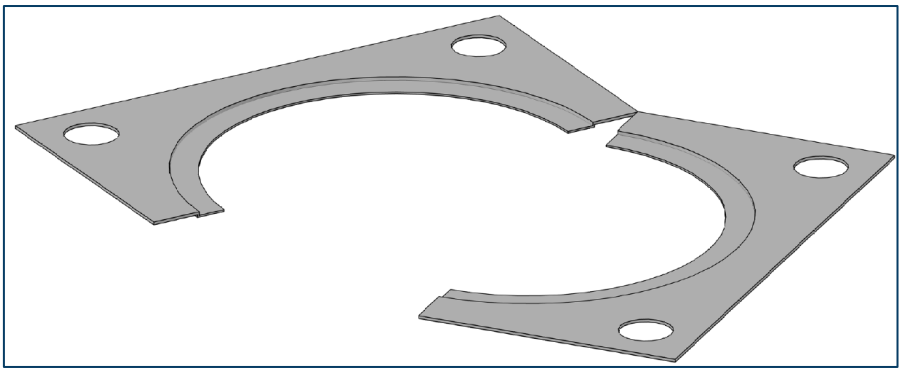

Figure 3-8: 3D schematic view of Metallic frame

The sealant composition ranged between 50-55 wt% SiO2, 10-12 wt% Al2O3, 20-23 wt% CaO and 10-12 wt%Na2O. The sealant, labeled as SACN, was produced as a glass by melting the appropriate raw materials in different proportions and by heating at 1500°C for 1 hour in a platinum crucible; the melt was cast on a metal plate and the transparent glass was ground for differential thermal analysis (DTA) and hot stage microscopy experiments (HSM).

Preliminary studies of wettability of the sealing glass on CroFer®22APU alloy (as received and preoxidised at 950°C in air for 2 hours,) and on YSZ supported on NiO-YSZ anode (ASE) ceramic were carried out by heating microscopy or in a tubular oven under air or Ar atmosphere.

The CroFer®22APU/glass-ceramic sealant/ASE joined samples were obtained by placing the CroFer®22APU plates on the yttria-stabilised zirconia (YSZ) surface of the anode-supported- electrolyte with the glass slurry sandwiched in between. The slurry was made of a mixture of glass powder dispersed in ethanol (solid content 40 wt. %).

Heat-treatments were performed in a tubular oven (argon atmosphere) at a temperature above the glass softening point, without applying any load. Reproducible results, in terms of joint thickness and homogeneity were obtained. The joining thermal treatment was carried out from room temperature to 900°C with a dwelling time of 30 minutes at 900°C and a heating rate of 5°C/min. Two main crystalline phases were detected by X-ray diffraction (XRD) in the glass-ceramic obtained after the sealant heat-treatment necessary for the joining process: Ca2Al2SiO7 and NaAlSiO4.

Furthermore, some CroFer®22APU/glass-ceramic sealant/ASE samples were exposed to H2-3H2O atmosphere at 800°C for 500 hours, and to thermal cycles (air atmosphere) from room temperature to 800ºC for a period of 500 hours and 3000 hours.

Cross-sections of joined samples were characterized by scanning electron microscopy (SEM) after polishing. EDS analysis was carried out in order to detect any elemental diffusion into or away from the seal after H2-3%H2O atmosphere exposure and following thermal cycling at 800˚C and to examine for any chemical interactions between CroFer®22APU and cell with the glass-ceramic sealant at the three-phase-boundary under reducing and oxidizing conditions. An example of seal joint in the frame can be observed in Figure 3-10. These results can be found in Chapter 5.

Table 3-2: Characteristic temperatures and thermo mechanical properties of the proposed sealant

Glass-ceramic sealant	
T_g (℃)	670
Softening temperature (℃)	740
Thermal expansion coefficient (℃ $^{-1}$)	10.7 (300℃-500℃).
Temperature at η 10^4 dPa·s (℃)	1165

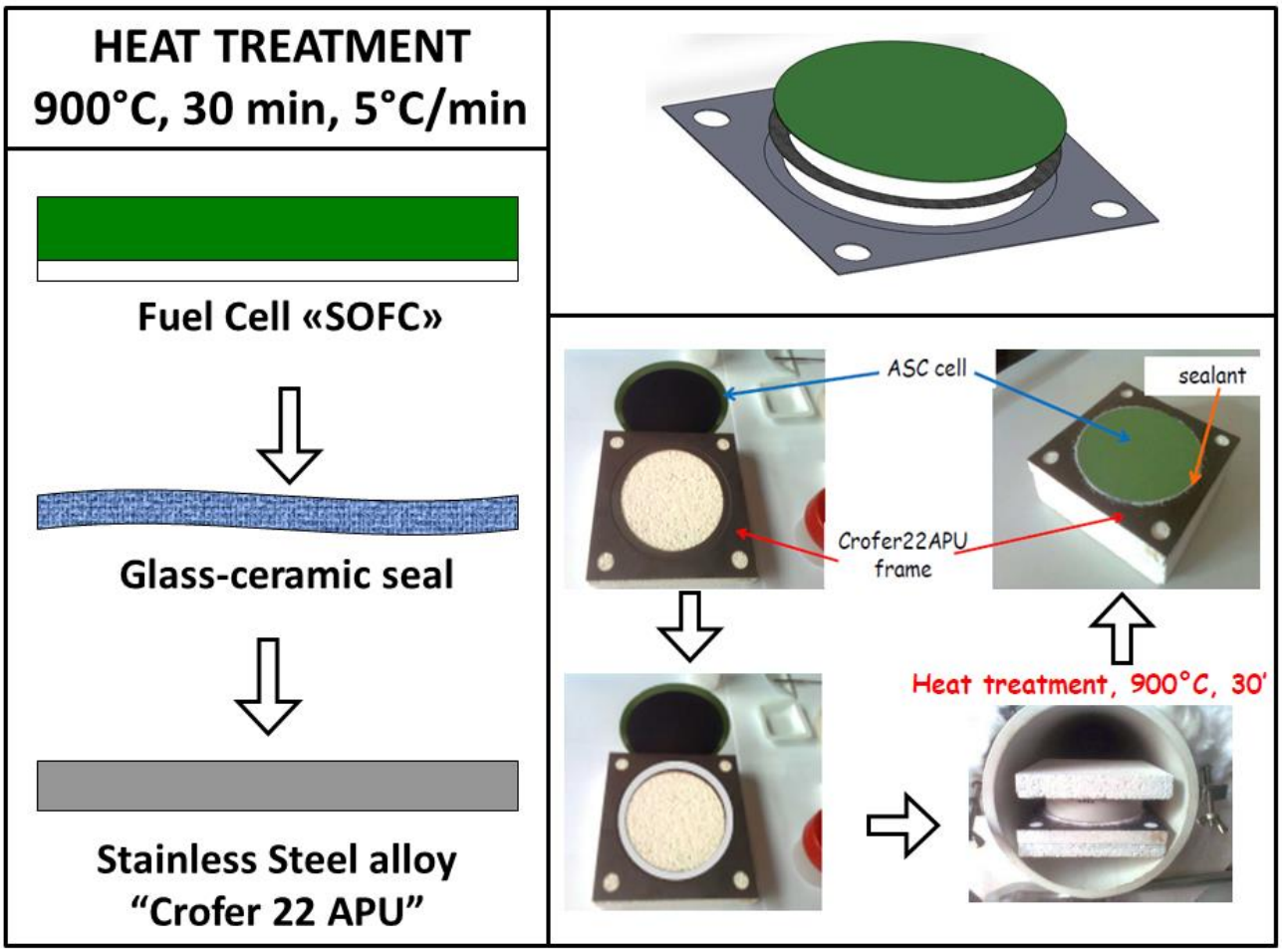

Figure 3-9: Joining CroFer® frame / glass-ceramic sealant / ASC cell unit procedure

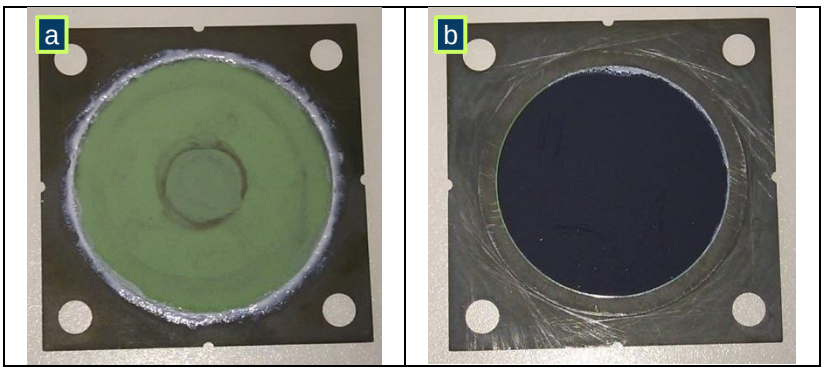

Figure 3-10: SOFC joined to metallic frame with glass ceramic seal to the:
a) Anodic side; b) Cathodic side.

3.1.5 Interconnect

This component presents two important functions: one related to the air distribution on the cathode side or to the fuel distribution on the Anode side to assure high efficiency of the chemical conversion; and the second function related the electrical connection of the cells.

A computational fluid dynamic study (CFD) was carried out to define interconnect geometry. It is important to properly choose a gas flow distribution geometry (flow field) of the interconnect plate to guaranty high performance of chemical reactions in the cell electrodes. In the cell surface, three main ways of dealing with the slow reaction rates are: the use of catalysts, raising the temperature and increasing the electrode area. The first two can be applied to any chemical reaction. However, the third is special to fuel cells and is very important. Indeed, electrode area is such a vital issue that the performance of a fuel cell design is often quoted in terms of the current per cm^2 [54].

However, the surface area is not the only issue; the electrode is made highly porous. This has the effect of greatly increasing the effective surface area. SOFC cell electrodes have a microstructure that gives them surface areas that can be hundreds or even thousands of times their straightforward 'length × width. On the other hand, the gas flow required for the porous electrode is higher than to straightforward area of the electrodes.

The CFD analysis for the interconnect definition was carried out in the framework of the Regional Project "The Design and in-house development of Solid Oxide Fuel Cell (SOFC) stacks for dealing with multiple fuels" (MULTISS).The developed design is in accordance to the flow field simulation and this is explained in the "Appendix A" of this thesis. Some results were exposed below.

Figure 3-11 shows the model mesh that was built for the tuning of the algorithms and the validation the gas flow field for the pins configuration.

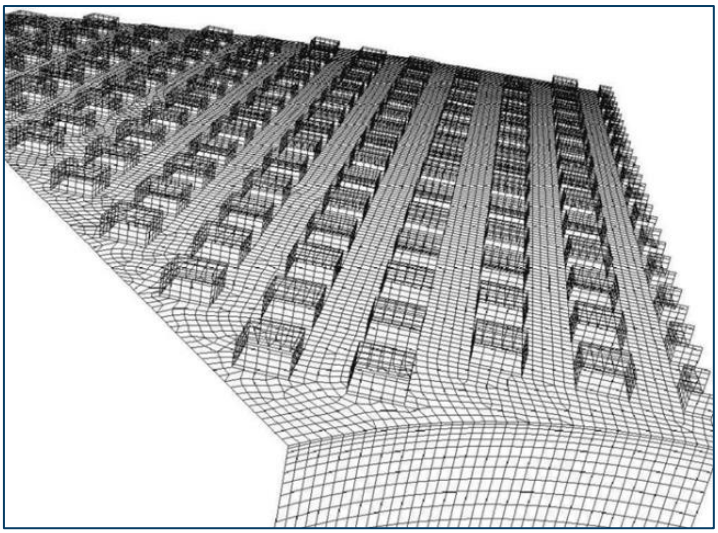

Figure 3-11: Example of the CFD mesh on the interconnector surface for the Pins configuration flow field.

Simulations in fact showed the presence of a “shadow effect” behind the geometry constraints of the interconnect (pins or channels) that significantly reduce the concentrations of the reactants in that zones. This implies that at high current density some part of the anode volume works very badly and the cell behaves as it had a lower active surface. These justify the diffusive limit of the polarization curves and suggest some strategies to reduce this effect and to obtain good performance also at high current density. Unfortunately, reducing this effect by decreasing the pins or channels width contrast with the electrical conduction need between electrode and interconnector. (See Figure 3-12).

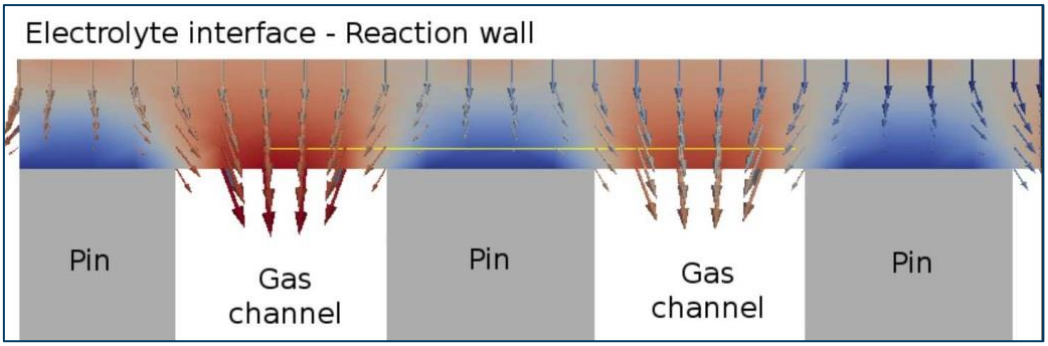

Figure 3-12 “Shadow effect” of the pins to the reactant diffusion in the electrode volume

After modeling work was utilized to optimize the gas flow inside the interconnects. Preliminary comparisons were made between circular cells and square cells varying the inlet and outlet size. The results show that the corner region is the worst ones in term of fluid distribution. So circular cell for this kind of inlet-outlet configuration was justified. (See Figure 3-13).

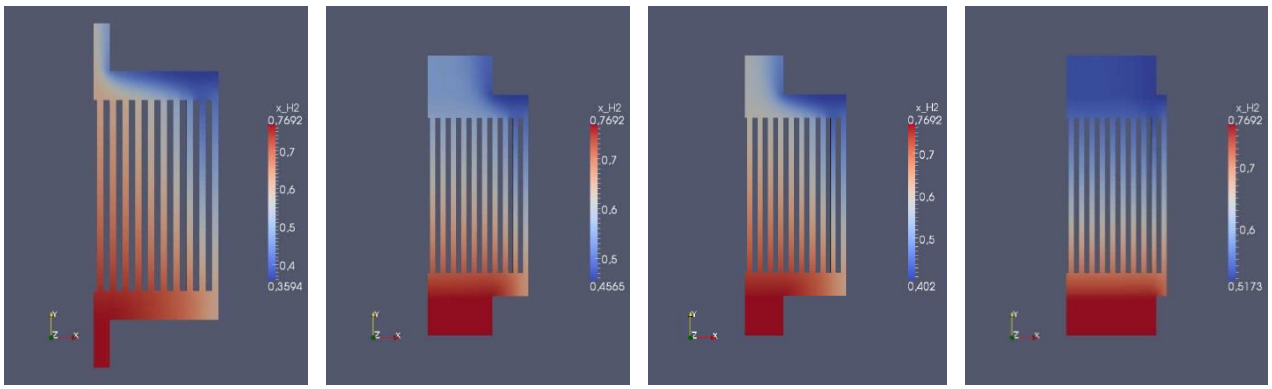

Figure 3-13: H_2 molar fraction distribution on the anode surface at different current densities in case of rectangular cells with channel flow field.

Then, using circular geometry, some simulations are made changing the ratio between the inlet and the outlet channel section, which is one of the most important parameters in fluid flow distribution. (See Figure 3-14)

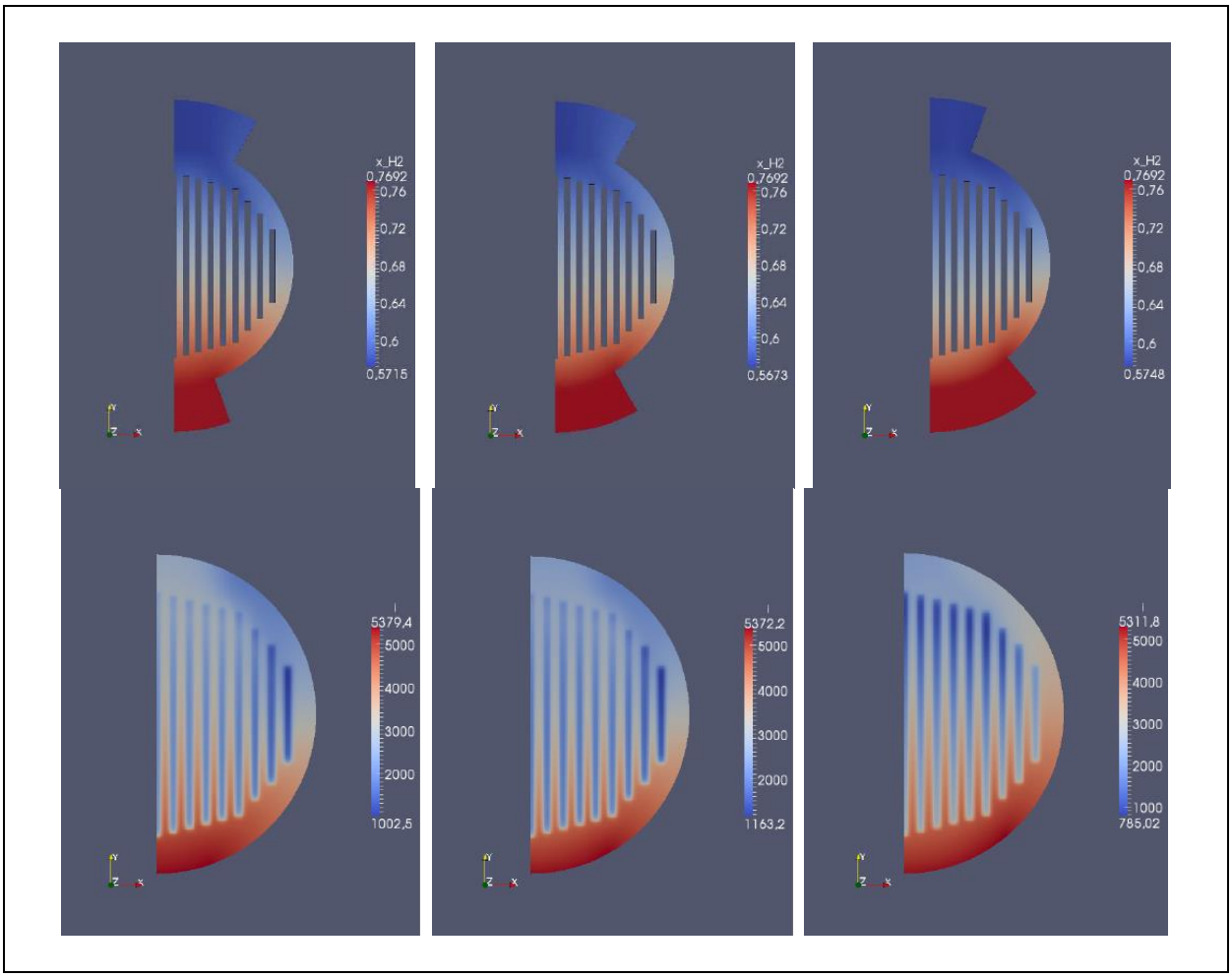

Figure 3-14: H_2 molar fraction distribution on the anode surface at different current densities in case of circular cells, with modification of the ratio between the inlet and the outlet channel section

Best results are obtained in those configurations with similar inlet and outlet dimensions. Variations in channels geometry (complex configurations or similar) could optimize the flow fields for a single operation point but simpler geometries work better for general purpose operations. We also experimented that a transversal channel can redistribute differences between longitudinal channels with positive effect. Since the electrical modeling is the less approximate part, the channel width and the ratio between channel and solid part widths was considered in conservative way.

Figure 3-15 shows the finally design for different interconnect plates of anode and cathode sides; and it is possible to note the different gas flow profiles (pins or channels) considered previously.

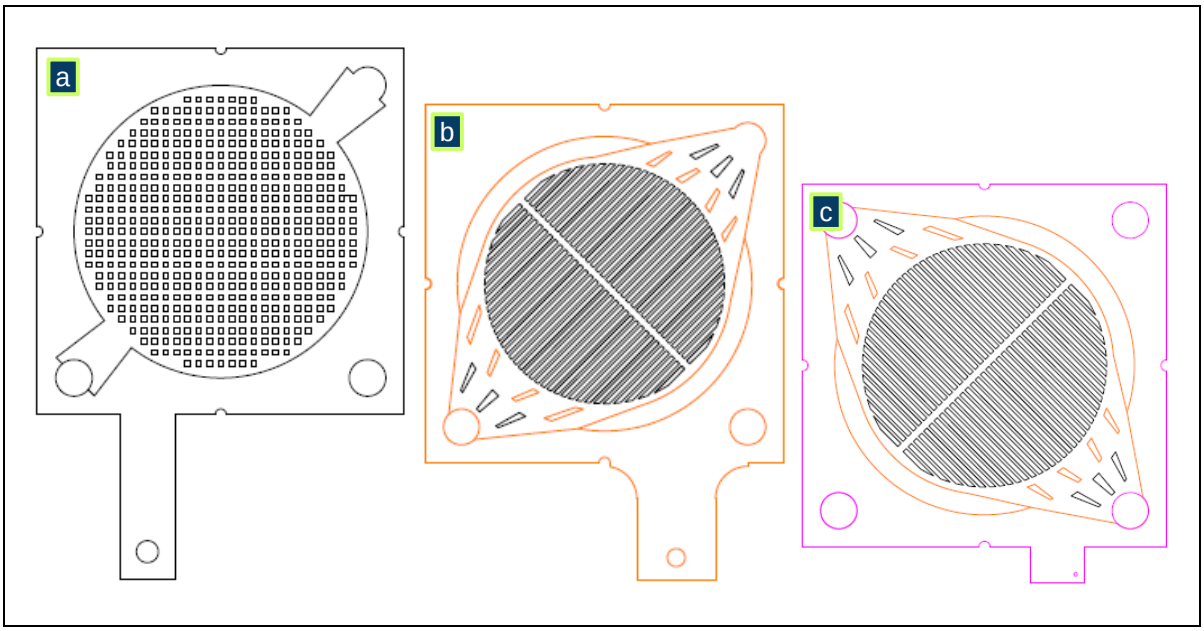

Figure 3-15: Interconnector with different gas flow designs. a) anode side with pin configuration, b) cathode side of bipolar interconnect with channel configuration and c) cathode end plate interconnect with channel configuration.

The material used for the interconnect fabrication was a commercially Ferritic stainless Steel with high amount of Chromium named Crofer® APU22 produced by ThyssenKrupp Germany. The thickness of the raw plate was 2.5 mm and the material was machined in accordance with the mechanical design done in this PhD investigation during the stack development phase.

The metallic mesh is an additional connector between the cell and the interconnect plate in anode side (nickel) as well as in cathode side (platinum). In this way, a good electrical connection and compatibility under operative conditions can be obtained (reduce for the anode and oxidant for the cathode). In this work, the meshes utilized were from Alfa Aesar - A Johnson Matthey Company, Platinum and Mikel Gauze 100 mesh. An example can be appreciated in Figure 3-16.

The metallic mesh improves and makes uniform the electrons distribution on the electrodes surface. It also reduces the contact resistance due to the malleability and the adaptation capabilty to the geometry of electrodes and interconnectors. The mesh has an excellent compatibility with the anode since they both are made of the same material. On the cathode side, it is necessary to use noble metals like Pt or Au for avoiding the surface oxidation between the interface electrode/interconnector. Other solution can be the use of inconel (Ni-based alloy) with a protective coating in order to reduce costs by substituting

the utilization of noble metals. In this way, the interconnector conductivity can be increased by reducing the contact resistance, as shown in Table 3-3.

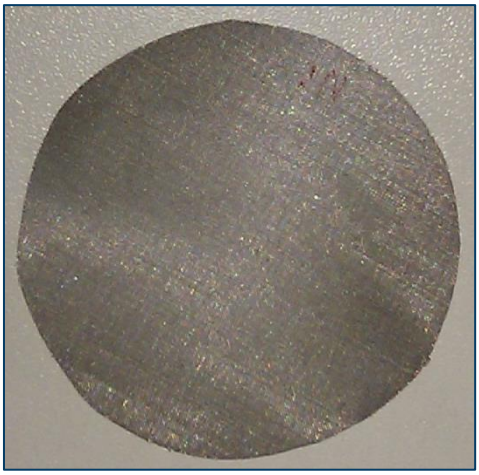

Figure 3-16: Platinum mesh (100 mesh)

Table 3-3: Electrical Conductivity of metals used in SOFC components

Element	Electrical Conductivity (x 10^7 Ohm.m)	Element	Electrical Conductivity (x 10^7 Ohm.m)
Ag	6.21	Co	1.72
Cu	5.88	Ni	1.43
Au	4.55	Fe	1.02
Al	3.65	Pt	0.96
Mg	2.33	CroFer®	1.81

Another step for the interconnect preparation consisted of the protective coating application on the interconnect surface. This coating was developed by Edison Research & Development Center Edison S.p.A [55,53] in the framework of MULTISS project. A thin $Mn_{1.5}Co_{1.5}O_4$ coating (1µm) was deposited on CroFer®22APU using thermal co-evaporation technique, followed by heat treatment in oxygen. Further details related to the coating fabricating technique and results are reported in [55].

3.1.6 Fuel Cell

This investigation was based on a commercial circular planar SOFC by HC stark with 80 mm diameter for anode and electrolyte, while the diameter of 70 mm was used for the

cathode. In this way, there was a gap of 10mm for the glass ceramic seal to join the cell with the frame. It was an anode supported type. The cell consisted of:

- Anode made of NiO-YSZ
- YSZ electrolyte (8 % mol. Yttria Stabilized Zirconia).
- Double layer cathode made of LSM (lanthanum strontium manganite) and YSZ-LSM (YSZ functional layer and a LSM current collecting layer).

The thickness of the anode was around 580 μm, the electrolyte layer was 4 μm thick, and the thickness of the cathode was around 45 μm.

3.2 Assembly procedure

In this paragraph, a detailed procedure for stack assembly is found. Every step carried out during this procedure is illustrated in Figure 3-17.

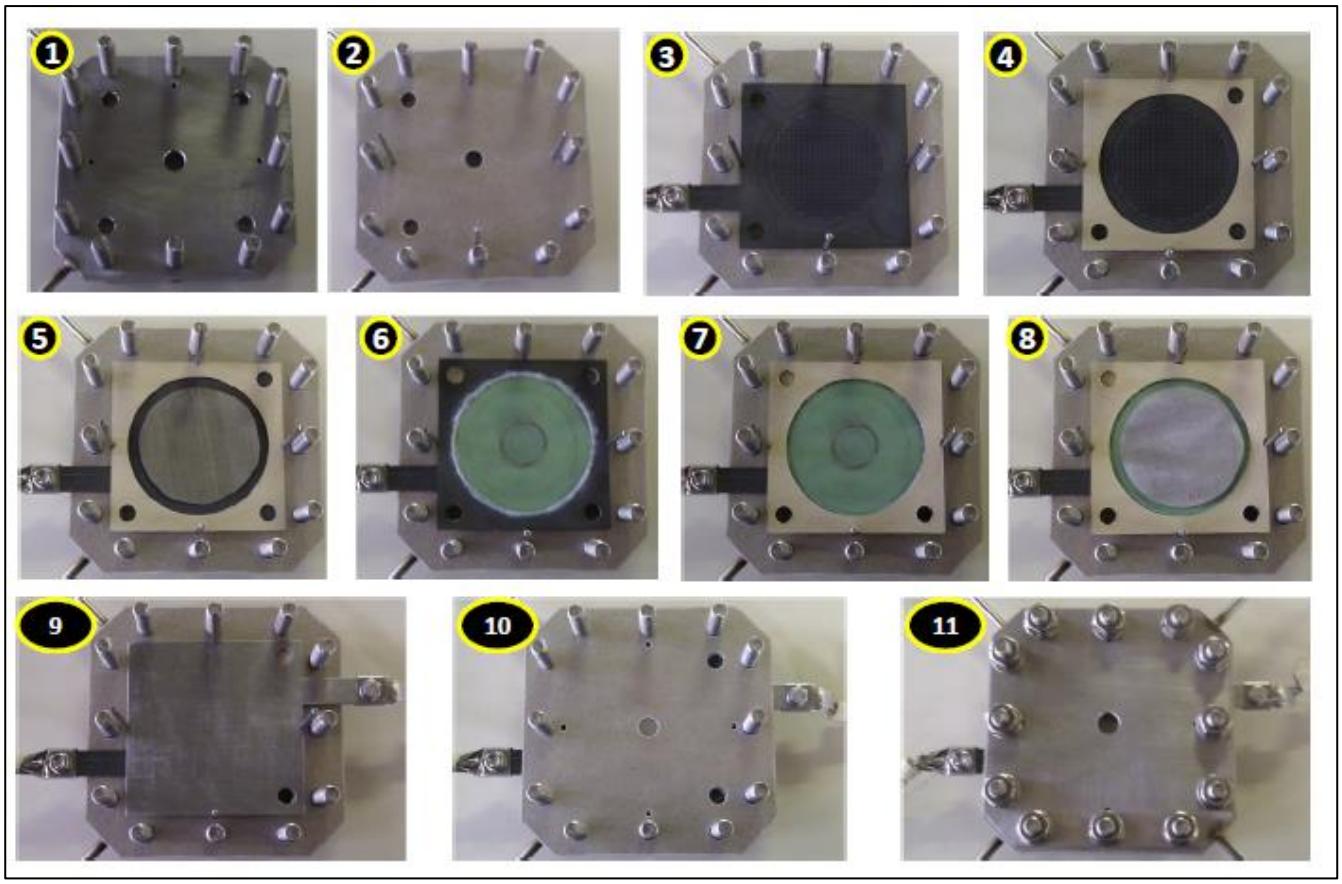

Figure 3-17: Steps for stack assembly procedure

1) Housing Stack Fuel. This element is the structure mechanical support due to it maintains pressure equalized in fuel cell stack (50N) during test. A second function is given by the Air and Fuel distribution in the stack because it has the inlet manifold. This component must be coupled with its external counterpart, which has the outlet manifold.

2) Mica Insulation. Two functions are guaranteed: electrical insulation; and sealing between the stack structure and housing component.

3) Cathode End Plate This piece has two functions related to the air distribution on the Cathode side (developed design in accordance to the fuel field simulation); and the electrical wire connection.
4) Mica Insulation. This material brings the functions related to the electrical insulation and the sealing between the cathode plate and the frame plate (cell joint).

5) Electrical connector Cathode side. This part brings the electrical connection between the cathode cell and the metallic plate. The materials used must keep a high electrical conductivity at high temperatures (around 800°C) and oxidant atmosphere.

6) Fuel Cell type anode supported (ASC). This part is constituted by three basic elements of stack: Frame: It is a thin CroFer® plate, which supports the jointed cell. Sealing glass-ceramic Cell.

7) Mica Insulation. In addition to the electrical insulation, this material seals the anode plate and the frame plate (cell joint).

8) Electrical connector Anode side. This part brings the electrical connection between the anode cell and the metallic plate. The materials used must keep a high electrical conductivity at high temperatures (around 800°C).

9) Anode End Plate. This piece has two functions related to the fuel distribution on the Anode side (developed design in accordance to the fuel field simulation); and the electrical wire connection.

10) Mica Insulation. Two functions are guaranteed: electrical insulation; and sealing between the stack structure and housing component.

11) Housing Stack Fuel. This part has the same function that the housing shown at the beginning of this sequence. It must be coupled with its internal counterpart, which has the inlet manifold.

The procedure shown above was developed to allow the assembly of multi cells configuration. Some pictures of the prototypes produced with one cell and 3 cells are reported as follows.

Mono cell configurations	Multi cell configurations (3 cells)
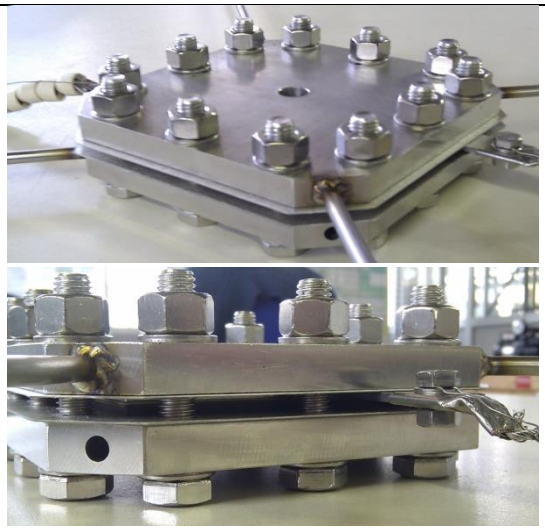	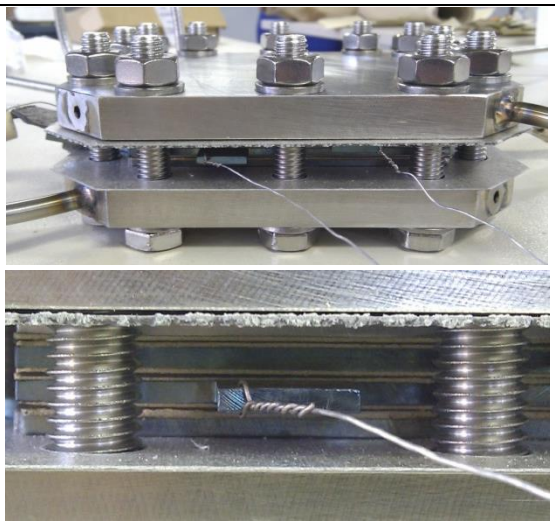

SOFC Stack Testing

A short-stack of planar cells was designed, developed and built. In this section, the experimental results obtained with short-stacks of mono cell and multi cells configurations are presented and analyzed.

Two standard configurations were defined and tested:

1. *One cell configuration.* The aim consisted of testing the assembly stack system in order to evaluate the mechanical structure and material compatibility, thermo-fluid-dynamic field and electrical connection. Other aspect to study is the cathode protection from Cr poisoning by means of a protective coating.
2. *Three cells configuration.* The idea was to verify the scale-up of the system from the lab design to a higher power system. Additionally, a high duration test was performed to verify the system stability. A fuel system was integrated based on simulated biogas used as primary fuel source.

The conditions used during testing of short stacks are summarized in Table 4-1. Results obtained from every test will be extensive presented and discussed in the next paragraphs.

Table 4-1: The experimental conditions used for the shorts-stacks tested

Test	Test name	Cell number	Flow field	Protective Coating	Time (hours)
I	m1STACK	1	Pins	no	250
II	m2STACK	1	Pins	yes	375
III	STACK 1	3	Channels	yes	200
IV	STACK 2	3	Channels	yes	•

4.1 **Test I:** Stack on mono cell configuration without protective coating.

Scope of this test was to verify the stack design, assembly procedure and proper operation of seal glass-ceramic based cell assembly. The duration of this test was 250h. The gas flow design in the interconnect plate was Pins configuration (see Figure 3.11). No protective coating was deposited on the interconnectors.

The stack stability was tested in Open Circuit Voltage (OCV) conditions and then different flow rates of H_2 were used in order to verify the stack response with different fuel utilization (FU), as can be seen in Figure 4-1.

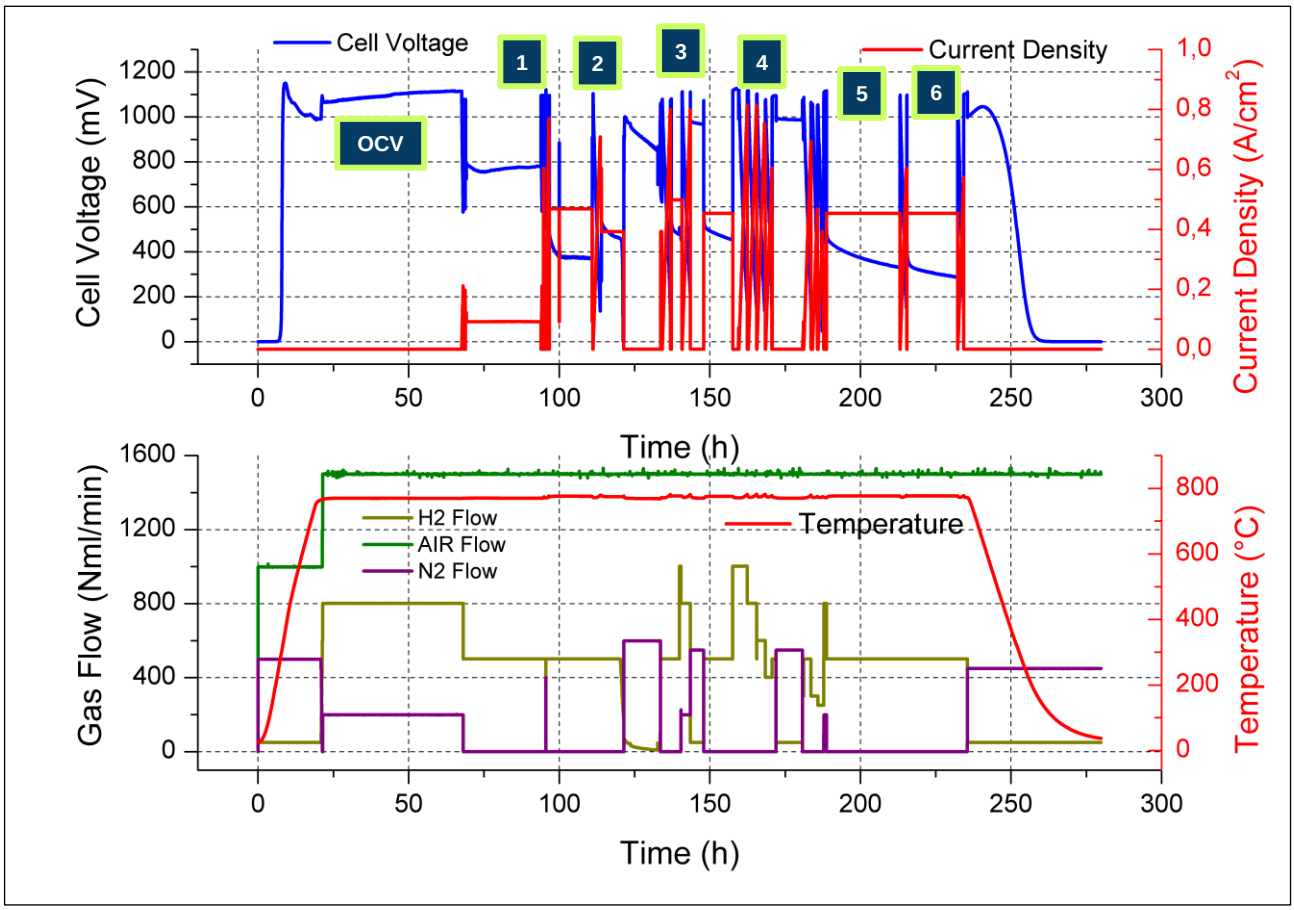

Figure 4-1: Galvanostatic performance of the m1STACK.

During the first 75 hours, in the OCV condition it is possible to note a slightly increase of the voltage. This increase can be explained by a normally activation of the electrode.

The polarizations tests (I-V curves) were done to check the degradation of the stack. These tests were completed with the same gas flow rate of H_2 (500 Nml/min), as seen in Table 4-2.

Table 4-2: Referential time for the I-V curve done with H_2 (500 Nml/min)

Test	Time (h)
1	95
2	110
3	150
4	170
5	185
6	220

Different flow rates conditions of H_2 were tested in the whole test duration. The respective results were taken from the polarization curve form (I-V curve) to evaluate the stack behavior and response with FU variations.

Figure 4-2 presents the decreasing performance of the stack under the same flow rate of H_2 (500 Nml/min) during all time tested. Specifically, in the beginning on the test 1 and 2 (see Figure 4-1 for timing reference) is evident the activation process of the electrode and the assessment of the electrical connection between the cell and the interconnect plate. These affirmations were confirmed with ASR curve presented in the Figure 4-3.

Additionally, the maximum power of the stack (during third test) after 140 hours was obtained at high current conditions (from 0.5 A/cm2) as seen in Figure 4-2. In fact, this maximum power value corresponds to the minimum curve of ASR (see Figure 4-3), which is related to the ASC3 cell value. On the other hand, the decreasing performance of the stack was begun after the third test. The progress degradation was noted on the tests 4, 5 and 6 in Figure 4-2 and Figure 4-3.

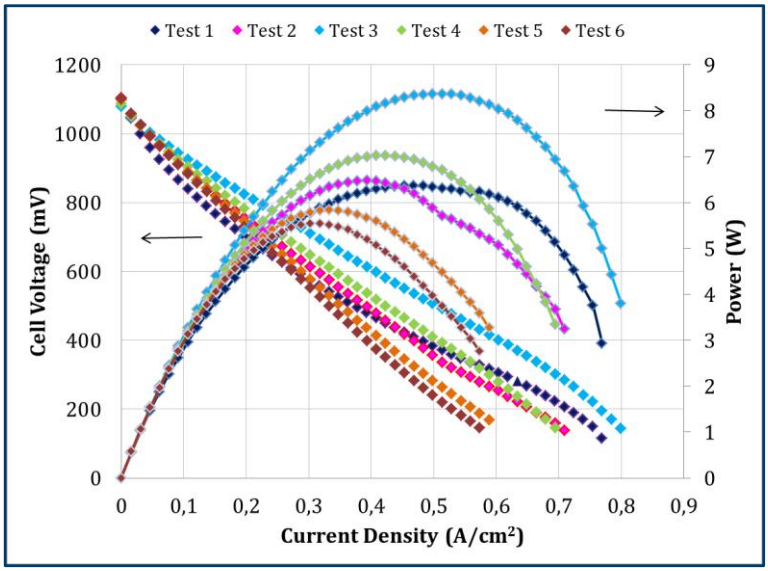

Figure 4-2: I-V curve with the same H_2 flow rate (500 Nml/min) to verify the m1Stack performance during all time test.

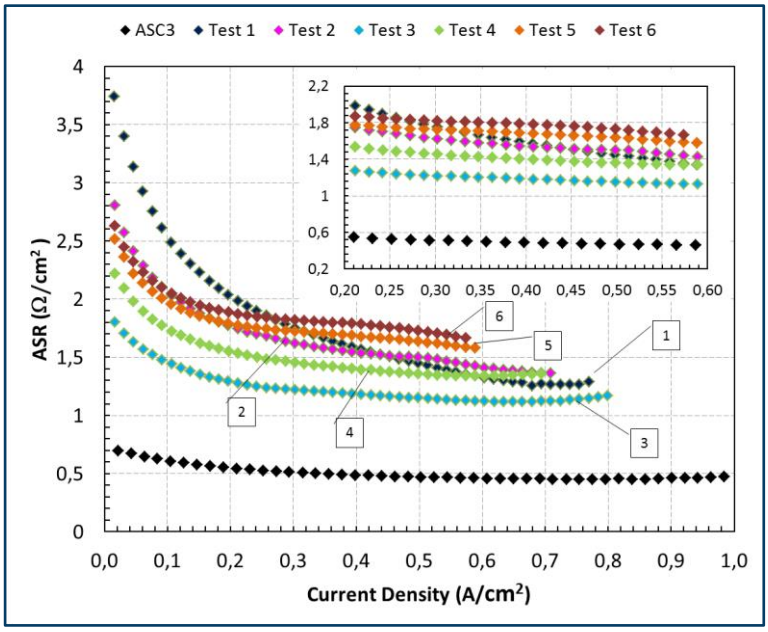

Figure 4-3: Comparison of the ASR during all time test at 500 Nml/min of H_2

Other interesting result was the decreasing performance of the stack with the variation of the H_2 flow rates, as presented in Figure 4-4. This is more evident for H_2 flow rates lower than 400 Nml/min at high current conditions (from 0.5 A/cm^2). This means that the stack is limited in power generation with low H_2 flow rates and high Fuel Utilization. For this reason, the optimization of the flow field of plates was carried out.

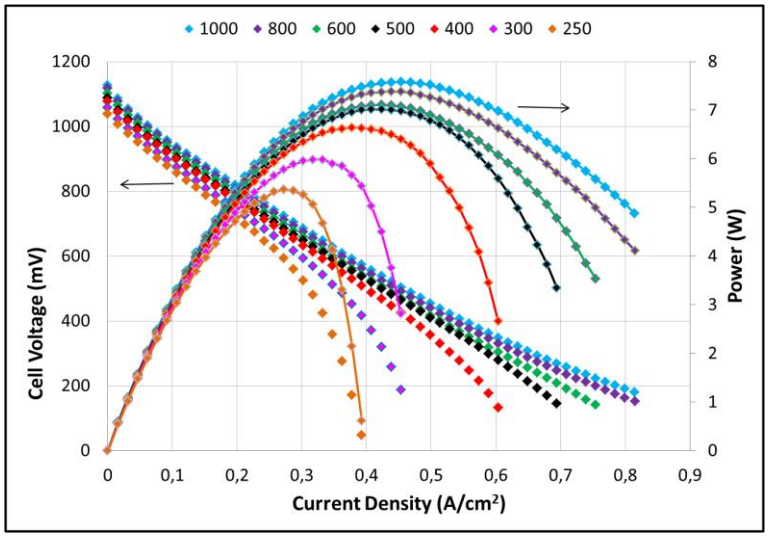

Figure 4-4: I-V curve with different flow rates (250 – 1000 Nml/min) to verify the m1Stack performance in a short time.

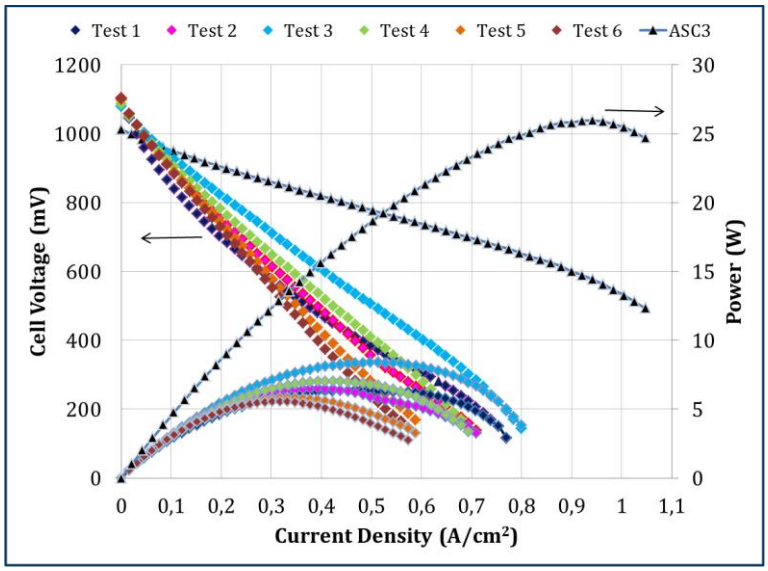

Figure 4-5: I-V curve with the same H_2 flow rate (500 Nml/min) to verify the m1Stack performance during all time test.

The I–V curve of the stack and the output performance of the individual cells is shown in Figure 4-5. The maximum power of the stack was 8.5W, while the ASC3 cell produced a power peak of 27W when fed with the same flow rate of H_2 (500 Nml/min). This difference represents an energy loss around 70% with respect to the total capacity of power production of the cell. These losses can be attained to the ohmic losses due to the contact resistance between interconnectors and cell.

4.2 **Test II:** Stack on mono cell configuration with protective coating

Scope of this test was to check the stack performance and durability using a protective coating of the interconnector face in contact with the cathode electrode to avoid its Cr poisoning. The protective coating was produced by Edison Research & Development Center Edison S.p.A [53, 55]. The duration of this test was of 375 h, as can be seen in Figure 4-6.

The stack stability was tested in OCV conditions during the first part, and then different flow rates of H_2 were used in order to verify the stack response with different fuel utilization. The stack was stable for more than 300 hours under electrical load and without apparent degradation.

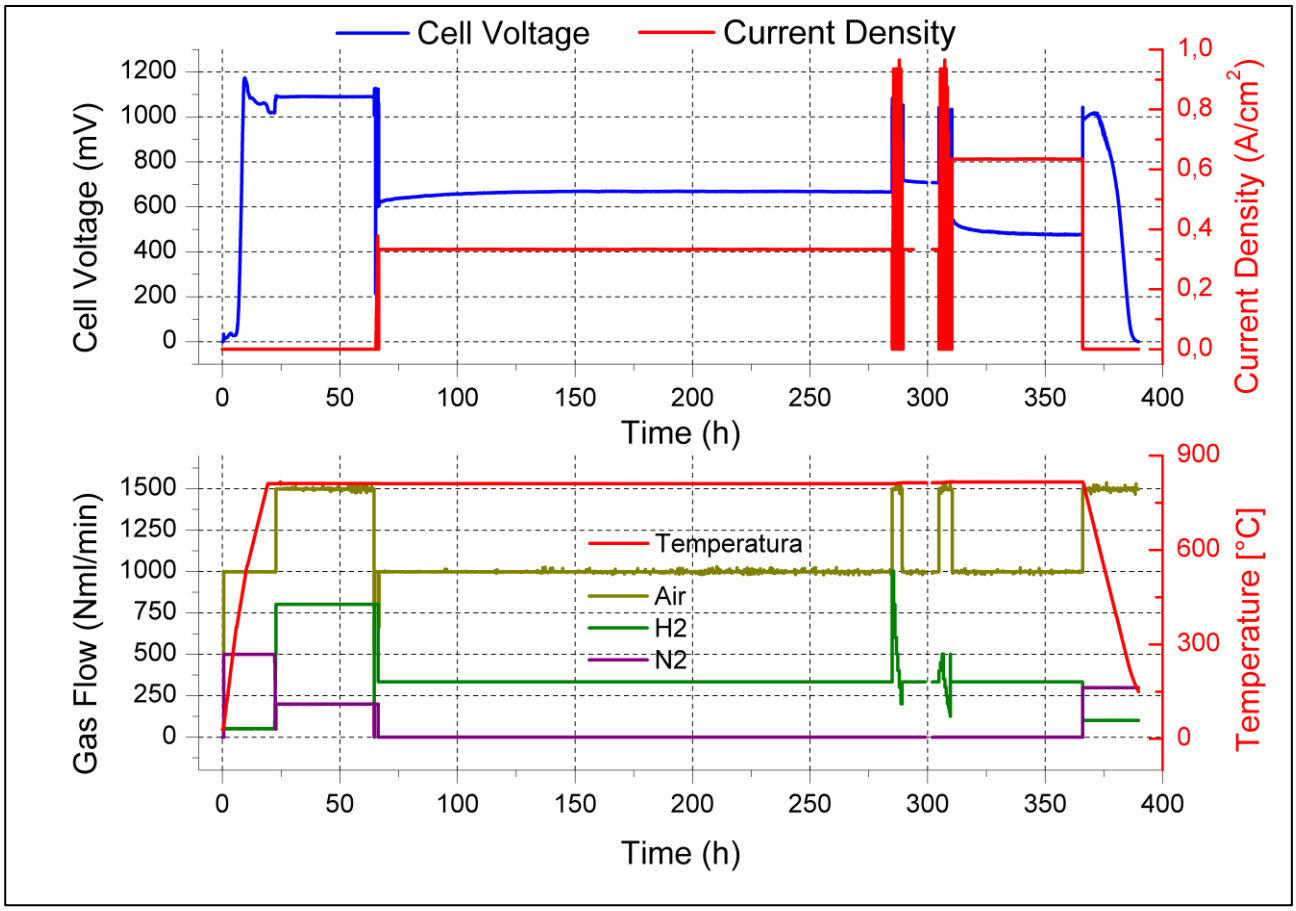

Figure 4-6: Galvanostatic performance of the m2STACK

Figure 4-7 notices the evaluation of the polarization, power, efficiency and fuel utilization obtained with the variation of the flow rate of H_2 on the m2Stack test.

The maximum efficiency was about 29% with a FU of 80%. An evident improvement was obtained in comparison with m1STACK. In fact, the maximum power on the m2Stack is 20% higher than the m1Stack (11 vs. 8.5 W). Additionally, higher current densities were obtained with lower hydrogen flow rates.

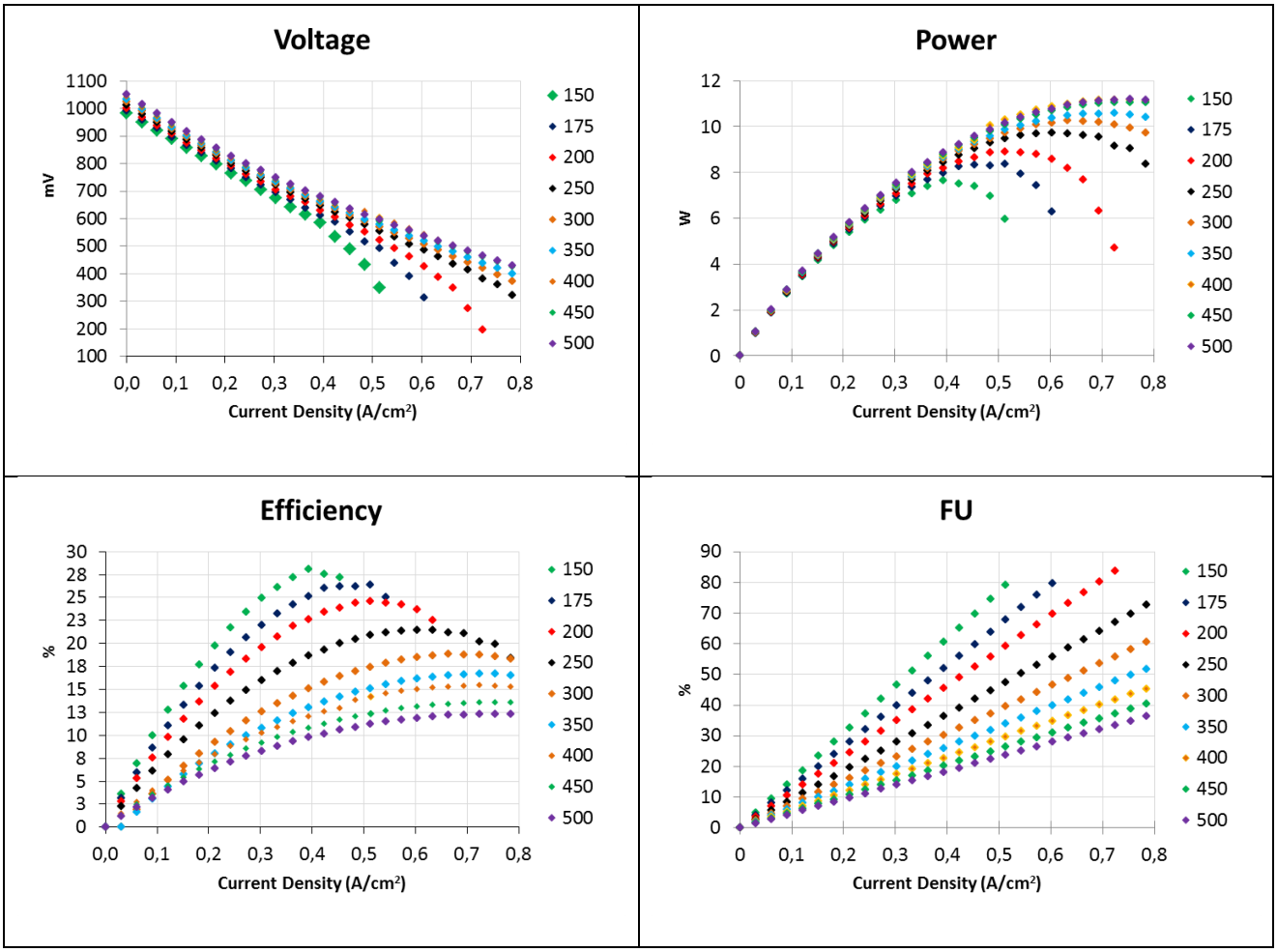

Figure 4-7: Polarization, power, efficiency and FU of the m2STACK

The I–V curve of the stack and the output performance of the individual cells shown in Figure 4-8. The maximum power of the stack was 11W, while the ASC3 cell produced a power peak of 27W when it was feeding with the same flow rate of H_2 (500 Nml/min). This difference represents an energy loss of 60% of the total that the cell can produce. These losses can be attained to the ohmic losses due to the contact resistance between interconnectors and cell. A slight improvement of 10% of power produced was obtained in comparison to m1Stack.

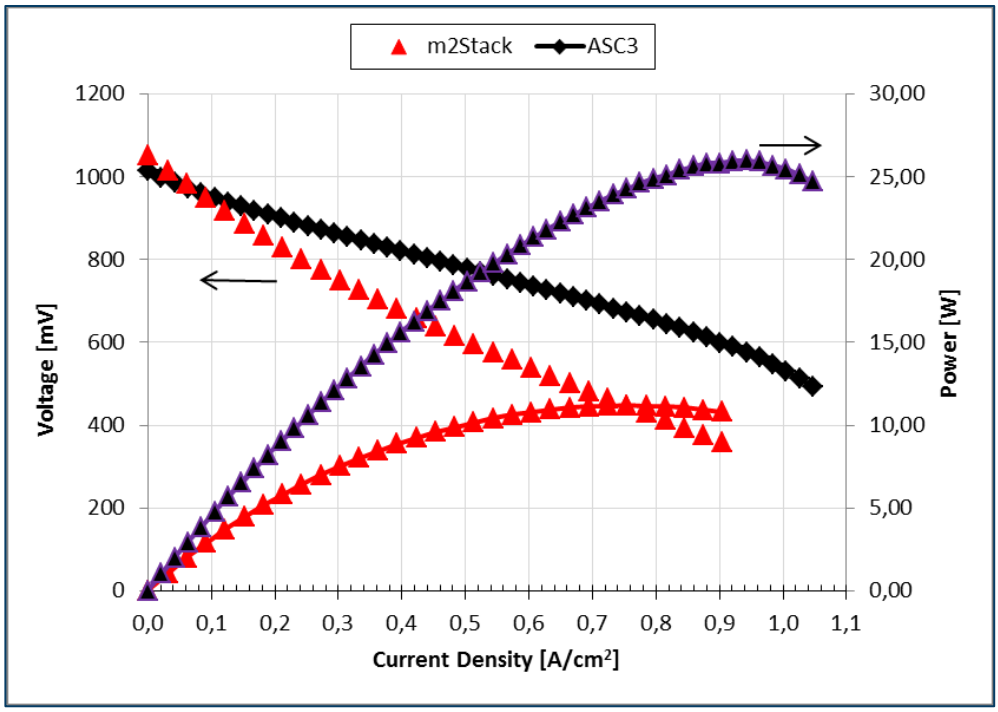

Figure 4-8: I-V curve with the same H_2 flow rate (500 Nml/min) to verify the m2Stack performance during all time test.

Moreover, the ASR value of the m2Stack reported in the Figure 4-9 shows an enhancement in confront with the ASR value of the m1Stack. The protective coating represents betterment for the stack system. During 375 hours of test, there was no evidence of voltage decreasing at load current conditions. So, there were no indications related to cathode Cr poisoning. On the contrary, the test on m1Stack revealed voltage decay from 150 hours. This is a clear indication of cathode Cr poisoning.

Finally, the optimization of the flow field of plates should be carried out to reduce the ASR values of the stack. Also, a reduction of the interconnect thickness is necessary. In this way, the ohmic losses will decrease whereas the power stack performance increases.

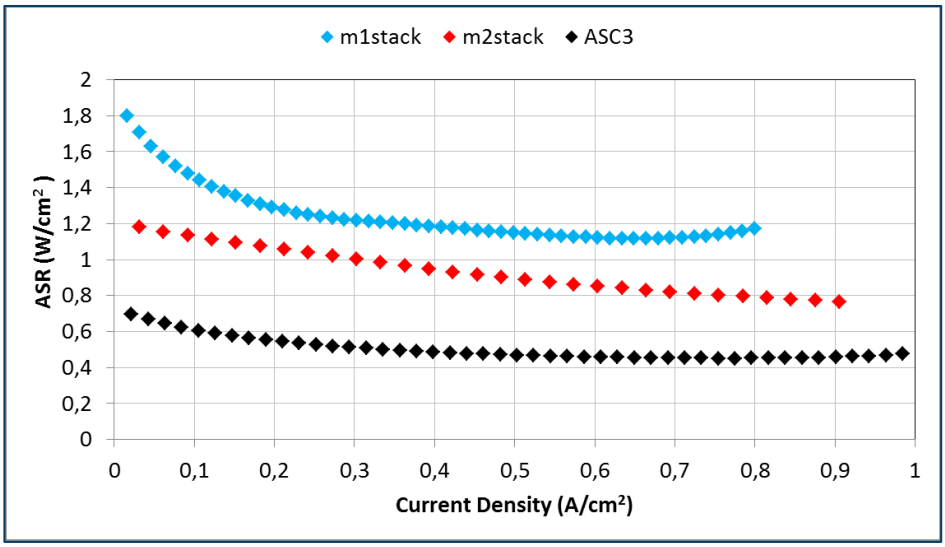

Figure 4-9: Comparison of the ASR in m1Stack and m2Stack.

4.3 **Test III:** Stack on three cell configuration with protective coating

Scope of this test was to verify the stack design and the scaling up to assembly procedure and the electrical stability of the developed stack in multi cell configuration.

Other innovation was the modification of flow field of cathode and anode plates by changing from pin configuration (used in the previous mono cell) to channels configuration (used in the new 3 cells short-stack), as shown in Figure 3.13 b and c).

The stability was tested in Open Circuit Voltage conditions during the first part of test and then the stack was supplied with 1000 Nml/min flow of H_2 (effective 333 Nml/min x cell) to analyze the stack response and durability. These values are the maximum operating values in this test because of lab instrumental limitations.

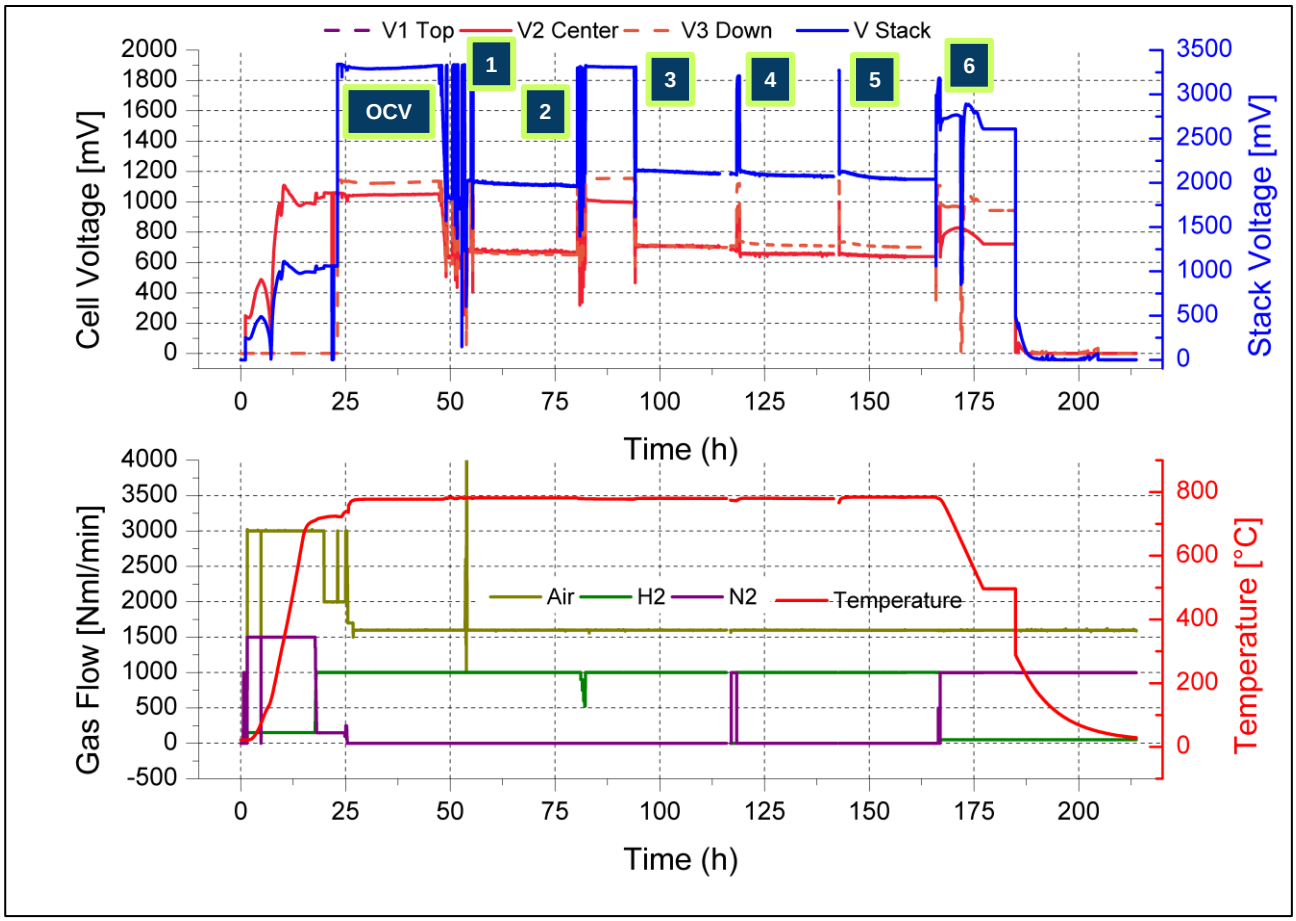

Figure 4-10: Galvanostatic performance of the STACK 1.

The specify polarizations tests (I-V curves) were done to check the degradation of the stack. These tests (see Table 4-2:) were completed with the same gas flow rate of H_2 (333 Nml/min).

Table 4-3: Referential time for the I-V curve done with H_2 (333 Nml/min)

Test	Time (h)
1	50
2	80
3	100
4	125
5	150
6	175

Although the stack was stable, 3 cells did not present the same behavior (see Figure 4-10 and Figure 4-11). The top and down cells exhibited better performances at low current. On the contrary, the central cell performed better at high current.

This test was influenced by two electrical blackouts: one of 40 minutes and the other one was about 20 minutes the day after. These events caused the automatic closure of the H_2 safety electrovalve. Probably, they caused the partial anode oxidation. In consequence, it was not possible to perform this test for a long time.

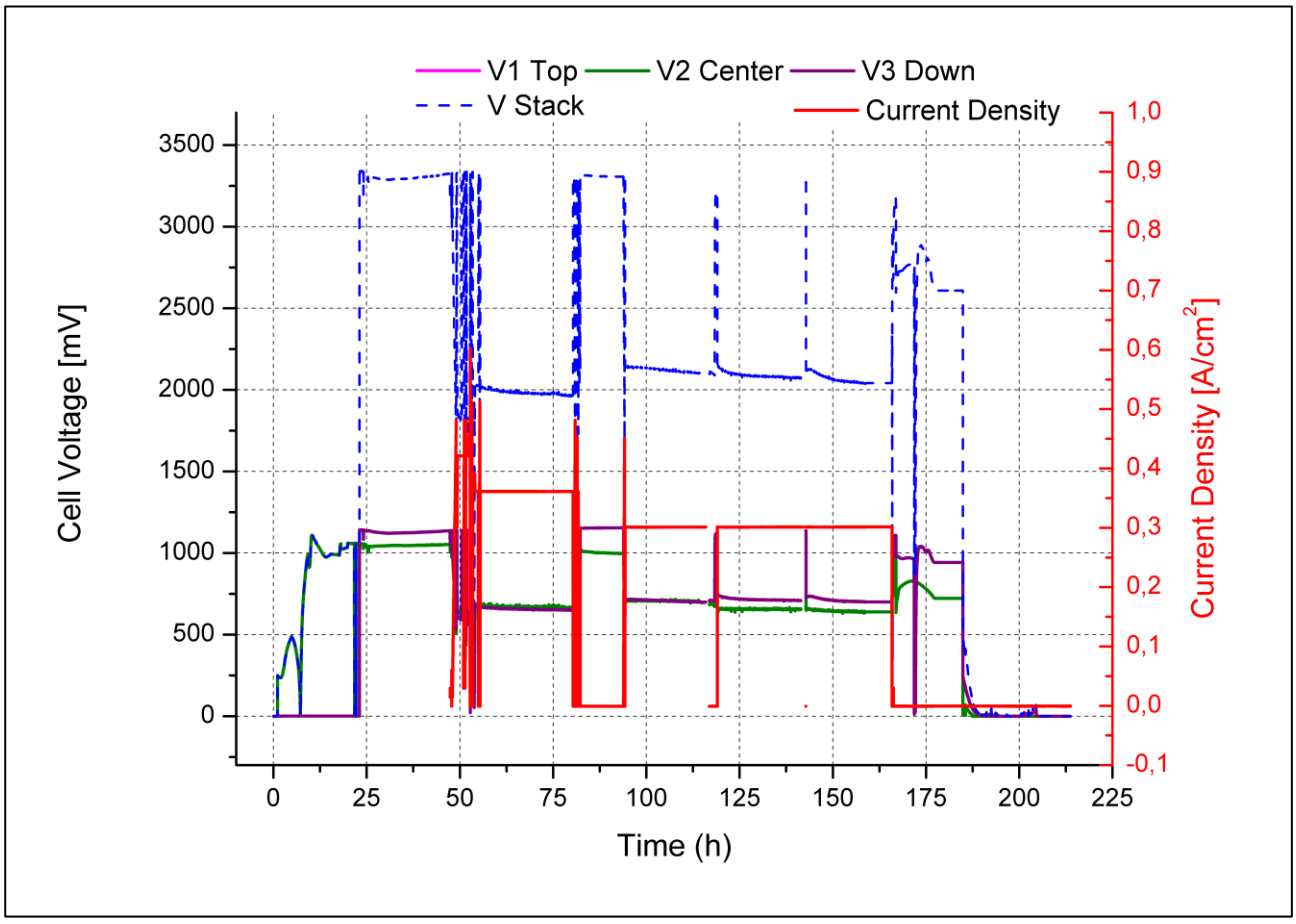

Figure 4-11: I-V curves for the 3 cells of the STACK1

In Figure 4-12, it is possible to note a detrimental effect in the internal fuel dynamic in the stack, especially in case of the response obtained at high current conditions. Also, tests with the same flow rate (H_2: 333 Nml/min; Air: 533 Nml/min per cell) have been performed to investigate the fuel cell degradation during tests completion (200 hours). (See Table 4-3).

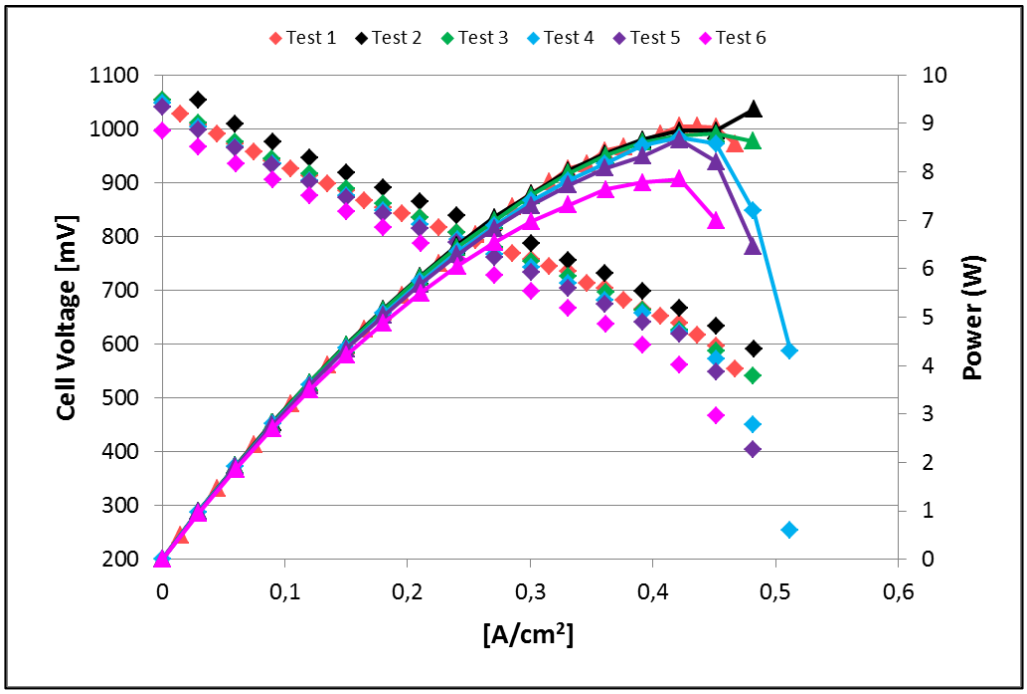

Figure 4-12: I-V curve with the same H2 flow rate (333 Nml/min x cell) to verify the stack performance during all time test.

Additionally, the ASR value of the Stack 1 (3 cells configuration) reported in the Figure 4-13 shows an enhancement at low current conditions. In particular, a significant reduction of ASR values was reached at the end of the test (Test 6) in comparison with the previous ones. Taking into account these results, it is necessary to perform experiments for a higher duration in order to assure the electrodes activation and electrical connections assessment.

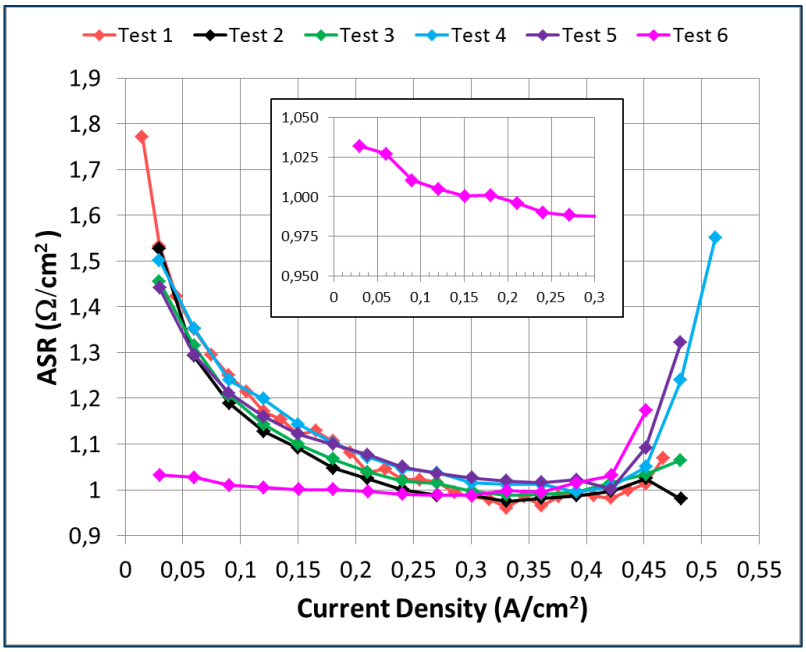

Figure 4-13: Comparison of the ASR values during all time test for stack1

4.4 **Test IV:** Stack on three cell configuration with protective coating fed with simulated reformed biogas.

Scope of this test was to verify the electrical stability of the developed stack in multi cell configuration fed with simulated reformed biogas. This test was executed in the framework of the PRIN2008 project.

One innovation was the modification of a fuel composition, changing the H_2 with a simulated biogas. For this, it was necessary the implementation of a cleaning (desulfurization) and reforming system.

Figure 4-14 shows a scheme of SOFC stack integration with simulated reformer biogas, while Figure 4-15 presents the Piping & Instrumentation Diagram (P&ID) of SOFC stack fed with simulated reformed biogas. This test bench (see Figure 4-16) was developed and built in Energy Department of Politecnico di Torino to operate with the two systems in an independent way to assure the correct functioning of both systems before integration.

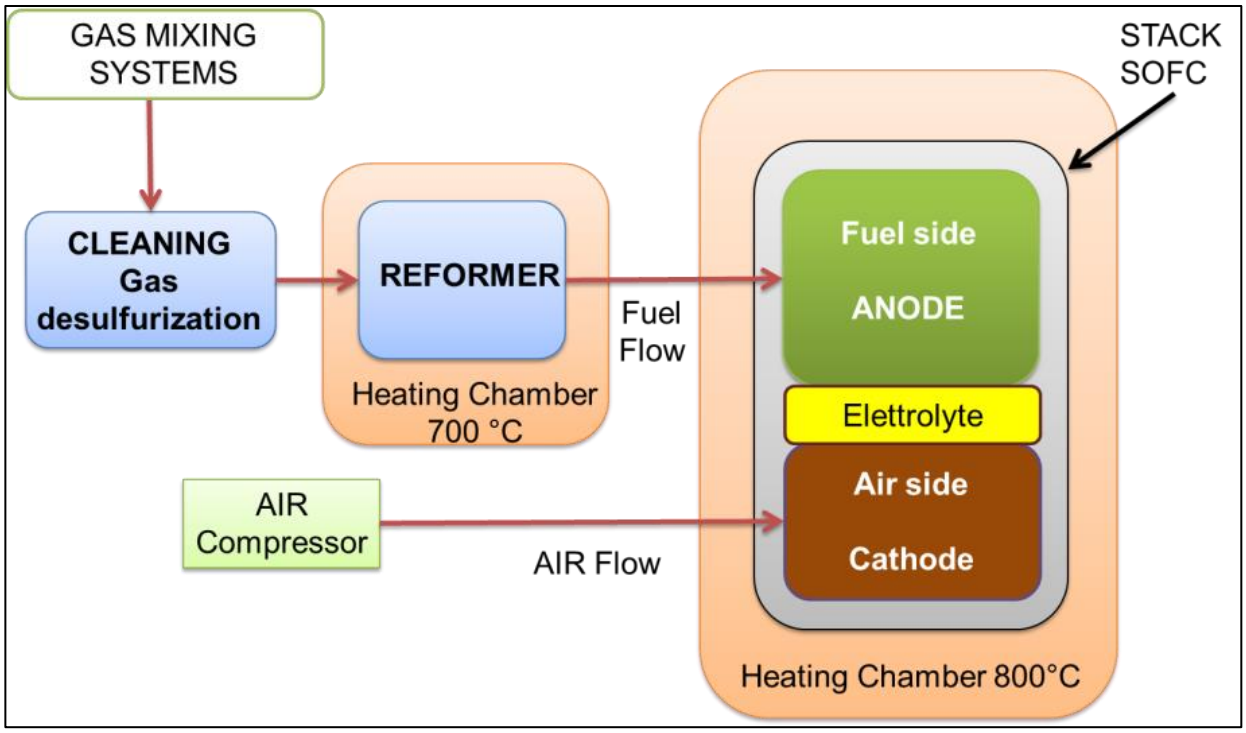

Figure 4-14: Schematic process of SOFC stack fed with simulated reformed biogas.

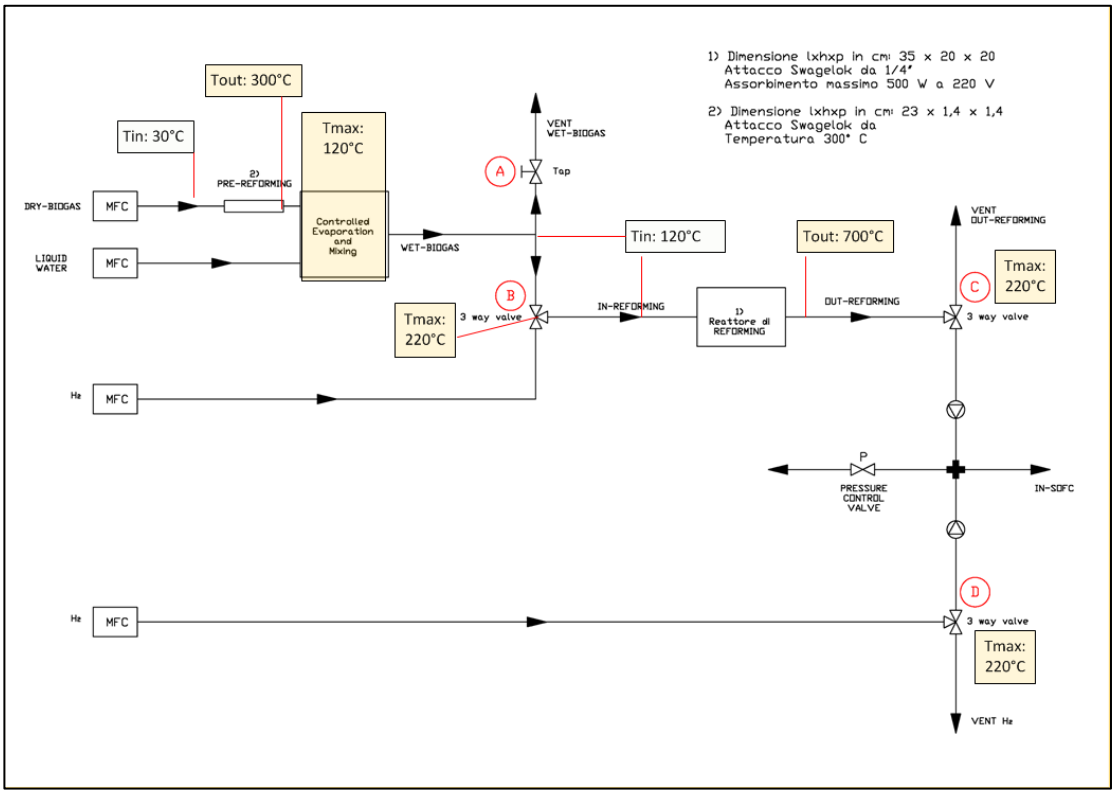

Figure 4-15: Piping & Instrumentation Diagram (P&ID) of SOFC stack fed with simulated reformed biogas

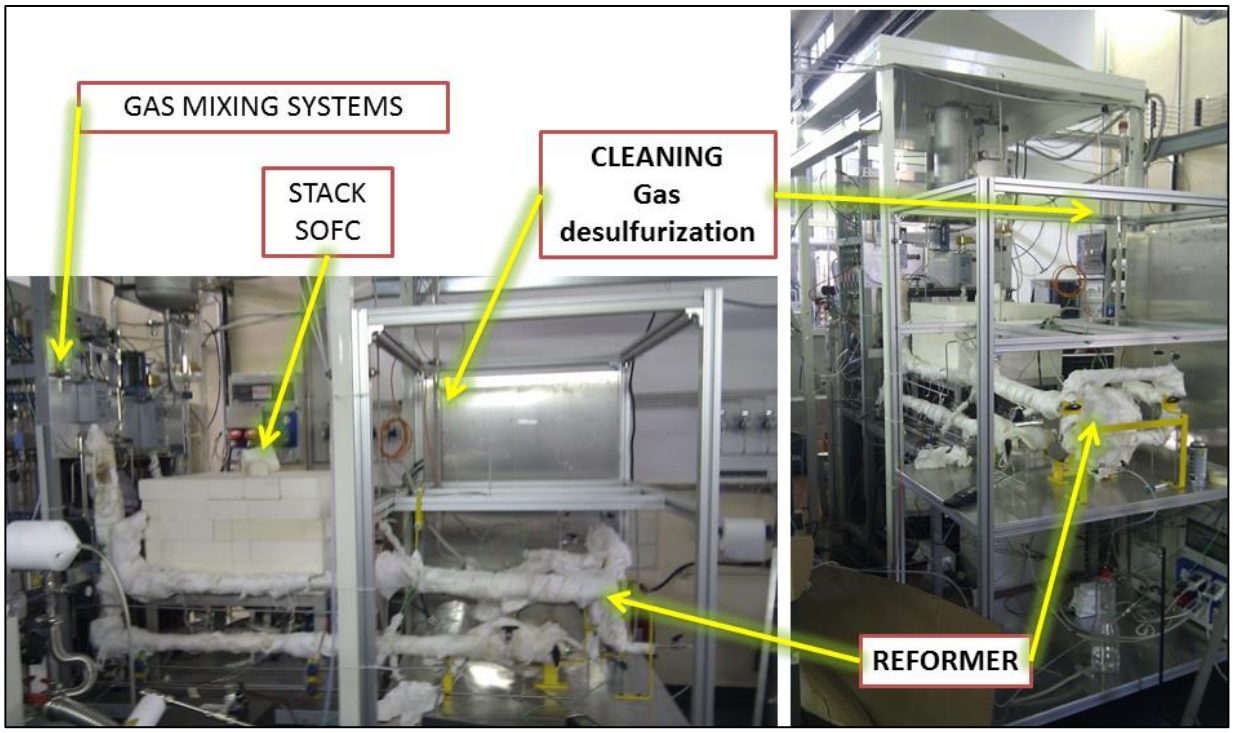

Figure 4-16: Test Bench Developed by Energy Department of Politecnico di Torino for tested SOFC stack fed with different fuel.

Figure 4-17 notices the electrochemical performance of the Stack2. In the first part of the test, the stack was fed with H_2 and next it was integrated with the simulated reformer biogas system. Electrical stable conditions were obtained for more than 500 hours with a current density around 0.1 A/cm^2. The stack and the biogas fuel system were integrated for the last 300 hours of test.

Unfortunately, the hydrogen inlet pipe was broken after 50 hours. The safety system avoids the total damage of the stack, nevertheless two of the three cells were affected: V1 around 80% and V2 (about 40%). Since the cell 3 did not reveal any damage and the reformer properly worked, it was decided to continue the experiment until 500 hours.

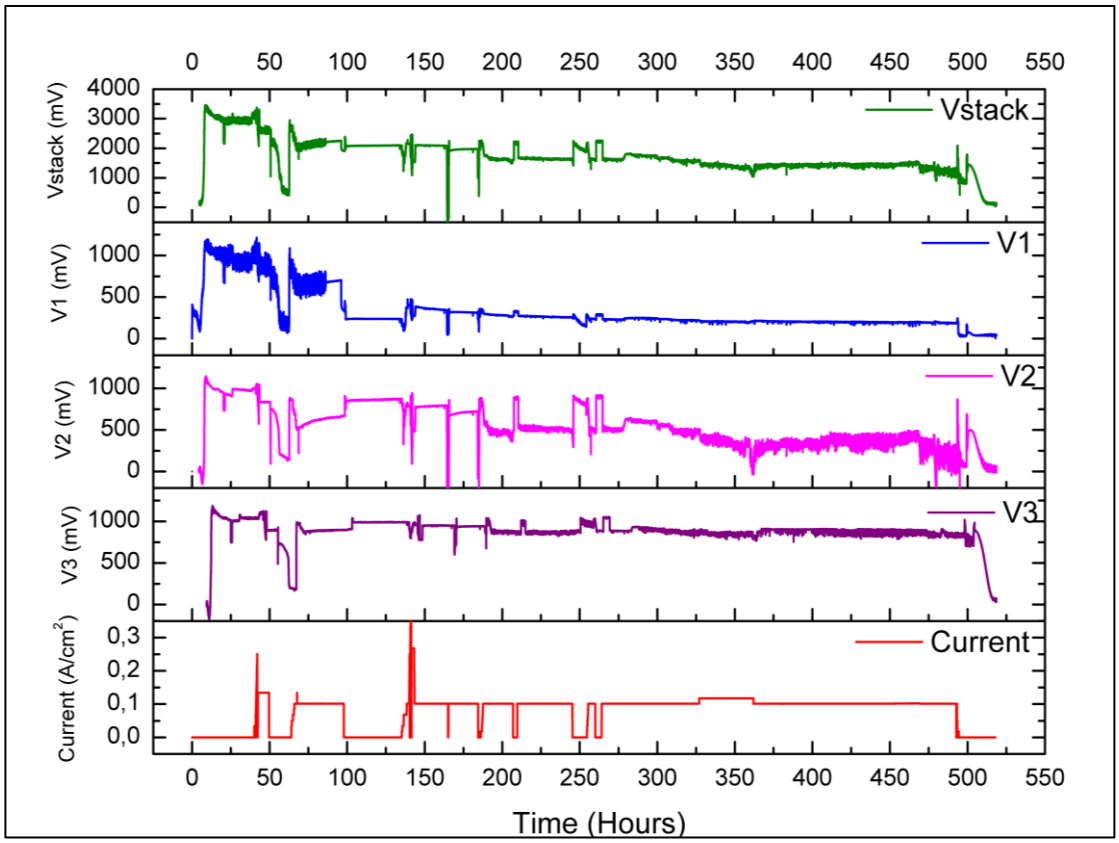

Figure 4-17: Galvanostatic performance for > 500 h in Stack2.

This test was satisfactory completed regard to the integration of both systems, as can be seen in Figure 4-18, where it is possible to note the inlet and outlet gases in the critical point of the system (simulated biogas, cleaning, reformer and stack).

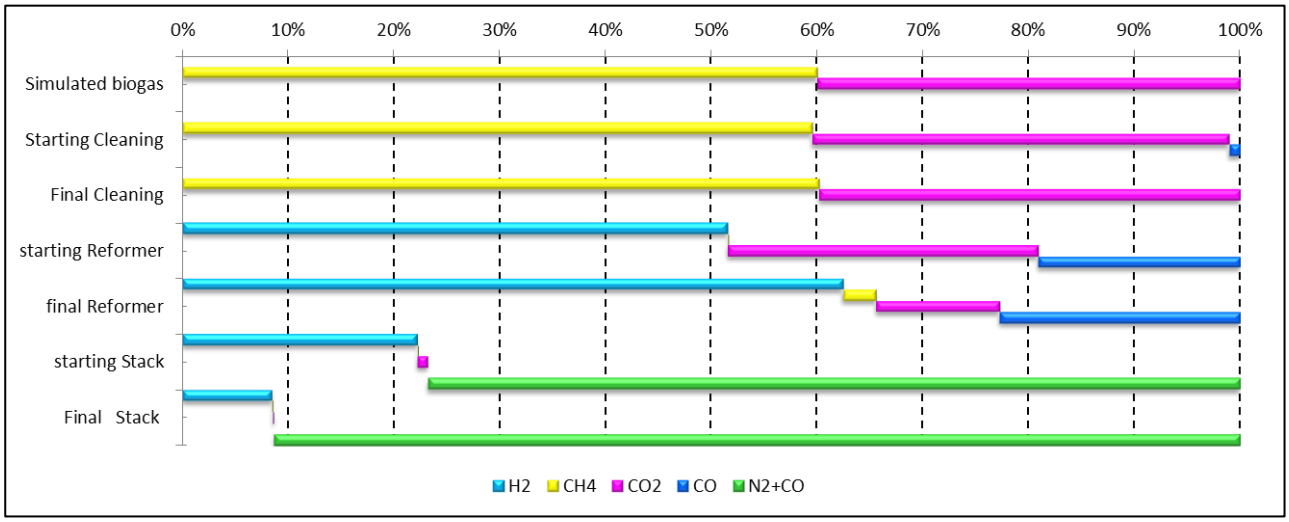

Figure 4-18: Gases composition during the SOFC stack integration phases with simulated biogas system.

In fact, the desulphurization and reforming system satisfactorily worked due to they allow feed the SOFC stack as seen in Table 4-4, where the simulated biogas polluted with sulfur was cleaned (desulphurization) and the reformer converted the CH_4 into CO_2

Table 4-4: Gases composition during the SOFC stack integration phases with simulated biogas system.

		Cleaning section		Reformer		Stack	
	Simulated biogas	**Starting Cleaning**	**Final Cleaning**	**starting Reformer**	**final Reformer**	**starting Stack**	**Final Stack**
H_2	0,00	0,00	0,00	51,50	62,39	22,19	8,47
CH_4	60,00	59,17	59,89	0,02	3,16	0,01	0,04
CO_2	40,00	39,19	39,64	29,34	11,66	0,98	0,18
CO	0,00	1,09	0,00	19,14	22,78	0,00	0,00
N_2+CO	0,00	0,00	0,00	0,00	0,00	76,87	91,32
H_2S (ppmv)	32,07	0,00	0,00	0,00	0,00	0,00	0,00

SOFC Stack Characterization

The short-stacks tested were submitted to post mortem examination and the respective results, in terms of mechanical structure, material compatibility and durability are analyzed are presented and analyzed in this Chapter. Other aspect that was studied regards the cathode protection from Cr poisoning by means of a protective coating. The conditions used during testing of short stacks are summarized in Table 4.1.

Figure 5-1 shows the prototypical SOFC stack before and after testing. It is evident the oxidation occurred in housing plates and bolts. In consequence, another stainless steel should use with better performances at high temperatures (800°C) not only from corrosion resistance point of view but also with a good mechanical stability and durability.

BEFORE	AFTER
	
	

Figure 5-1: Developed SOFC stack: before & after testing

The housing material was stainless steel AISI 316L. This alloy offers higher creep, stress-to-rupture, and tensile strength at elevated temperature. In addition, L-graded (low carbon content) is resistant to sensitization (precipitation of chromium carbide along the grain boundaries) in short-term exposures at high temperatures [56]. The sensitization phenomenon results in susceptibility to intergranular corrosion, since the grains become depleted in chromium and lose their corrosion resistance (see Figure 5-2). The intergranular corrosion susceptibility occurs during long term exposures at elevated temperatures (400-850°C). This explains the material degradation observed in housing plates and bolts after long thermal cycling tests.

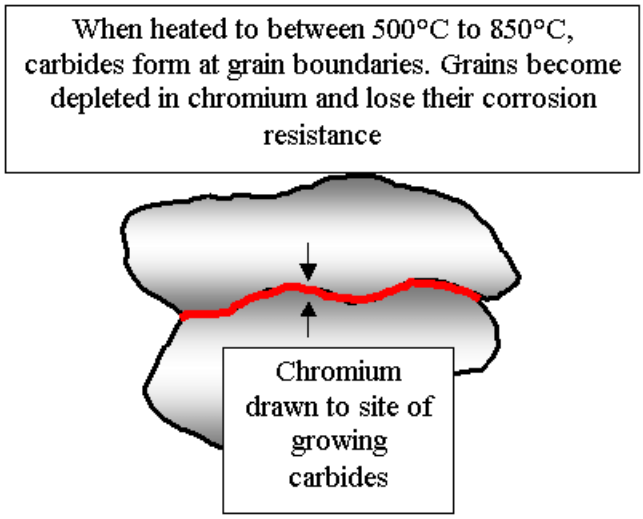

Figure 5-2: Scheme of the sensitization phenomenon in austenitic stainless steel.

A solution could be to replace the AISI 316L with AISI 316Ti, which is a Titanium stabilized graded. This proposal looks for the prevention of intergranular corrosion, since incorporating strong carbide formers or stabilizing elements such as titanium or niobium in the stainless steels. These elements have a much greater affinity for carbon than chromium, then, carbide formation with these elements reduces the carbon available in the alloy for formation of chromium carbides. The Table 5-1 shows the chemical composition differences between these alloys.

Table 5-1: Chemical composition of AISI 316, 316L and 316Ti [*from IMS S.p.a.*]

AISI 316							
C	Mn	Si	Cr	Ni	Mo	N	Others
≤0.070	≤2.00	≤1.00	16.50÷18.50	10.00÷13.00	2.00÷2.50	≤0.11	S≤0.030 P≤0.045
AISI 316L							
C	Mn	Si	Cr	Ni	Mo	N	Others
≤0.030	≤2.00	≤1.00	16.50÷18.50	10.00÷13.00	2.00÷2.50	≤0.11	S≤0.030 P≤0.045
AISI 316Ti							
C	Mn	Si	Cr	Ni	Mo	Ti	Others
≤0.080	≤2.00	≤1.00	16.50÷18.50	10.50÷13.50	2.00÷2.50	5xC÷0.70	S≤0.030 P≤0.045

On the other hand, the bolts material is the same for the housing plates. The main issue is related to the loss of tightening torque at elevated temperatures, although the applied

torque took into account the calculated torque at ambient and at 800°C. The stack is subjected to thermal cycling that does not allow an appropriate control of the compression system when 800°C are reached. Considering this aspect, another compression system (e.g: braces) could be used for having better control.

The effect of the tightening torque loss can be appreciated in Figure 5-3, due to the oxidation signs presented in the compressive seal gaskets, which were subsequently reduced by H_2. In this way, leakages between the housing and the end plate interconnect is evident. The gases could leak during the cooling phase of the stack, because the bolts are shrunk by thermal effects losing then the tightening torque.

It is also possible that leakages occur during testing. In particular, the temperature increases after the application of electrical current, due to the Joule effect.

In order to enhance the stack performance, it would be necessary to optimize or developed a new compression system which can guarantee a good control of tightening torque to avoid leakages.

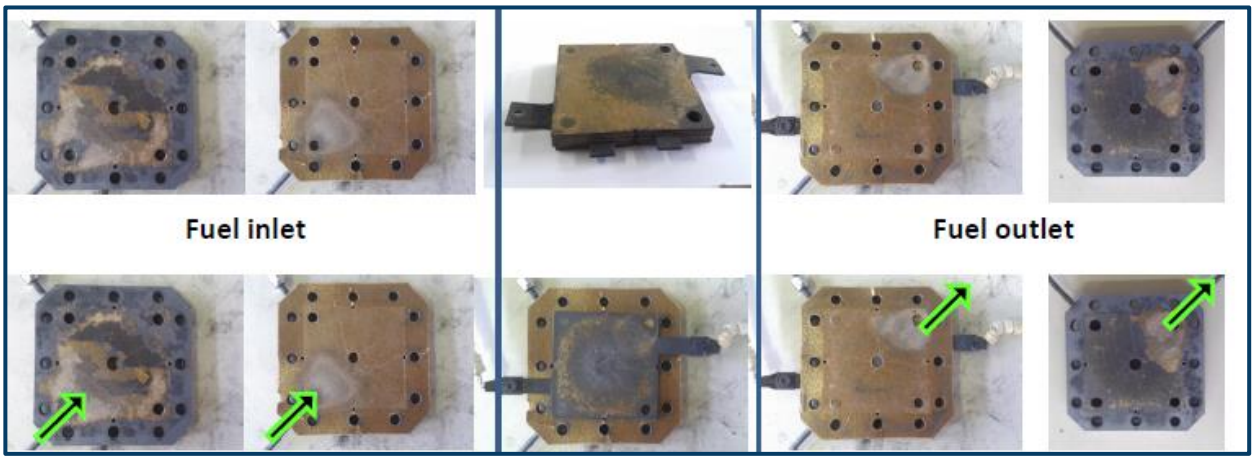

Figure 5-3: Housing plates after stack disassembly

5.1 POST MORTEM ANALYSIS ON m1STACK

Figure 5-4 shows a schematic cross section view of the ASC cell joined to the Crofer22APU frame (submitted to 250 hours of tests in m1STACK), that has been cut in

different zones and sections. The sketch reported in Figure 5-4 will be used as a reference for post mortem analyses of the tests described above.

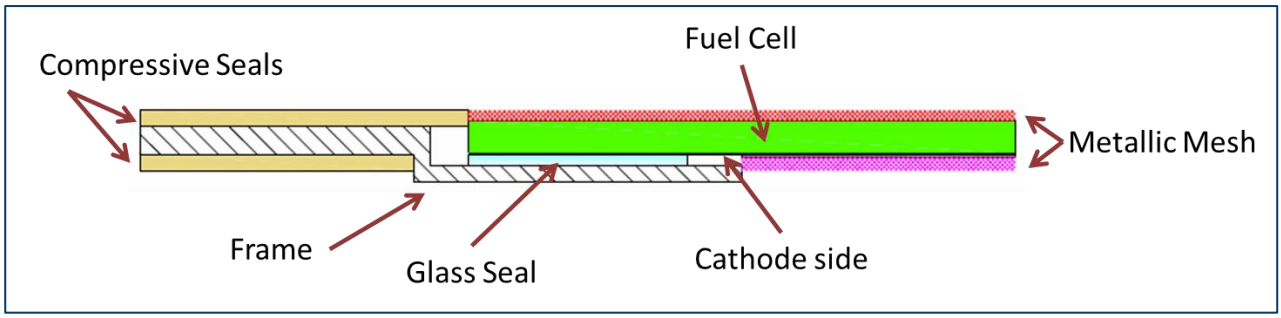

Figure 5-4: Schematic cross section view of the ASC cell joined to the frame

Figure 5-5a, shows a SEM cross section of Crofer22®APU/glass-ceramic sealant after 250 hours of m1STACK test. The interface between the glass-ceramic sealant and the Crofer®22APU is homogenous, free of cracks and voids; the preoxidation layer on the Crofer®22APU is still visible. No elements (Cr and Mn) diffusion was detected into the glass-ceramic sealant, as demonstrated by the EDS elements mapping reported in Figure 5-6.

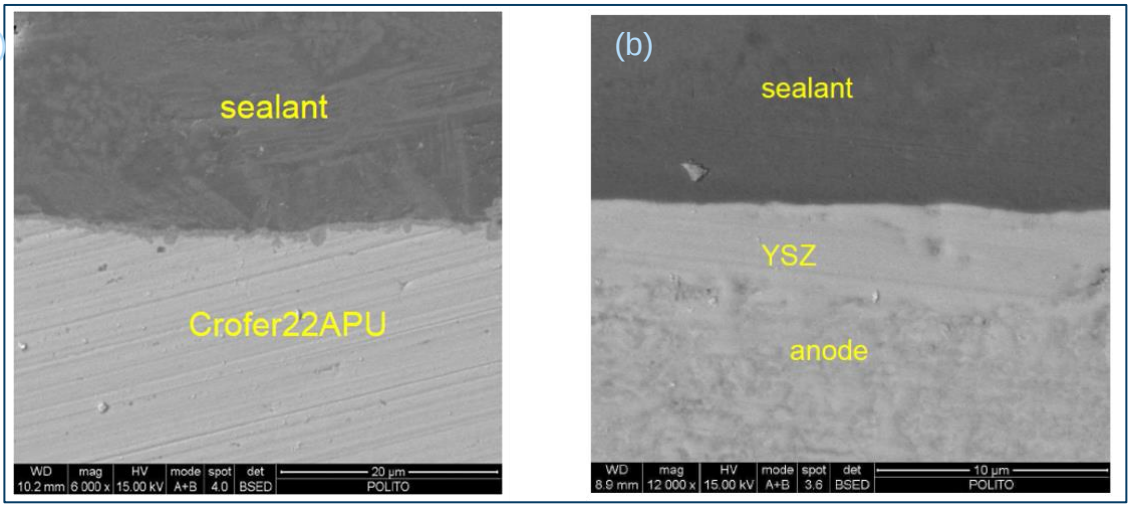

Figure 5-5: SEM cross section of Crofer22APU/glass-ceramic sealant after 250 hours of m1STACK test.

Figure 5-5b, shows the SEM cross section of YSZ/glass-ceramic sealant interface; it can be observed that the interface is still sound and continuous and the very thin YSZ electrolyte (5 µm) is not cracked.

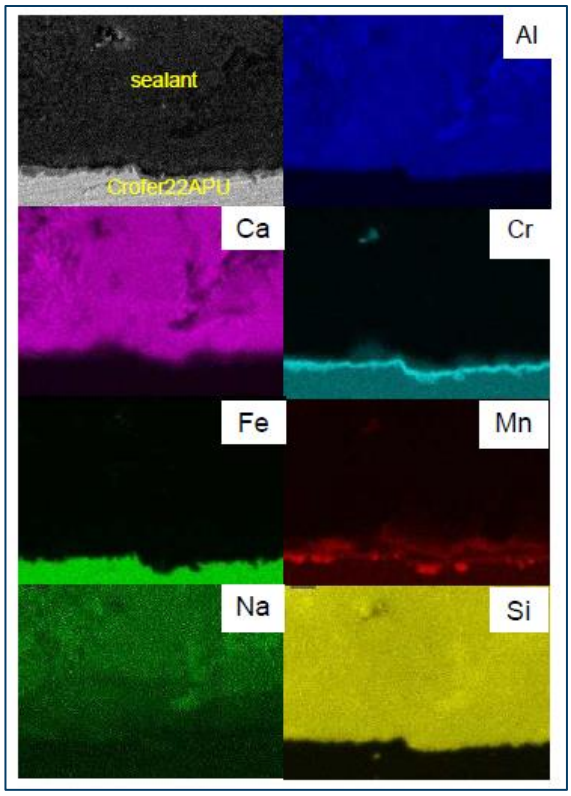

Figure 5-6: SEM and EDS analyses Crofer22APU/glass-ceramic sealant/air side three phase boundary

Further SEM and EDS analyses were focused at the Crofer22®APU/glass-ceramic sealant/air side three phase boundary. The microstructure at the edges of the samples around the glass-ceramic sealant/Crofer®22APU interface was also investigated in order to examine the presence of any corrosion products. The SEM micrograph reported in Figure 5-7 did not reveal any anomalous corrosion of the Crofer®22APU interconnect.

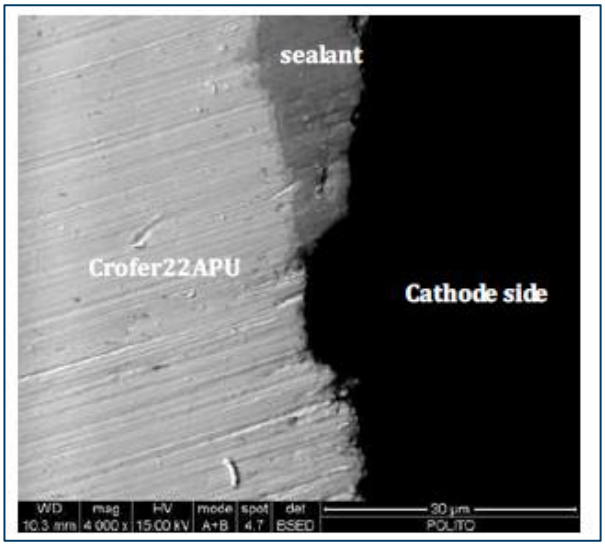

Figure 5-7: SEM micrograph Crofer22APU interconnect

Examinations on the cathode area close to the interface with YSZ are reported in Figure 5-8 a and b and show the Mn, Cr spinel oxide faceted crystals deposited on the LSM cathode surface; these faceted crystals contain manganese and are generally considered to be a spinel phase.

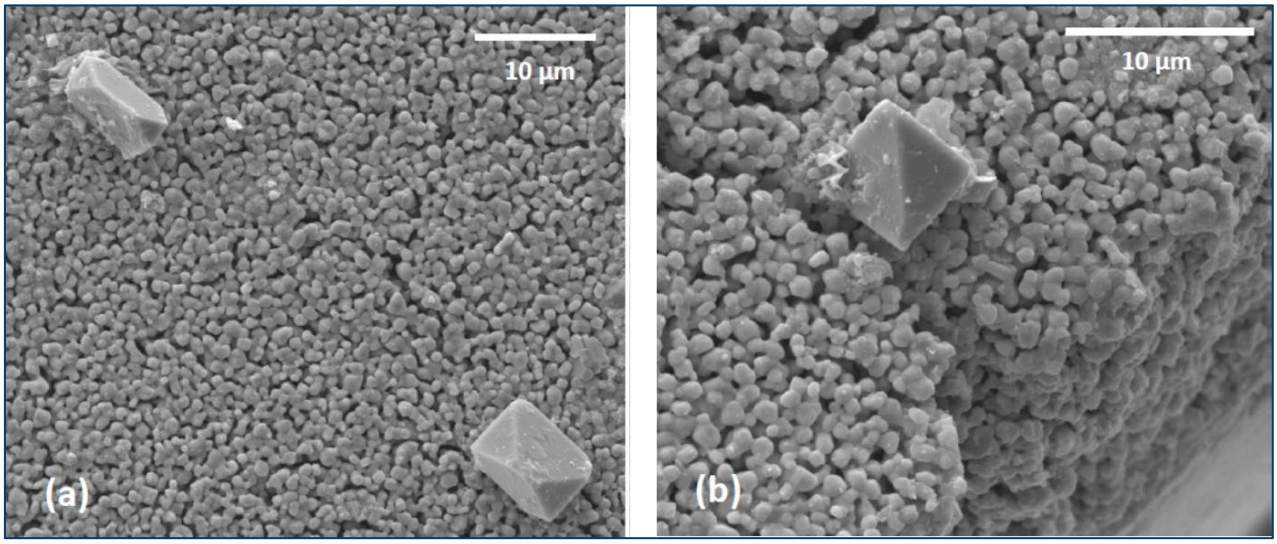

Figure 5-8: (a) and (b): Faceted crystals formed on the cathode surface after m1stack test.

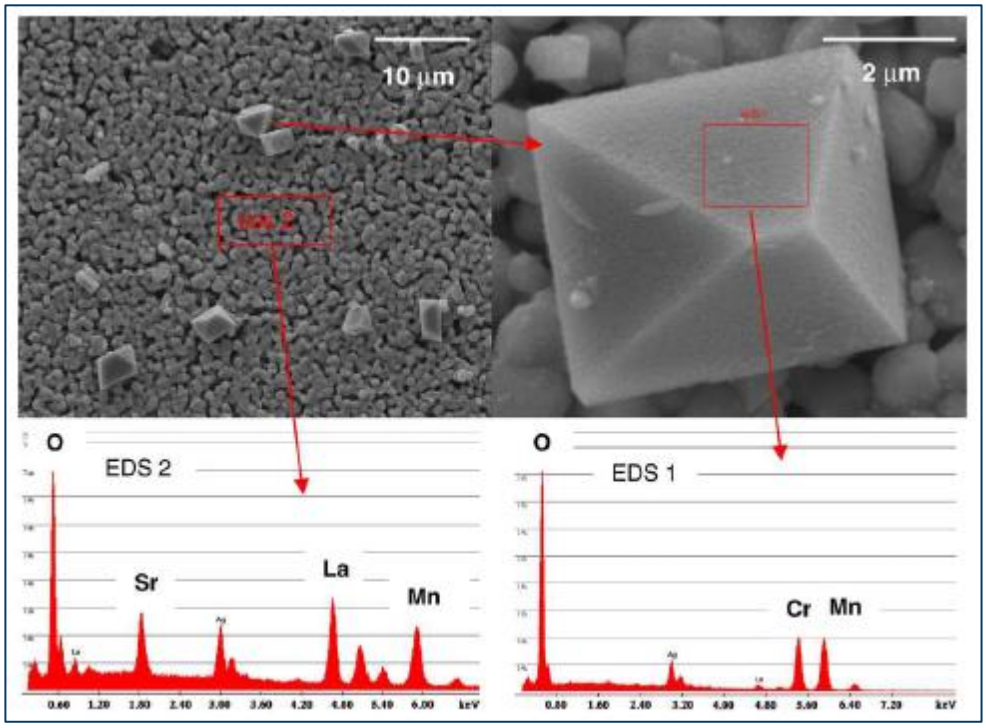

Figure 5-9: SEM cross-section of the SRU (area A) after thermal ageing experiments

Figure 5-9 shows a LSM cathode top view, close to the electrolyte interface: some deposited crystals can be observed on the cathode surface. EDS analysis conducted on these crystals revealed the presence of chromium, manganese and oxygen suggesting the formation of a $(Cr, Mn)_3O_4$ spinel phase.

In fact, one of the major degradation mechanisms in SOFCs is cathode poisoning by chromium from vaporization of the metallic interconnect [57]. The chromium transport occurs primarily through the formation of Cr^{6+} containing species, such as CrO_3 or $CrO_2(OH)_2$, from oxidation of chromium oxide in the interconnect [58]. This phenomenon degrades the performance of the cathode under polarization, because it causes associated chemical changes of the LSM phase as well the new spinel phase formation occurs. Furthermore spinel blocks pores and thus impedes the oxygen reduction required for the function of the cell. Chromium poisoning has been observed in chromium-based [59], nickel-based [60] and iron-based [61] interconnect alloys. In order to avoid this phenomenon, a protective coating was deposited on the interconnector of m2stack, as found in the next section.

5.2 POST MORTEM ANALYSIS ON m2STACK

This test is different from m1STACK, because of the presence of $Mn_{1.5}Co_{1.5}O_4$ coating on Crofer22APU frame and on Crofer22APU pins. We report a brief description of the coating preparation and characterization. A thin $Mn_{1.5}Co_{1.5}O_4$ coating (1µm) was deposited on Crofer22APU using thermal co-evaporation technique, followed by heat treatment in oxygen. The produced coating (see Figure 5-10) exhibited a dense crystalline structure with grain size of about 200 nm. The coating/substrate interface is continuous and pores free; the coating average thickness is 1µm. Further details related to the coating fabricating technique and results are reported in [55].

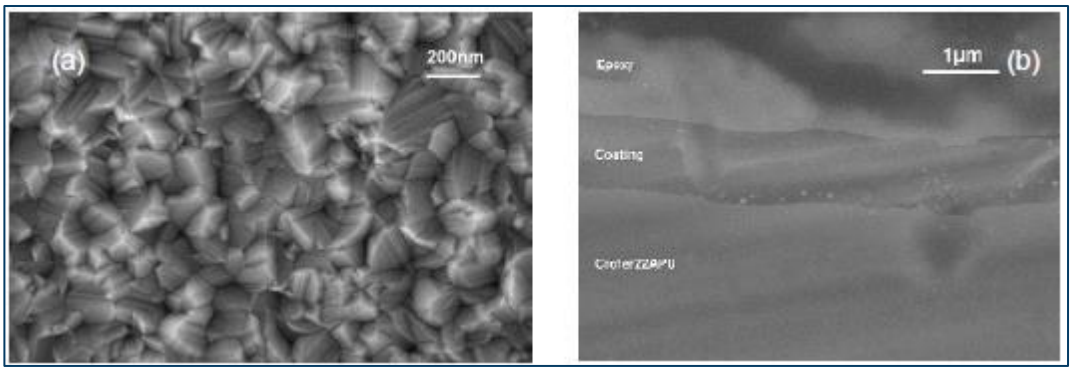

Figure 5-10: FESEM plane and cross section view of $Mn_{1.5}Co_{1.5}O_4$ coated on Crofer22APU

The compatibility of the $Mn_{1.5}Co_{1.5}O_4$ coating with the glass-ceramic sealant was preliminary tested; SEM cross section of the as prepared SACN glass ceramic sealant on $Mn_{1.5}Co_{1.5}O_4$ coated Crofer22APU is shown in Figure 5-11. The interface between the glass ceramic sealant and the $Mn_{1.5}Co_{1.5}O_4$ spinel coating on Crofer22APU is continuous and crack free, due to a good thermal expansion coefficient match of the glass ceramic sealant (10.7×10^{-6} C^{-1}) with that of $Mn_{1.5}Co_{1.5}O_4$ spinel (10.8×10^{-6} C^{-1}) coating on Crofer22APU.

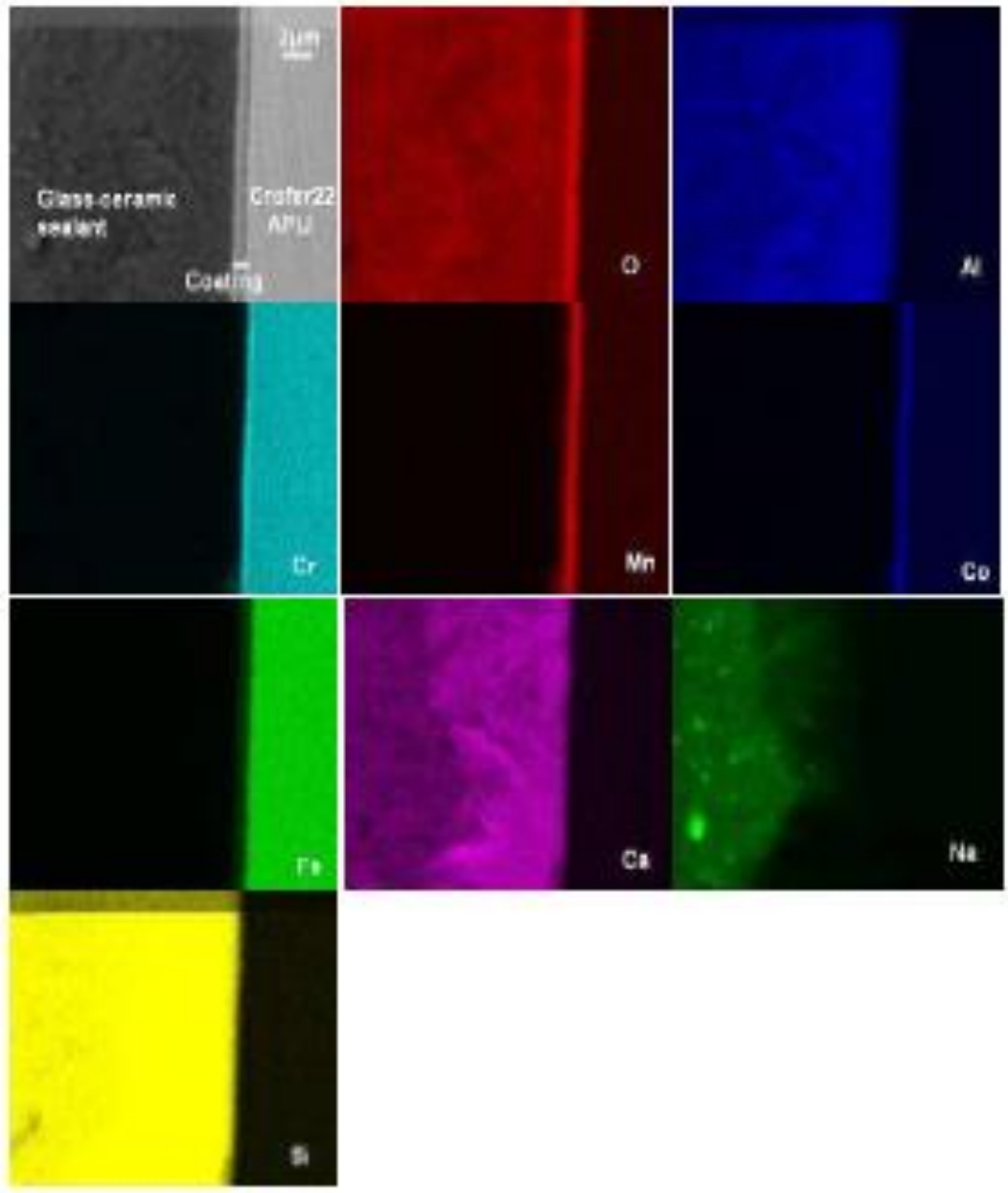

Figure 5-11: SEM cross section. Interface between the glass ceramic sealant and the $Mn_{1.5}Co_{1.5}O_4$

Nevertheless, for the assembly of the m2STACK it was decided to deposit Mn1.5Co1.5O4 coating on Crofer22APU frame only in the area not in direct contact with the glass-ceramic sealant. The glass-ceramic sealant was subsequently deposited in direct contact with the preoxidised Crofer22APU.

The stack was stable for more than 300 hours (under electrical load) and without apparent degradation. As in the case of m1STACK test. The interfaces between the glass-ceramic sealant and both the Crofer22APU and YSZ are homogenous, free of cracks and voids, as reported in Figure 5-12 a and b respectively.

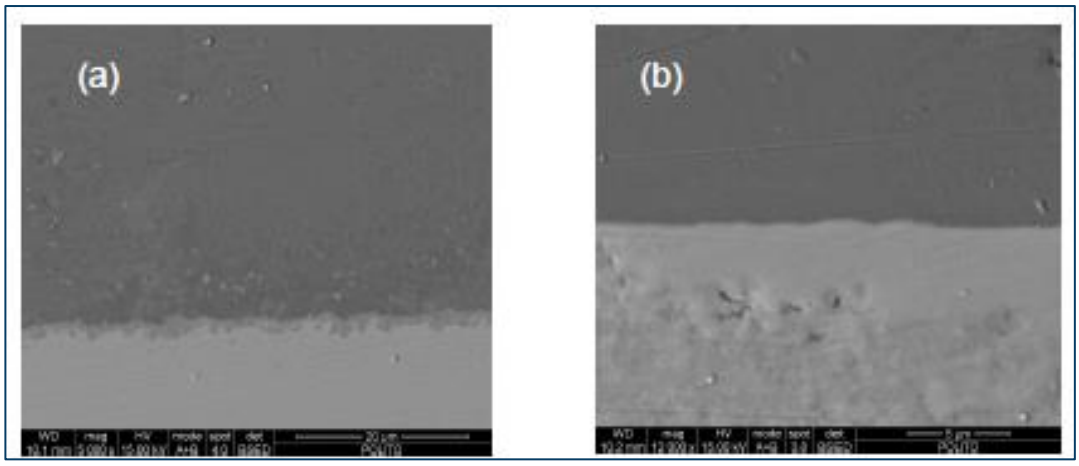

Figure 5-12: The interfaces between the glass-ceramic sealant and both the Crofer22APU and YSZ

It must be highlighted that SEM investigations carried out on the cathode surface did not reveal the presence of the Mn Cr spinel oxide faced crystals, as reported in Figure 5-13; this was an experimental evidence of the effectiveness of the $Mn_{1.5}Co_{1.5}O_4$ spinel coating on Crofer22APU, thus preventing cathode Cr poisoning

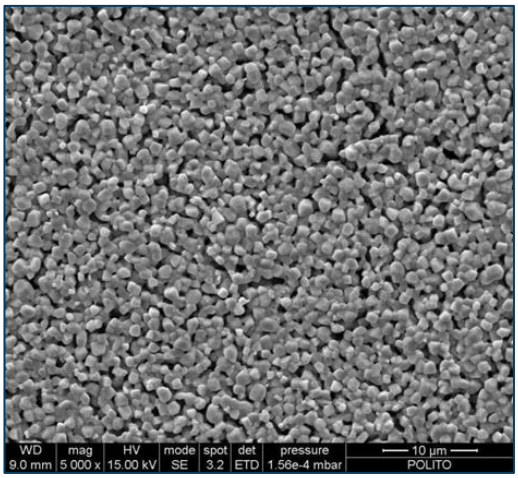

Figure 5-13: The Mn1.5Co1.5O4 spinel coating on Crofer22APU

5.3 POST MORTEM ANALYSIS ON STACK 1 (3 cells configuration) test

Figure 5-14 show a picture of the stack after the disassembly. Mica adhesion to the surface of the Crofer22APU plate is evident.

Figure 5-14: STACK 1 after the disassembly

Figure 5-15 shows a picture of the frame of the top cell in the stack after disassembly; glass-ceramic sealant (white) is evident only in some areas, the remaining glass ceramic sealant was found to be on the cell side, still adherent to the YSZ electrolyte.

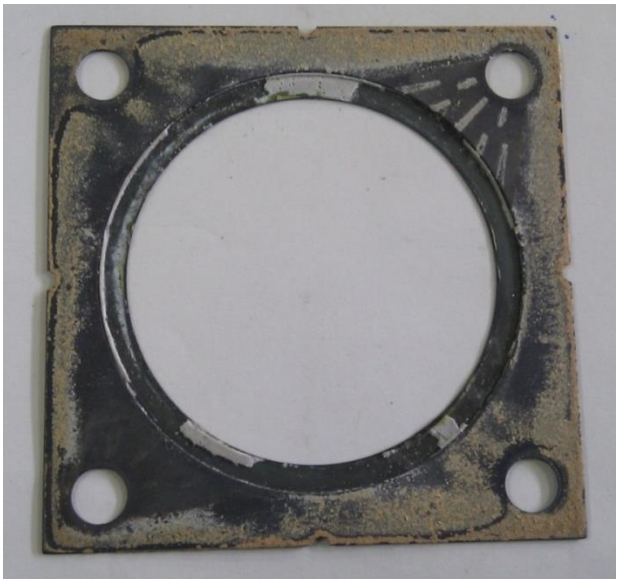

Figure 5-15: Top view of the frame cell 1 in the STACK 1

As in the case of the previously described post mortem tests, it was decided to cut small samples in the most significant areas; a SEM magnification of Crofer22APU and the glass-ceramic sealant at the 3-phase boundary (at the cathode side) is reported in Figure 5-16, showing a good adhesion of the sealant to the Crofer22APU.

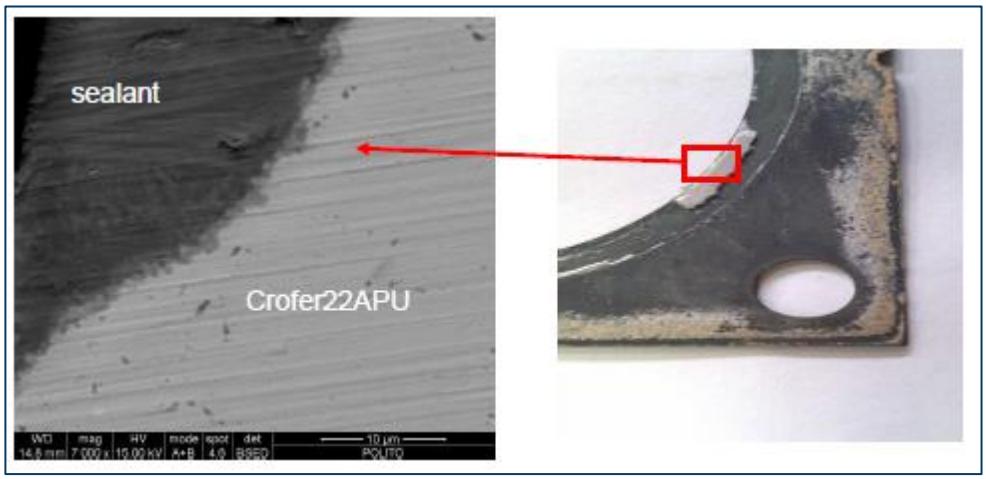

Figure 5-16: SEM magnification of Crofer22APU and the glass-ceramic sealant at the 3-phase boundary

SEM magnifications of the red and the blue area respectively are reported in Figure 5-17

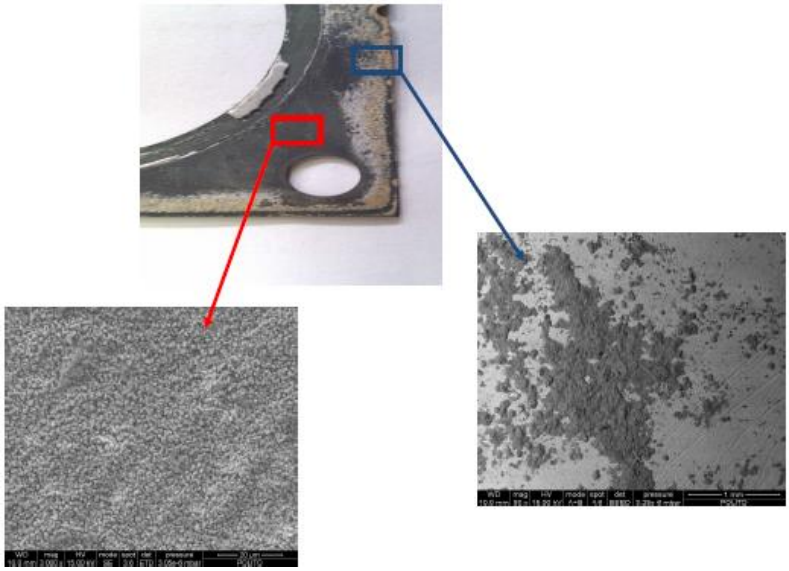

Figure 5-17: Top view magnifications of the frame

The SEM magnification of the blue area clearly shows the residual mica stick to the $Mn_{1.5}Co_{1.5}O_4$ coated Crofer22APU frame. The magnification of the red area show the

$Mn_{1.5}Co_{1.5}O_4$ coating on the Crofer22APU; the coating microstructure is seen to be homogenous and without defects.

Figure 5-19 shows the top view of the LSM cathode/YSZ interface, where no Mn, Cr spinel oxide crystal were observed, thus demonstrating an effective protection of the $Mn_{1.5}Co_{1.5}O_4$ coating against Cr cathode poisoning. It is important to mention that the verification of Cr presence was done at the cathode/electrolyte interface, because after the chromium evaporation occurs from the interconnect surface, a gas transport of chromia vapour contacts the cathode surface (interconnect/cathode interface), then it reacts and it diffuses into cathode until reduction and deposition occurs at cathode/electrolyte interface as schematically is illustrated in Figure 5-18.

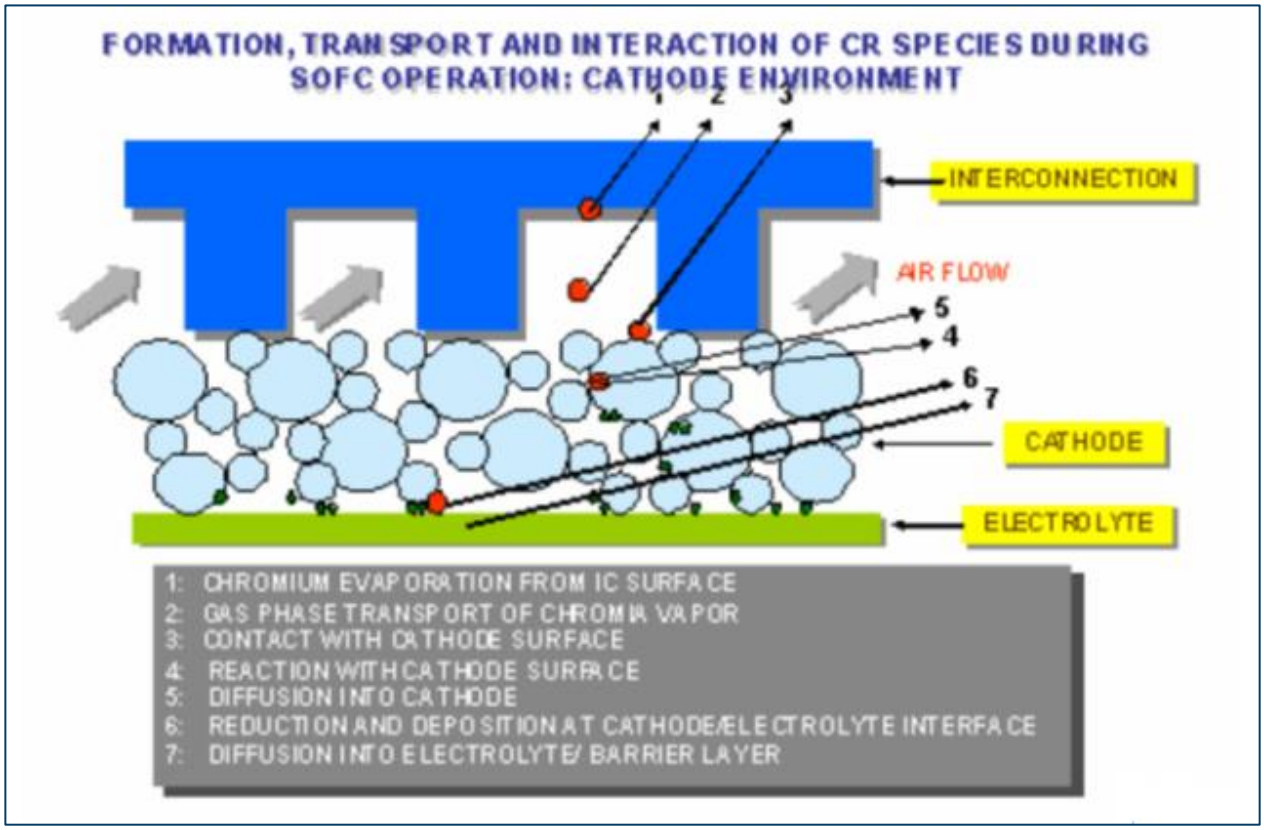

Figure 5-18: Scheme about formation, transport and interaction of Cr species during SOFC operation.

Figure 5-19: Top view of the LSM cathode/YSZ interface

Post-mortem examinations were conducted on different areas of the Crofer22APU frame/glass-ceramic sealant/ASC cell.

The stack was stable for more than 300 hours (under electrical load) and without apparent degradation. The interfaces between the glass-ceramic sealant and both the Crofer®22APU and YSZ are homogenous, free of cracks and voids.

Conclusions

In this PhD thesis, a planar Solid Oxide Fuel Cell stacks were designed, built, tested and analyzed. This investigation was carried out in the framework of the Regional Project “The Design and in-house development of Solid Oxide Fuel Cell (SOFC) stacks for dealing with multiple fuels” (MULTISS) and the National Project PRIN2008.

The general objective consisted in the development and in-house production of SOFC short-stacks of planar anode-supported geometry for dealing with multiple fuels. In consequence, the following main activities were done and the respective conclusion can be drawn:

1. Determination of the stack geometry by means of test of commercial anode-supported cell (“ASC3” NiO/YSZ anode, YSZ electrolyte, LSM cathode).

   Preliminary comparisons were made between circular cells and square cells varying the inlet and outlet size This study was done by using a numerical modeling (see Appendix A) of flowfield in interconnect plates. This activity was carried out in the framework of MULTISS Project. The results showed that the corner regions are the worst ones in term of fluid distribution. Then, the cell circular geometry was selected.

   The tests were done by using a commercial cell anode-supported type (ASC3) from H.C. Starck with diameter of 80mm for anode and electrolyte, while the diameter of 70 mm was used for the cathode. In this way, there was a gap of 10mm for the glass ceramic seal to join the cell with the frame. Additionally, the other stack components will have a square geometry to facilitate their manufacturing process and to reduce cost.

2. Materials selection of stack components (interconnectors, housing, frame, compressive and bonded seals), according to compatibility at high temperatures (800°C) in terms of thermal expansion, stack mechanical structure, degradation and electrical characteristics (insulator or conductor).

   The material chosen for the interconnector and the frame was a ferritic stainless steel known as Crofer® 22APU. At temperatures up to 900°C a chromium-manganese oxide layer is formed on the surface of Crofer ® 22APU which is thermodynamically very stable and possesses high electrical conductivity. The low coefficient of thermal expansion (11.9 $\cdot 10^{-6}$/K) is matched to that ceramics typically used for high temperature fuel cells in the range from room temperature to 800°C.

   The housing material utilized was stainless steel AISI 316L. This alloy offers higher creep, stress-to-rupture, and tensile strength at elevated temperature. In addition, it is resistant to sensitization (precipitation of chromium carbide along the grain boundaries) in short-term exposures at high temperatures. The sensitization phenomenon results in susceptibility to intergranular corrosion during long term exposures at elevated temperatures (400-850°C). This explains the material degradation observed in housing plates and bolts after long thermal cycling tests.

   With respect to the compressive seals, two types were selected to guarantee a proper gas tightness and electrical insulation. The first one was Thermiculite® 866 (Flexitallic, UK) placed between the frame and the interconnect plate; whereas the second one was Flexible Mica Paper (Fuel Cell Materials) positioned between the interconnect endplate and the housing.

   On the other hand, the bonded seal used to hermetic join the frame with the electrolyte was developed by DISAT Politecnico di Torino in the framework of MULTISS Project. This research group has widely experience in glass ceramic based materials. In fact, they developed a new sealant based on sodium-calcium-aluminum-silicate-glass ceramic, which has a thermal expansion coefficient of 10.7 x 10^{-6} $°C^{-1}$. This value is compatible with YSZ and Crofer® 22APU substrates.

3. Design, development and production of short-stack components adapted on planar ASC3 cell:
   - Frame in stainless steel Crofer®22APU to join the cell with SiO_2-CaO-Al_2O_3-Na_2O sealant providing an effective gas stream separation between the anode and cathode side.

The performance of a glass-ceramic sealant in two SOFC short stack configurations was tested and evaluated. The glass-ceramic sealant demonstrated an excellent chemical and thermo mechanical compatibility with both Crofer®22APU and YSZ components providing excellent hermeticity.

- Interconnect in stainless steel Crofer22APU taking into consideration the following aspects from the numerical modeling developed at DENERG Politecnico di Torino in the framework of MULTISS project:
    - Two flow fields (pins and channels) to prevent shadow effect at high current density were calculated.
    - The inlet and outlet gases dimensions were calculated to facilitate the fuel and air distribution in order to minimize the ohmic losses due to contact resistance.
    - The flow configuration selected for the bipolar interconnects was cross-flow fluid configuration, which is usually utilized to feed standard circular cells.

- Deposition of coating on interconnect surface for cathode protection from Cr poisoning. The coating based on $Mn_{1.5}Co_{1.5}O_4$ was developed by Edison Research & Development Center, Edison S.p.A, in the framework of MULTISS project.

- For the Housing plates, the loss of tightening torque at elevated temperatures, although the applied torque (50N) took into account the calculated torque at ambient and at 800°C.

4. Building of short planar anode-supported SOFC stacks. This activity was focused on the implementation of innovative and simple procedures, which allowed power capacity scale-up in accordance to power requirements.

5. Performance and electrochemical testing of short stacks under steady state conditions. It were tested two different configurations as mentioned below:

    - One cell configuration. The assembly stack system was tested to evaluate the mechanical structure and material compatibility, thermo-fluid-dynamic field and electrical connection. In addition, the cathode protection from Cr poisoning was examined by means of coating deposition on the interconnect surface. In this

way, a comparison was done between m1stack (without coating) and m2stack (with protective coating). In the m2stack test (where $Mn_{1.5}Co_{1.5}O_4$ coating was previously deposited on Crofer22APU) carried out at ~0.3 A cm^{-2} and an FU of 25%, no voltage degradation was observed during the galvanostatic experiment of 360 h at 800°C.

- Three cells configuration. The system scale-up from the one cell design to a short-stack was verified as well as the system stability thanks to a high duration test.

  In addition, a simulated reformed biogas fuel system (desulfurization and reforming) was integrated to the Stack2. This aspect represents an innovation, since the modification of fuel composition was carried out, by changing from H_2 fuel to simulated biogas.

6. Stacks disassembly and Post mortem characterization of stack components (interconnectors, frame, sealant, protective coating and ASC cells). The mechanical structure, material compatibility, durability and cathode protection from Cr poisoning were examined by using Scanning Electron Microscopy (SEM) and Energy Dispersion Spectroscopy (EDS). This activity was carried out in collaboration with Department of Applied Science and Technology (DISAT) of the Politecnico di Torino and Edison Research & Development Center Edison S.p.A, in the framework of MULTISS project.

Finally, the main conclusions can be drawn as follows:

- The short stack development in a reliable and reproducible way was confirmed.
- It was demonstrated that the assembly procedure was efficient thank to the ease procedure and time reduction in the production of the different configurations.
- SOFC stack assembly feasibility to operate in steady state conditions was demonstrated.
- The protective coating of the interconnector face in contact with the cathode electrode improved the stack stability as demonstrated with testing.
- The power capacity increasing of stack unit was obtained by using a simple scaling procedure.

- The short stack with 3 cells configuration performs and is stable.
- SOFC stack operation with simulated biogas feeding was proved.
- Cleaning gas and reforming system were integrated with SOFC stack in steady state condition for more than 300 hours.

Recommendations and Future works

Some recommendations are mentioned below as a consequence of the lessons learned during this research. In the same way, future works and applications are presented.

- Changing material of housing and bolts from AISI 316L to 310S; which combines excellent high temperature properties with good weldability and ductility, is designed for high temperature service. AISI 310S resists oxidation in continuous service at temperatures up to 1150°C when reducing sulfur gases are not present. This alloy is also used for intermittent service at temperatures up to 1040°C.
- Development of a new compression stacks system in order to automatically control the tightening torque.
- Performing tests of long duration (>1000 h) to verify the stack stability and durability.
- Modeling and design a complete BoP around the SOFC short-stack.
- Energetic and economic analysis of the SOFC introduction in market applications.

A. Appendix

Modeling and design of the single planar SOFC

The CFD analysis for the interconnect definition was carried out in the framework of the Regional Project “The Design and in-house development of Solid Oxide Fuel Cell (SOFC) stacks for dealing with multiple fuels” (MULTISS).[53,62,63]

Modeling plays an important role in this project. The two main goals are:

4 to understand, demonstrate and describe certain phenomena that happen inside the cell and housings difficult to observe during the tests;
5 to perform a large number of virtual tests in order to optimize some aspect or part of the system, such as minimizing pressure drops or improve fluids distribution.

Many post mortem analysis in fact reveal that somewhere the fluid flow was unstable or that temperature values are abnormal in some part of the cell. Intuitive justifications are provided after experimental tests, and through the simulations these hypothesis are confirmed. Furthermore it is possible to circumscribe the main involved phenomena and eventually to perform simulations to emphasize only them. After that, a large number of simulations to research the better configuration or to perform topology optimizations are done.

Modeling solid oxide fuel cells mainly consists in coupling traditional algorithm for solving multi species Navier-Stokes equations with some routine that simulate the electrolyte behavior. In commerce many tools for CFD (computational fluid dynamic) exist, and some of them already provide adequate routines to simulate fuel cells in general and SOFC in particular.

Often the quality of these codes is very high, but two inconvenient have to be underlined: first of all the high (in some cases prohibitive) licensing costs, and second that one can only do what the tools are designed for. This aspect could be a strong limitation in research activities where one wants to simulate only certain phenomena, or develop models that differ from the standard ones, or implement the “wrong physic” to confirm or disprove some hypothesis. Moreover licensing costs represents barren costs in research project because they have to be considered like a consumables and not reusable when project ends. For all these reasons the attention is focused on the OpenFOAM® CFD tool that is open source (no license cost has to be taken into account) and it is fully customizable basing on our needs (middle-high C++ knowledge is necessary). This software provide some precompiled Navier-Stokes solvers for fluid flows and porous media but the multi species mass and thermal transport are not well implemented and no fuel cells

integrated module already exists. In this project the standard code was updated with a new multi species mass transport library developed during the project and an own SOFC code was implemented. Of course part of time was spent for building modeling instrument and not for simulations research. But in this way people that worked in this field obtained an high level formation and they really increase their knowhow both in CFD in general and in SOFC simulations in particular. This represent a long term investment because this knowledge can be fruitfully reutilized in other projects. The large amount of work dedicated to build multi-species transport library and to develop the SOFC code finally converged into a publication.

Modeling single cells presents some difficulties characteristic of the problem. First of all, we have to consider that the domain is limited respect to the real system, and boundary conditions can heavily modify the model behavior and results especially from the thermal point of view. In fact we didn't know the exact temperature distribution around the cell but only some temperature constrains far from it. Furthermore the combustion of the exhausts at the cells border drastically change the thermal field in that zones. Complete system model required too many computational resources and even if we can have them we risk to lose our main target that is the cell simulation and topology optimization. For this reason many isothermal simulation were performed that give us acceptable results. Domain limitations also give us some difficulties to numerically describe the combustion around the cell from a gas composition point of view. In fact the dynamic of combustion is affected from the external cell environment conditions such as oxygen availability and thermal constrains. Another problem encountered during the simulations concern the mesh generation. Many cell components are characterized by very high aspect ratio (ratio between the minimum and maximum dimensions). For example the cathode has a diameter of 80 mm and a thickness of 0.034 mm. An adequate grid resolutions along the thickness implies a big resolution along other dimensions so the total number of elements quickly increases. For this reason many studies of mesh-independent are performed in order to prove the quality of our meshes.

Activity

The first modeling step is the mesh generation and the most complex component from this point of view is the interconnect. The meshes used for simulations in MULTISS project are generated following two main process:

- parametric script for generating simple geometries for repetitive simulations used in model tuning, validation and topological optimization;
- standard pre-processing method starting from CAD software, exporting the geometry into a grid generator tool and finally importing the mesh to utilize it with the CFD code.

In the first case very controllable mesh quality can be obtained and the mesh generation is directly coupled inside an automatic process. This is a very useful functionality to obtain a complete SOFC simulation tool, in fact for an end user it is sufficient to tune some settings

to obtain an own mesh (based on some predefined geometry). The second mesh generation process is more similar to what happened in industrial environment. In this case it is possible to design more complex geometry fully coupled with other components. In this case particular attention has to be placed on mesh quality in order to prevent abnormal behavior of the grid generation tool.

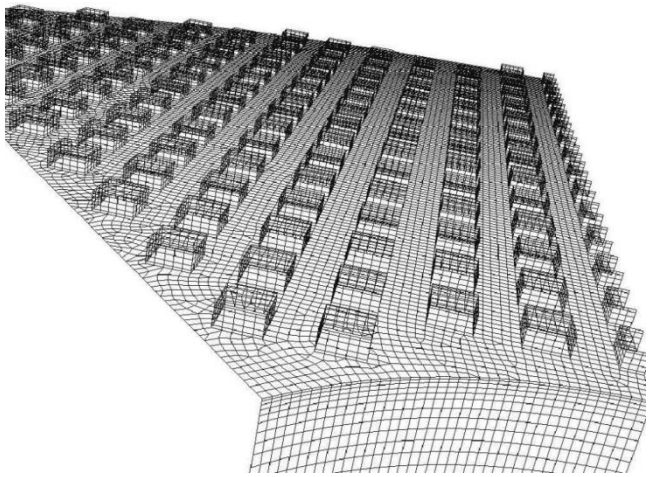

Figure A-1: Example of the mesh on the interconnector surface

Once the model and the mesh are built the next step is the tuning of the algorithms and the validation. The philosophy used is to use the real physic values for parameters that have it (porosity, tortuosity, etc…) and to respect the relations between parameter used to tune the model (for example between anode and cathode exchange current density). The validation process showed that the differences between 2D and 3D model is appreciable only at medium-high current density.

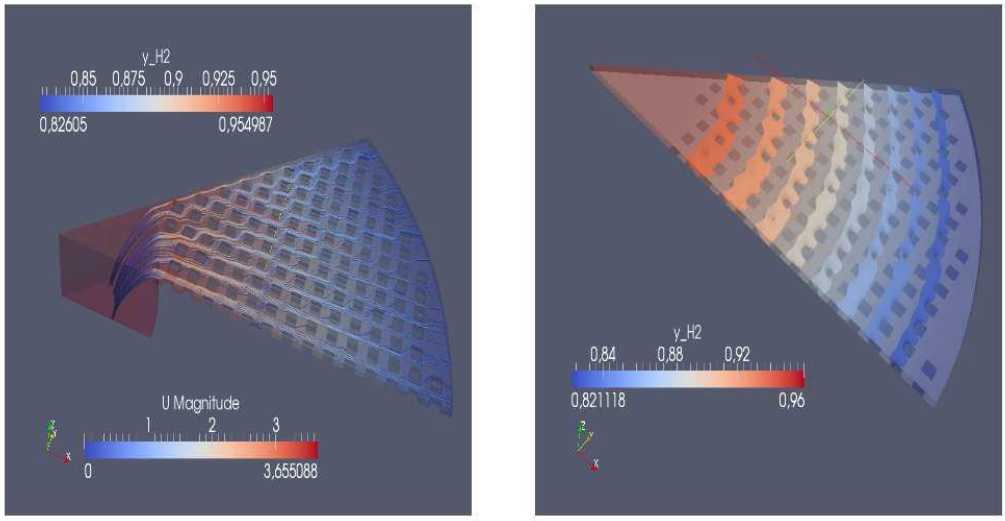

Figure A-2: H2 molar fraction at the anode surface as a function of current density in case of 2D (left) and 3D (right) models

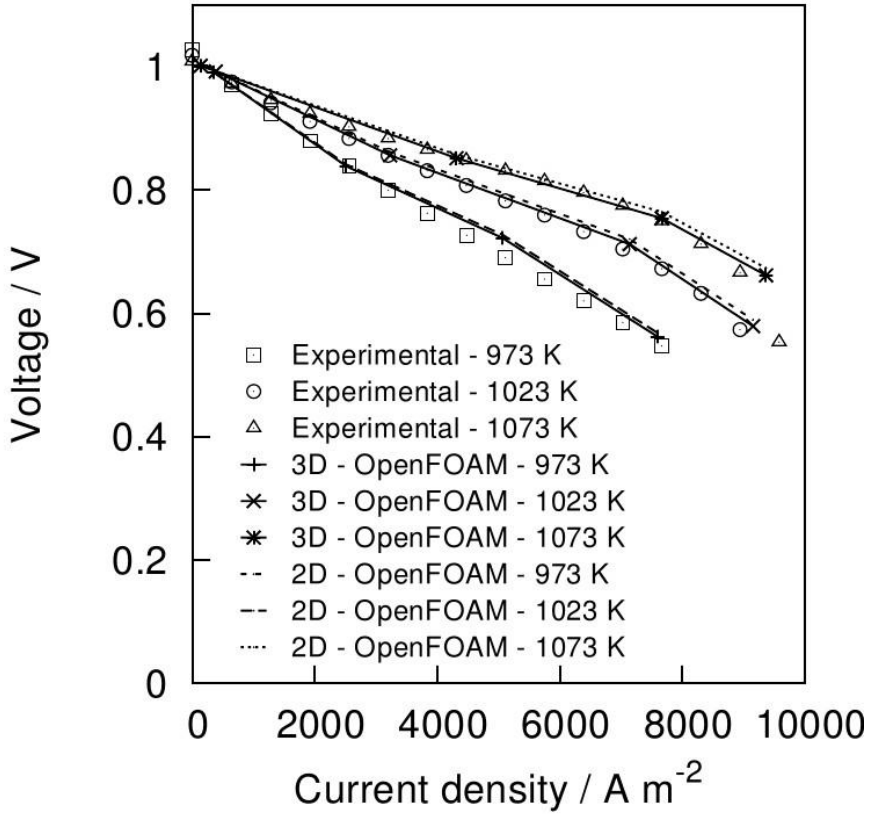

Figure A-3: Experimental and model polarization curves in case of 2D and 3D models

In general simulated curves overlap the simulated ones very well. At high current density 2D simulation over predict the voltage and the polarization curves don't fall down in the diffusive limiting region. This is due to the absence of any geometric fluid channels impedances in that simulation. Simulations in fact showed the presence of a "shadow effect" behind the geometry constraints of the interconnect (pins or channels) that significantly reduce the concentrations of the reactants in that zones. This implies that at high current density some part of the anode volume works very bad and the cell behaves as it had a lower active surface. This justify the diffusive limit of the polarization curves and suggest some strategies to reduce this effect and to obtain good performance also at high current density. Unfortunately reducing this effect by decreasing the pins or channels width contrast with the electrical conduction need between electrode and interconnector.

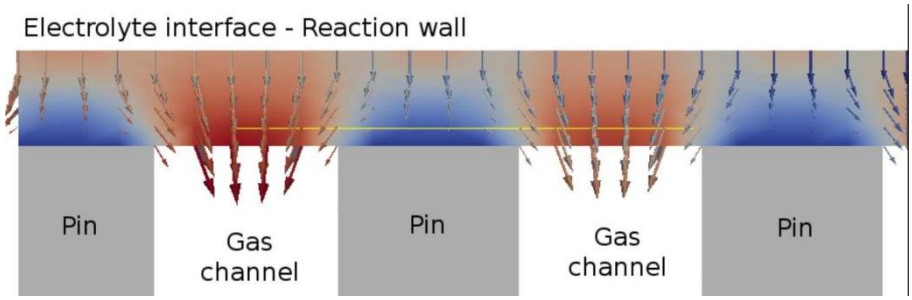

Figure A-4: "Shadow effect" of the pins to the reactant diffusion in the electrode volume

Another phenomenon that is explained through simulations is the lower experimental OCV value respect to the theoretical one during not sealed configuration tests. A little difference is expected due to gas leakage through the cell electrolyte and the measured value had to be justified in other way. We know that in the un-sealed configuration the exhausts burn outside the cell. This implies two main consequences: the increasing of the temperature and the variation of the reactant concentrations. The interested zone affected by this two phenomena is the annular region at the border of the cell, quite big even if it takes a little ray unit. An approximate combustion model (steady state, laminar, Arrhenius reaction rates, low grid refinement, etc…) was implemented because it was not the main aim of our works, but it however gave an explanation to the observed OCV phenomena.

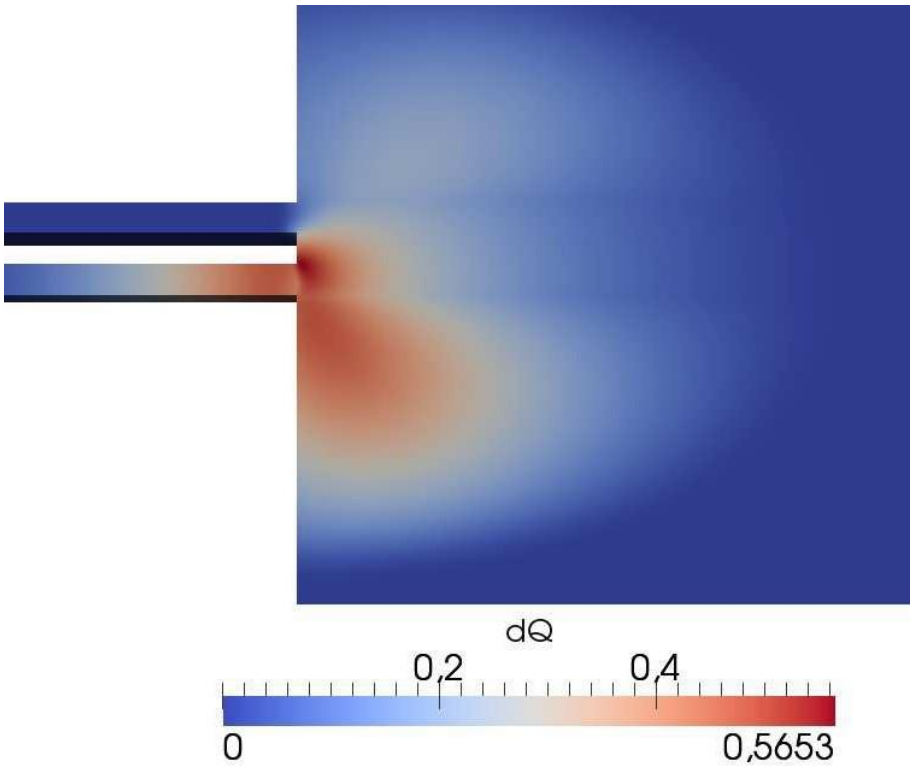

Figure A-5: Heat flow for burning reaction at the border of the un-sealed cell

When the anodic fluid flow is high enough (every cases where a quantity of molar flux on nitrogen is added) the combustion mainly occurs outside the cell but the diffusive effects on the reactants are present also inside the gas channels. So there is a zone of the cells in which the temperature is higher, the oxygen is nearly absent, the hydrogen is lacking and the water is present in abundance. All these factors contribute to reduce the Nernst potential. The entity of this reduction is comparable with the measured OCV. More accurate results could be achievable modeling combustion in more accurate way.

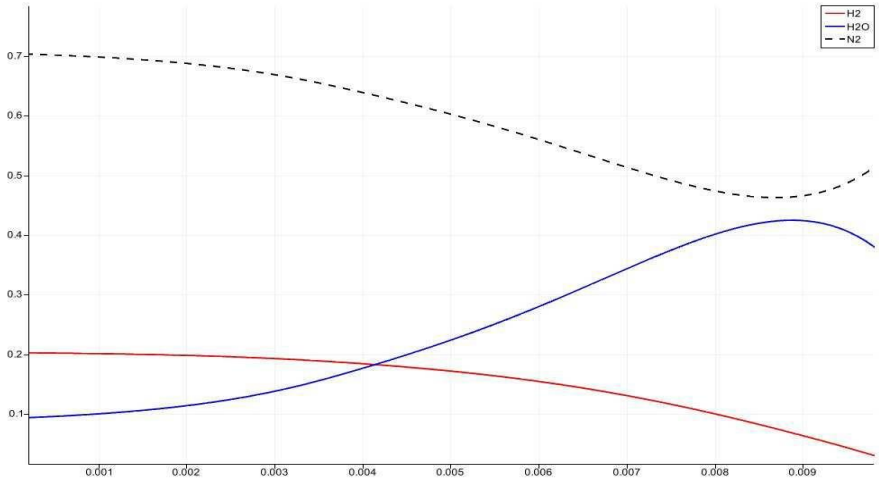

Figure A-6 Distribution of molar fraction along the cell ray in case of un-sealed cell

First simulations are used to understand and explain physic phenomena. After modeling work was utilized to optimize the gas flow inside the interconnects. Preliminary comparisons were made between circular cells and square cells varying the inlet and outlet size. The results shows that the corner region are the worst ones in term of fluid distribution. So circular cell for this kind of inlet-outlet configuration was justified.

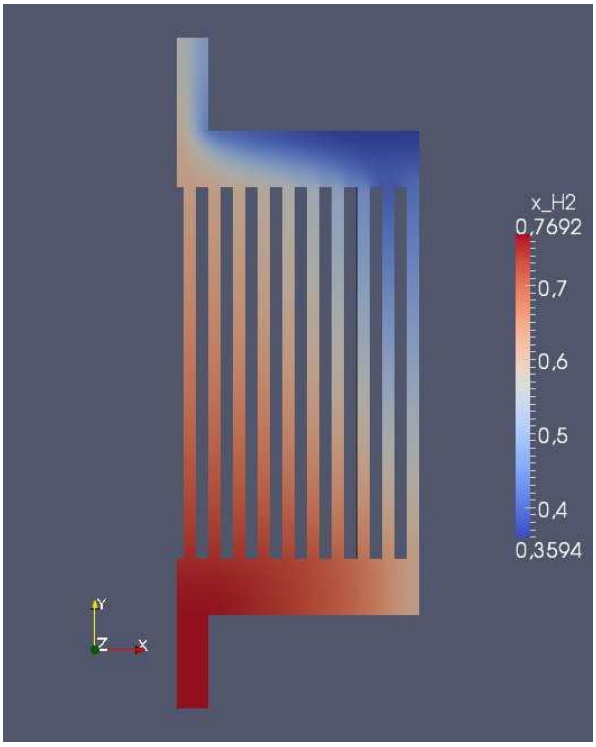

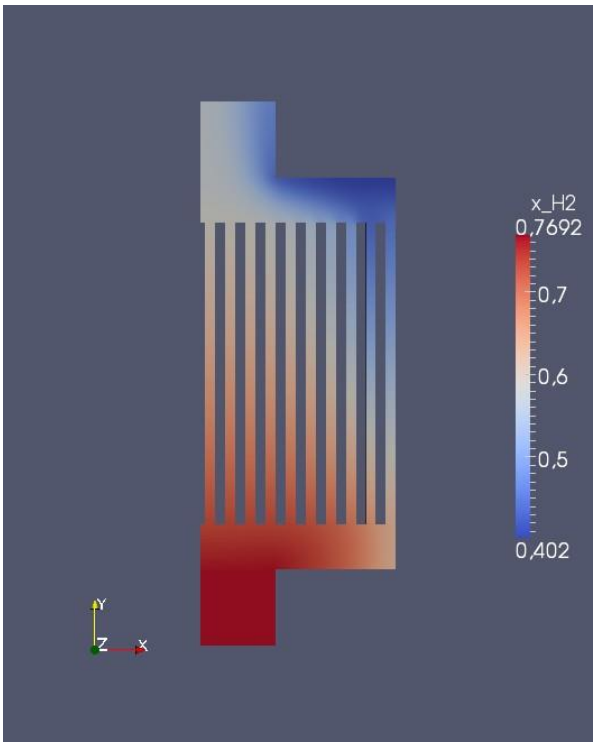

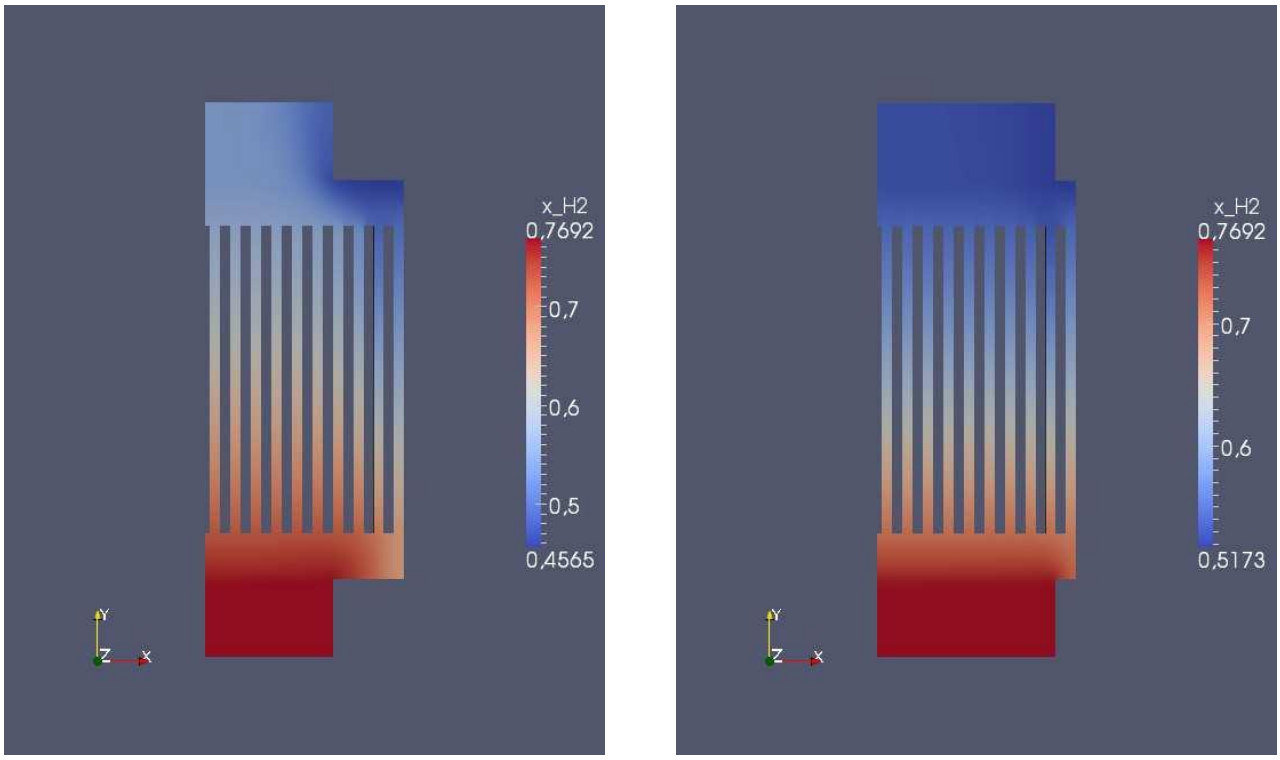

Figure A-7: H2 molar fraction distribution on the anode surface at different current densities in case of rectangular cells

Then, using circular geometry, some simulations are made changing the ratio between the inlet and the outlet channel section, that is one of the most important parameters in fluid flow distribution.

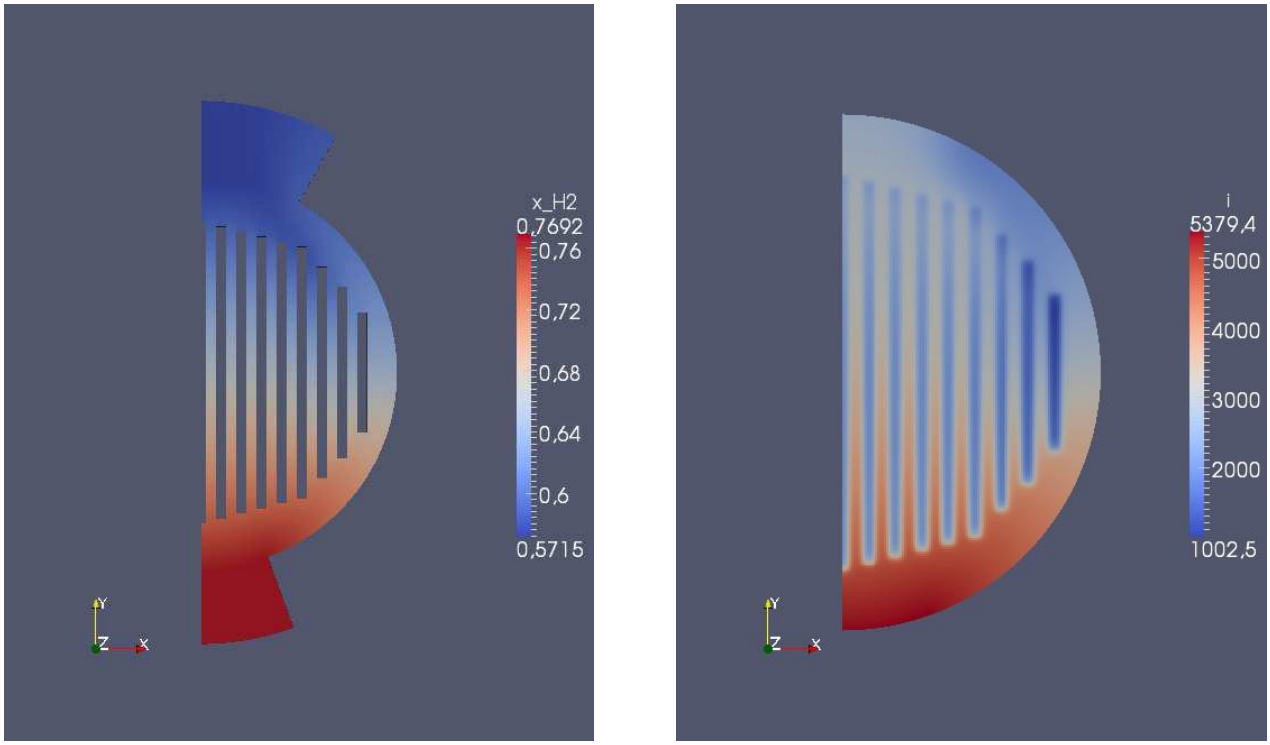

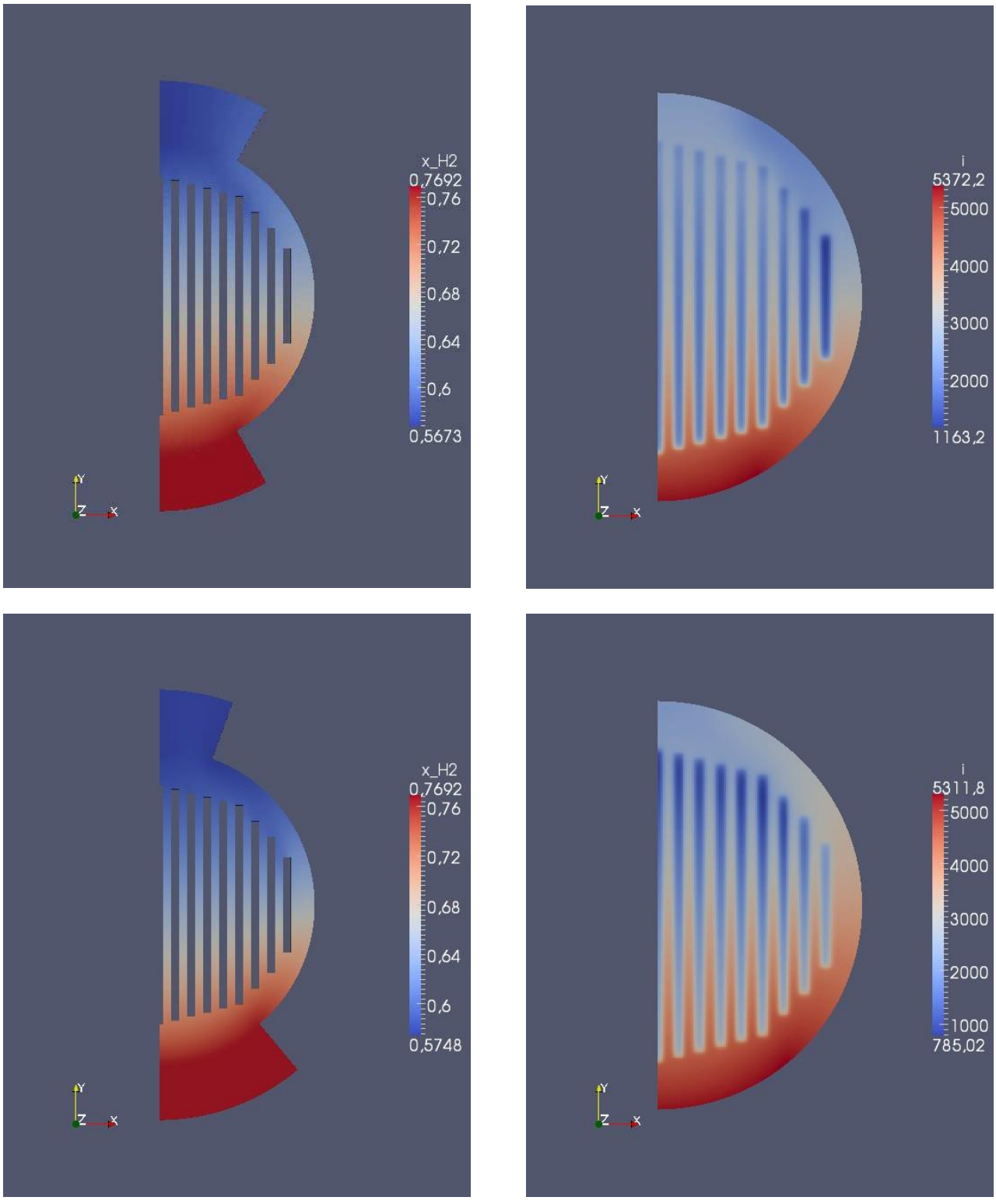

Figure A-8: H2 molar fraction distribution on the anode surface at different current densities in case of circular cells, with modification of the ratio between the inlet and the outlet channel section

Best results are obtained in that configurations with similar inlet and outlet dimensions. Variations in channels geometry (complex configurations or similar) could optimize the flow fields for a single operation point but simpler geometries work better for general purpose operations. We also experimented that a transversal channel can redistribute differences between longitudinal channels with positive effect. Since the electrical modeling is the less approximate part, the channel width and the ratio between channel and solid part widths was considered in conservative way.

Finally some simulations are performed about the anodic and cathodic flow configuration. Standard circular cells are usually fed by cross flow fluid configuration. Counter flow configuration could work better both in term of gas distribution and in term of current and temperature distribution. Unfortunately the optimal configuration require two different inlet manifold. This could increase the complexity of the system so it was not considered for preliminary tests.

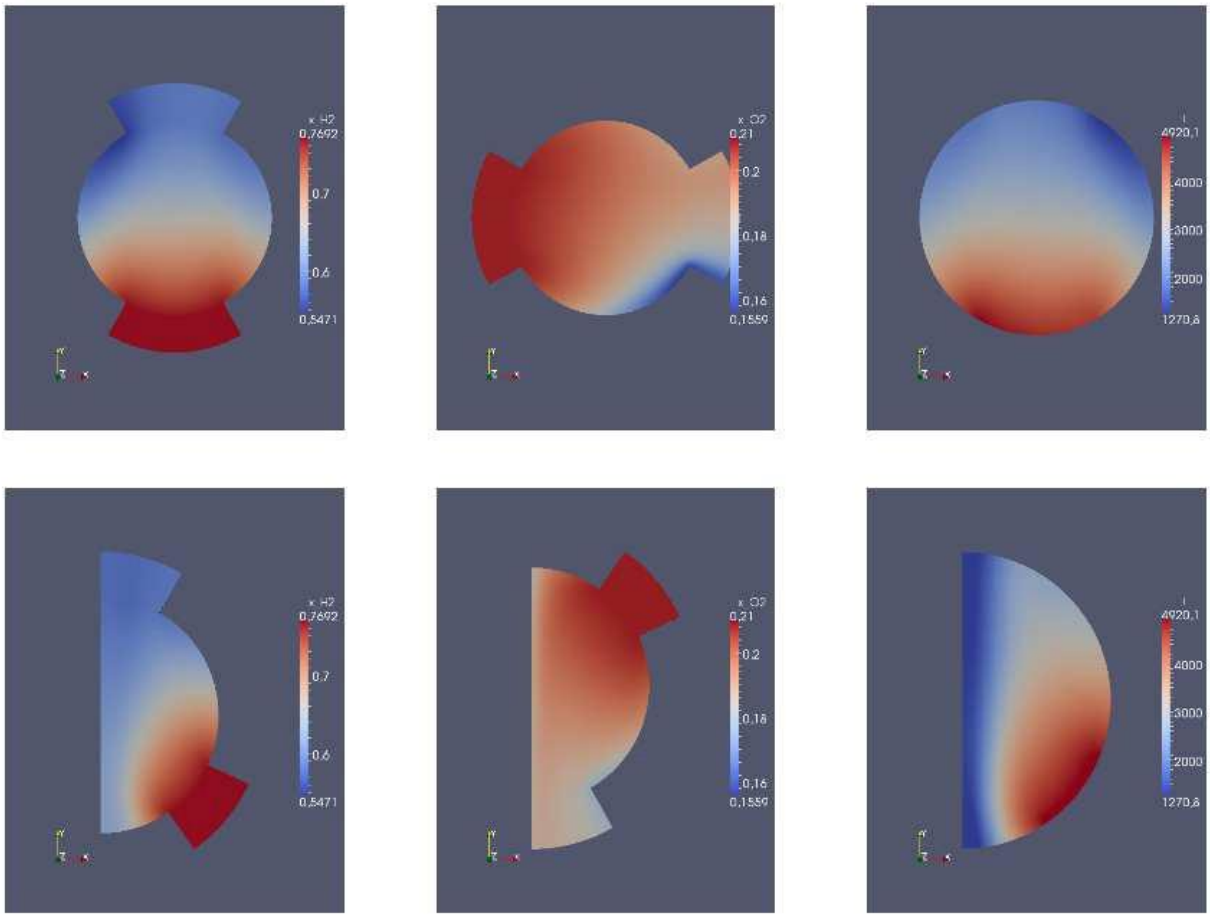

Figure A-9: H2 and O2 molar fraction distribution on respectively the anode and cathode surfaces at different current densities in case of circular cells, in case of different flow configuration (cross- flow, multiple inlet, etc)

Conclusions

At the end of Single Repeated Unit (SRU) simulation process, many parameters are fixed and some rules are defined in order to optimize the geometry.

Modeling suggests that the width of the channels has to be thicker as much as possible in order to prevent shadow effect at high current density.The inlet and outlet dimensions are increased to facilitate the fuel distribution.

The ratio between fuel channel width and interconnect width is set to one to minimize the ohmic losses due to contact resistance. Further simulations with comparison with experimental results suggest that the ratio can be set to two or three without increase the electric resistance and improving fluid dynamic performances.

The results can be improved increasing the meshes resolution and upgrading some models like combustion, mass and heat transfer, etc… This can be done only increasing the complexity of the model and only for one cell.

Considering the future stack point of view the model was built in order to obtain best results with minimum computational requirement. For optimization also economic/manufacturing constraints are considered in order to provide a geometry realistically feasible.

B. Appendix

Electrical Conductivity and Resistivity at 295K

Li 1.07 9.32	Be 3.08 3.25	... Electrical conductivity x $10^7/\Omega$ m Electrical resistivity x $10^{-8}\Omega$ m									B	C	N	O	F	Ne ... ...
Na 2.11 4.75	Mg 2.33 4.30	...									Al 3.65 2.74	Si	P	S	Cl	Ar ... ...
K 1.39 7.19	Ca 2.78 3.6	Sc 0.21 46.8	Ti 0.23 43.1	V 0.50 19.9	Cr 0.78 12.9	Mn 0.072 139	Fe 1.02 9.8	Co 1.72 5.8	Ni 1.43 7.0	Cu 5.88 1.70	Zn 1.69 5.92	Ga 0.67 14.85	Ge	As	Se	Br	Kr ... ...
Rb 0.80 12.5	Sr 0.47 21.5	Y 0.17 58.5	Zr 0.24 42.4	Nb 0.69 14.5	Mo 1.89 5.3	Tc .7 14	Ru 1.35 7.4	Rh 2.08 4.8	Pd 0.95 10.5	Ag 6.21 1.61	Cd 1.38 7.27	In 1.14 8.75	Sn 0.91 11.0	Sb 0.24 41.3	Te	I	Xe ... ...
Cs .50 20.0	Ba 0.26 39.	La 0.13 79.	Hf 0.33 30.6	Ta 0.76 13.1	W 1.89 5.3	Re 0.54 18.6	Os 1.10 9.1	Ir 1.96 5.1	Pt 0.96 10.4	Au 4.55 2.20	Hg* 0.10 95.9	Tl 0.61 16.4	Pb 0.48 21.0	Bi 0.086 116.	Po 0.22 46.	At	Rn ... ...
Fr	Ra	Ac	...													
...			Ce 0.12 81.	Pr 0.15 67.	Nd 0.17 59.	Pm	Sm 0.10 99.	Eu 0.11 89	Gd 0.070 134	Tb 0.090 111.	Dy 0.11 90.0	Ho 0.13 77.7	Er 0.12 81.	Tm 0.16 62.	Yb 0.38 26.4	Lu 0.19 53.	...
...			Th 0.66 15.2	Pa	U 0.39 25.7	Np 0.085 118.	Pu 0.070 143.	Am	Cm	Bk	Cf	Es	Fm	Md	No	Lr	...

Figure B-1: Data from Kittel, Introduction to Solid State Physics, 7th Ed.

Referenced to G. T. Meaden, Electrical resistance of metals, Plenum, 1965.

References

[1] K. Aleklett, " Lower output target for Iraq", Association for the Study of Peak Oil and Gas (ASPO), www.peakoil.net , (28-01-2013).

[2] UK International Climate Fund, http://www.dfid.gov.uk/Documents/publications1/uk-int-clim-fund-tack-clim-chge-red-pov.pdf , (28-01-2013).

[3] O. Edenhofer et al, “Renewable Energy Sources and Climate Change Mitigation”, Intergovernmental Panel on Climate Change (IPCC), http://www.ipcc.ch/publications_and_data/publications_and_data_reports.shtml#SRREN (28-01-2013).

[4] United Nations Framework Convention on Climate Change (UNFCCC) http://unfccc.int/meetings/doha_nov_2012/meeting/6815/php/view/reports.php, (28-01-2013).

[5] BlueGen “Big efficiency from a small electricity generator” http://www.bluegen.info/AU_benefit_1/, (28-01-2013).

[6] E. Ivers-Tiffée et al, “Why Going Nano with Fuel Cells?”, Center for Functional Nanostructures (CFN), http://www.cfn.kit.edu/653.php, (17-02-2013).

[7] National Energy Technology Laboratory, “Solid Oxide Fuel Cells and Critical Materials: A Review of Implications”, J. Thijssen, (2011).

[8] EG&G Technical Services, Inc.(2004) “Fuel Cell Handbook (Seventh Edition)”. U.S. Department of Energy.

[9] J. Thijssen, “The impact of scale-up and production volume on SOFC manufacturing cost”. National Energy Technology Laboratory, Department of Energy USA, (2007).

[10] N.Q. Minh, T. Takahashi “Science and technology of ceramic fuel cells”. Elsevier, Amsterdam., (1995).

[11] K. Kendall, N.Q. Minh and S.C. Singhal in High Temperature Solid Oxide Fuel Cells: Fundamentals, Design, and Applicatons, eds. S.C. Singhal, K. Kendall, Elsevier Advanced Technology, 2003, pag 199-224.

[12] Qiang Hu, Shaorong Wang, Ting-Lian Wen, “Analysis of processes in planar solid oxide fuel cells”, Solid State Ionics 179 (2008) 1579–1587.

[13] J. W. Kim, A. V. Virkar, IC. Z. Pung, K. Mehta and S. C. Singhal, J. Electrochem. Soc., 146 (1999) p. 69.

[14] Armstrong TR, Stevenson JW, Pederson LR, Raney PE (1996) J Electrochem Soc 143:2919.

[15] Huczkowski P, Christiansen N, Shemet V, Piron-Abellan J, Singheiser L, Quadakkers WJ (2004) Mater Corros 55:825.

[16] Stanislowski M, Wessel E, Hilpert K, Markus T, Singheiser L (2007) J Electrochem Soc 154:A295.

[17] Paulson SC, Birss VI (2004) J Electrochem Soc 151:A1961.

[18] Neumann A, Menzler NH, Vinke I, Lippert H (2009) ECS Trans 25(2):2889.

[19] DOE Report (reference 39463-02): Assessment of Planar Solid Oxide Fuel Cell Technology. October 1999, by Arthur D. Little, Inc.

[20] Schmidt H, Brückner B, Fischer K (1995) In: Dokiya M, Yamamoto O, Tagawa H, Singhal SC (eds) Proc. 4th Int. Symp. SOFC (SOFC-IV). The Electrochemical Society, Pennington, NJ, p 869

[21] Larring Y, Norby T (2000) J Electrochem Soc 147:3251.

[22] Quadakkers WJ, Greiner H, Hänsel M, Pattanaik A, Khanna AS, Mallener W (1996) Solid State Ionics 91:55.

[23] Deng XH, Wei P, Reza Bateni M, Petric A (2006) J Power Sources 160:1225.

[24] Yang ZG, Xia GG, Stevenson JW (2005) Electrochem Solid State Lett 8:A168

[25] Zahid M, Tietz F, Sebold D, Buchkremer HP (2004) In: Mogensen M (ed) Proc. 6th Eur. SOFC Forum, Lucerne, vol 2. European Fuel Cell Forum, Oberrohrdorf, Switzerland, p 820.

[26] Petric A, Huang P, Tietz F (2000) Solid State Ionics 135:719.

[27] Donald I.W. (1993) J Mater Sci 28:2841. doi:10.1007/BF00354689.

[28] K. Huang, 7th European Fuel Cell Forum 2006, Lucerne 3-5 July 2006.

[29] S.C Singhal. et al., Journal of the Electrochemical Soc., Vol. 146 (1), pp. 69-78 (1999).

[30] A. Atkinson,“UK Research on Fuel Cells", UK Energy Research Centre, http://www.ukerc.ac.uk/support/tiki-index.php?page=JointUK-SouthAfricaWorkshopOnEnergyResearch200206), (17-02-2013).

[31] B. Rietveld, et al., ASME 1st European Fuel Cell Technology and Applications.

[32] J.-H. Lee et Al., Journal of Power Sources, V. 159, pp 478-483, 2006.

[33] P.W. Li, et Al., Journal of Power Sources, vol. 124, pp. 487-498, 2003.

[34] P. Asinari et Al., Proceedings of ESDA2006, 8th Biennial ASME Conference on Engineering Systems Design and Analysis, 4-7 July, 2006, Torino, Italy.

[35] .N. H. Menzler et al., Journal of Power Sources, (2005), 152, 156–167.

[36] .K. S. Weil, (2006) JOM, 58, 37-44.

[37] N. P. Bansal et al., Journal of Power Sources, (2005), 147, 107–115.

[38] P. Batfalsky et al., Journal of Power Sources, (2006) 155, (2), 128-137.

[39] T. Lipman and D. Sperling, "Market Concepts, Competing Technologies and Cost Challenges for Automotive and Stationary Applications", in W. Vielstich et al. (Eds.), Handbook of Fuel Cells - Vol. 4, Chichester, England: John Wiley & Sons Ltd., p. 1318-1328, 2003. .

[40] P. Lamp, J. Tachtler, O. Finkenwirth, P. Mukerjee and S. Shaffer, "Development of an Auxiliary Power Unit With Solid Oxide Fuel Cells for Automotive Applications", Fuel Cells, Volume 3, Issue 3, p. 1-7, 2003.

[41] D. Nikbin, "Micro SOFCs: Why Small Is Beautiful", The Fuel Cell Review, Volume 3, Issue 2, p. 21-24, 2006.

[42] L. Blum, W. A. Meulenberg, H. Nabielek and R. Steinberger-Wilckens, "Worldwide SOFC Technology Overview and Benchmark", International Journal of Applied Ceramic Technology, Volume 2, Issue 6, p. 482-492, 2005.

[43] T. Ishihara, N. M. Sammes and O. Yamamoto, "Electrolytes", in S. C. Singhal and K. Kendall (Eds.), High Temperature Solid Oxide Fuel Cells, New York: Elsevier Ltd., p. 83-117, 2003.

[44] O. Yamamoto, "Low Temperature Electrolytes and Catalysts", in W. Vielstich et al. (Eds.), Handbook of Fuel Cells - Vol. 4, Chichester, England: John Wiley & Sons Ltd., p. 1002, 2003.

[45] M. Gödickemeier, K. Sasaki, L. J. Gauckler and I. Riess, "Electrochemical Characteristics of Cathodes in Solid Oxide Fuel Cells Based on Ceria Electrolytes", Journal of the Electrochemical Society, Volume 144, Issue 5, p. 1635-1646, 1997.

[46] J. M. Bae and B. C. H. Steele, "Properties of La0.6Sr0.4Co0.2Fe0.8O3-δ (LSCF) Double Layer Cathodes on Gadolinium-Doped Cerium Oxide (CGO) Electrolytes - I. Role of SiO2", Solid State Ionics, Volume 106, Issue 3-4, p. 247-253, 1998.

[47] V. Dusastre and J. A. Kilner, "Optimisation of Composite Cathodes for Intermediate Temperature SOFC Applications", Solid State Ionics, Volume 126, Issue 1-2, p. 163-174, 1999.

[48] A. Mai, V. A. C. Haanappel, S. Uhlenbruck, F. Tietz and D. Stöver, "Ferrite-Based Perovskites As Cathode Materials for Anode-Supported Solid Oxide Fuel Cells Part I. Variation of Composition", Solid State Ionics, Volume 176, Issue 15-16, p. 1341-1350, 2005.

[49] B. C. H. Steele, "Oxygen-Transport and Exchange in Oxide Ceramics", Journal of Power Sources, Volume 49, Issue 1-3, p. 1-14, 1994.

[50] EG&G Technical Services/ U.S. Department of Energy: "Fuel Cell Handbook" (Seventh Edition); November 2004.

[51] Stevenson J. & all: "SOFC Seals: Materials Status", SECA Core Technology Program – SOFC Seal Meeting, July 8, 2003.

[52] "Intergranular Corrosion – Recognizition, mechanisms and prevention" http://www.corrosionclinic.com/types_of_corrosion/intergranular_corrosion_cracking.html, (30-01-2013).

[53] Santarelli M, & all; "Design and in-house development of solid oxide fuel cell (SOFC) stacks for dealing with multiple fuels". EDIZIONI POLITEKO, TORINO, pp. 1-124. ISBN 9788897862024(2012)

[54] Larminie J. and Dicks A., "Fuel Cell Systems Explained, Second Edition", Wiley, ISBN 0-470-84857-X

[55] Ajitdoss L.C.& all, "Mn1.5Co1.5O4 protective coatingon Crofer22APU produced by thermal co-evaporation for SOFCs", Materials Letters Volume 95, 15 March 2013, Pages 82–85.

[56] "Sensitization of Stainless Steel", http://www.solidmetals.net/2011/05/02/sensitization-of-stainless-steel/, (28-01-2013).

[57] Tu H. et al. J Power Sources 127 (1–2), 2004, 284–293

[58] Opila E.J. et al. J. Met 58 (1), 2006, 22–26

[59] Konysheva E. et al. J Electrochem Soc. 153 (4),2006, A765–773

[60] Matsuzaki Y. et al. J Electrochem Soc 148 (2), 2001, A126–131

[61] Fujita K. et al. J Power Sources 131 (1-2), 2004, 261–269

[62] Novaresio V. "An open source library for the numerical modeling of mass-transfer in solid oxide fuel cells", Computer Physics Communications, Volume 183, Issue 1, January 2012, Pages 125–146.

[63] Novaresio, V. "Numerical modeling of planar SOFC stack by open source code", Proceedings of EFC2009 Third European Fuel Cell Technology & Applications Conference - Piero Lunghi Conference December 15-18, 2009, Rome, Italy